January 2009

The Role of Astrocyte Activation in Infantile Neuronal Ceroid Lipofuscinosis

Shannon Macauley-Rambach
Washington University in St. Louis

WASHINGTON UNIVERSITY IN SAINT LOUIS

Division of Biology and Biomedical Sciences

Program in Neuroscience

Dissertation Examination Committee:

Mark Sands, Chair

Karen O'Malley

David Gutmann

David Holtzman

Mark Goldberg

Michael Wong

THE ROLE OF ASTROCYTE ACTIVATION IN INFANTILE NEURONAL CEROID LIPOFUSCINOSIS

by Shannon Lynn Macauley-Rambach

A dissertation presented to the Graduate School of Arts and Sciences of Washington University in Saint Louis in partial fulfillment of the requirements for the Degree of Doctor of Philosophy

December 2009

Saint Louis, Missouri

ABSTRACT OF THE DISSERTATION

The role of astrocyte activation in infantile neuronal ceroid lipofuscinosis (INCL)

by

Shannon Lynn Macauley-Rambach

Doctor of Philosophy in Biology and Biomedical Sciences (Neurosciences)

Washington University in St. Louis

Dr. Mark S. Sands, Chairperson

Infantile neuronal ceroid lipofuscinoses (INCLs), or Batten Disease, is an inherited neurodegenerative lysosomal storage disorder affecting the central nervous system (CNS) during infancy or childhood. Hallmark pathological changes include accumulation of autofluorescent material, neuronal loss, cortical thinning, and brain atrophy, which ultimately lead to cognitive deficits, motor dysfunction, seizure activity, and blindness. INCL is the result of mutations in the *CLN1* gene leading to a deficiency in the lysosomal enzyme, palmitoyl protein thioesterase 1 (PPT1). A mouse model of INCL, the PPT1-deficient (PPT1-/-) mouse, was recently created by a targeted disruption in the *CLN1* gene. The phenotype of the PPT1-/- mouse is similar to that found in human INCL patients, suggesting the PPT1-/- mouse is an authentic model of INCL. Although the clinical symptoms of disease are well described, the cellular mechanisms underlying these pathological changes and functional deficits remain poorly understood. Therefore, the first goal of this dissertation was to investigate the

temporal-spatial progression of disease in a mouse model of INCL. We demonstrated a profound neuronal and glial involvement underlying both physiological and functional deficits. From these studies, we also found the first pathological change observed was the upregulation of glial fibrillary acidic protein (GFAP), a marker of astrocyte activation, in the thalamus, cortex, and cerebellum. Focal regions of GFAP upregulation were an accurate predictor of future sites of neuronal loss. Since astrocyte activation is both helpful and harmful to an injured CNS, the second aim of this dissertation was to investigate the role of astrocyte activation in a mouse model of INCL using the GFAP-/-, Vimentin-/- mice. We demonstrated that astrocyte activation, as defined by GFAP upregulation, plays a protective role in INCL.

ACKNOWLEDGEMENTS

First, I would like to thank my thesis advisor, Mark Sands, for his mentorship during this journey. From the scientific rigor to the congenial work environment, Mark gave me with the opportunity to succeed in graduate school. I believe his “open door policy” reflected his open mind. I came to Mark with an interest in lysosomal storage diseases and the brain. Although a self proclaimed “non-neuroscientist”, Mark embraced the idea of investigating questions outside his area of expertise, demonstrating both a confidence in me as well as a confidence in sound, goal-directed science; both lessons will serve me well during my career. Together, through much conversation and mutual brainstorming, we devised not one, but ultimately, two projects that were as fascinating as they were challenging. Mark’s dedication to the field of lysosomal storage disease research and strong desire to ease the suffering of patients and families afflicted by LSDs are truly inspiring. I thank Mark for his determination, motivation, and freedom of thought. Perhaps most, I thank him for his passion for science and unwavering confidence in me.

In addition to my mentor, I would like to thank the personnel in the Sands Lab for making lab an absolutely outstanding “hostile working environment”. I believe it is the diversity of thought and personal experience from lab that has shaped my work in ways I can only imagine. Specifically, I would like to thank Kevin for his diligence; Adarsh for his critical input and laughter; Jacqui for her support and friendship; and Marie for being the only “lab mom” strong enough and kind enough to deal with us all.

I believe the adage “it takes a community to raise a child” also applies to graduate students attempting to complete their PhD dissertation. I cannot imagine completing my doctoral training without the support of the Wash U community, friends and family. First, I would like to thank my thesis committee for their support and critical evaluation. Always impressed by their insight and intellect, I am forever grateful for their collaborative spirit. I have also had the pleasure of collaborating with Jonathon Cooper’s Lab at Kings College – London. Specifically, I would like to thank Catherine Kielar for her technical help and thoughtful discussions concerning our work. Second, I would like to thank my friends, old and new, for giving me equal parts strength, distractions, and laughter to see this process though to completion. I was lucky enough to begin this process with a tremendous 2003 Neuroscience class. I cherish the scientific conversations as much as the shenanigans! And to all those outside of grad school, thank you for reminding me life exists outside the lab.

Specifically, I would like to thank my friend and previous mentor, Greg Stewart, for pushing me to excel at Genzyme and “softly” suggesting that I go to Wash U. Graduate school would have been a lot different experience without his mentorship. I would also like to thank my best friend and partner-in-crime, Hilary Luderer. A constant companion, friend, colleague, and confidant, she made the worst parts of graduate school tolerable and the best times so much more special!

Lastly, I’d like to thank my family, old and new, for their support during this process. I feel blessed to have a family that always believed in my aptitude,

even when I couldn't. My success is due to attributes I've borrowed from them- my mom's veracious tenacity, my dad's acute perception, and my sister, Kelly's, analytical precision. I am lucky to have a family that challenged me to excel, provided me with the fundamentals to succeed, and offered me plenty of laughter along the way. For this, I'm forever grateful. During my time in St. Louis, I was lucky enough to extend my immediate family by meeting my husband, Rob. His family has been unbelievably supportive of me during this process. I am exceptionally grateful to my mother-in-law, Libby, and father-in-law, Steve, who display a constant interest in my work and choose to celebrate my success as if it was their own.

Finally, I'd like to thank my husband, Rob, for well… everything. When I left for St. Louis, I never dreamed after 6 years I'd get a PhD and a loving husband. As trite as it sounds, there is no way I could have done this without him. His constant love and support grounded me when nothing seemed to work. His unyielding confidence gave me strength and determination when I lost hope. His laughter and kindness will forever pull me away from the bench and put a smile on my face. It is impossible to name all the ways in which he assisted me during this process. I will forever be humbled by his love, admiration, and support.

TABLE OF CONTENTS

LIST OF FIGURES

CHAPTER 1: Introduction

CHAPTER 2: Characterization of the forebrain & hindbrain pathology in the PPT1-/- mouse, a mouse model of INCL

CHAPTER 3: The role of astrocyte activation, as defined by GFAP upregulation, in a mouse model of INCL

ABBREVIATIONS

LSD	lysosomal storage disease
CNS	central nervous system
NCL	neuronal ceroid lipofuscinosis
INCL	infantile neuronal ceroid lipofuscinosis
GRODs	granular osmiophilic material
SAP A	saposins A
SAP D	saposins D
GFAP	glial fibrillary acidic protein
LINCL	late-infantile neuronal ceroid lipofuscinosis
JNCL	juvenile neuronal ceroid lipofuscinosis
ANCL	adult-onset neuronal ceroid lipofuscinosis
EEG	electroencephalography
PPT1	palmitoyl protein thioesterase 1
PPT1-/-	PPT1 deficient
mos	months
s	seconds
ERG	electroretinogram
WT	wildtype
PC	Purkinje cells
GLAST	glutamate aspartate transporter
GLT-1	glutamate transporter 1
Vim	Vimentin
GFAP-/-, Vim-/-	GFAP, Vimentin double knockout mouse
2KO	GFAP, Vimentin double knockout mouse
GFAP-/-, Vim-/-, PPT-/-	GFAP, Vimentin, PPT triple knockout mouse
3KO	GFAP, Vimentin, PPT triple knockout mouse
CO_2	carbon dioxide
PBS	phosphate buffered saline
PFA	paraformaldehyde
H&E	hemotoxylin & eosin
CE	mean coefficient of error
TBS	tris-buffered saline
GS	glutatmine synthetase
NGS	normal goat serum
H_2O_2	hydrogen peroxide
TdT	deoxynucleotidyl transferase
PAS	Periodic acid-Schiff stain
LGN	lateral geniculate nucleus
MGN	medial geniculate nucleus
VPM/VPL	ventral posterior thalamic nucleus
MD	mediodorsal
CM	central medial
Rt	reticular thalamus
PC	Purkinje cell

EAAT4	excitatory amino acid transporter 4
BBB	blood brain barrier
vim	Vimentin
IF	intermediate filament
S1BF	somatosenory barrel field cortex
OCT	optimal cutting temperature
V1	primary visual cortex
MCAO	middle cerebral artery occlusion
TCA	trichloroacetic acid
ETOH	ethanol
IL-	interleukin
GM-CSF	granulocyte macrophage colony stimulating factor
IFN-g	interferon gamma
MCP-1	monocyte chemotactic protein-1
MIP-1	macrophage inflammatory protein-1
RANTES	regulated upon activation, normal T-cell expressed, ands secreted
EB	Evan's blue
ERT	enzyme replacement therapy
AAV	adeno-associated virus
LV	lenti-virus
EAE	experimental autoimmune encephalomyelitis
TBI	traumatic brain injury

DEDICATION

My thesis is dedicated to all those patients and families suffering from lysosomal storage diseases. Your strength and determination is not only an inspiration, but also a constant reminder of what I am working for. Specifically, I'd like to dedicate my work to Tracy VanHoutan, his wife, and his beautiful children, Noah, Emily, and Laine. A father's determination to save his children is my motivation.

Chapter One

Introduction

INTRODUCTION

Lysosomal Storage Diseases: An Overview

Lysosomal storage diseases (LSDs) are a group of rare, inherited disorders involving both the visceral tissues and central nervous system (CNS) of affected patients (Hers, 1965; Neufeld, 1991). There are greater than 45 distinct metabolic disorders in total. LSDs affect approximately 1 in 5,000 live births, making these disorders one of the most common childhood genetic diseases (Meikle et al., 1999).

Each LSD is a discrete genetic disorder caused by a single gene mutation. In all cases, the genetic mutation of a particular protein causes a disruption in normal lysosomal function (Scriver, 2001). Most of the disorders are transmitted through autosommal recessive inheritance, but a subset of LSDs is X linked. The main function of the lysosome is the degradation of macromolecules into simpler metabolites. Most LSDs are due to defects in soluble lysosomal enzymes that are responsible for the catabolism of macromolecules. The mutations lead to the reduction (>90%) or complete ablation of enzyme activity for that specific protein. The remainder of LSDs is caused by mutations in key lysosomal membrane proteins, proteins involved in lysosomal enzyme trafficking, or proteins responsible for lysosomal enzyme activation (Neufeld, 1991; Winchester, 2004).

Regardless of the function of a given protein, most LSDs result in the accumulation of undigested substrates in the lysosomal compartment. As the undegraded product steadily accumulates within the organelle, both the size and number of lysosomes within a cell increases. Upon microscopic inspection, this

lysosomal accumulation gives the cell and its cytoplasm a “foamy” appearance; a hallmark characteristic of LSD pathology (Figure 1). Although the mechanism is still unknown (Ballabio and Gieselmann, 2009), accumulated substrates interfere with normal cellular processing, ultimately affecting the function of vital organs such as the brain, kidneys, liver, lungs, spleen, and heart (Macauley and Sands, 2009b; Neufeld, 1991; Scriver, 2001). The clinical signs associated with LSDs can include organomegally, skeletal deformities, pulmonary insufficiencies, immunologic abnormalities and cardiac defects. In addition to these systemic problems, CNS involvement occurs in 75% of all LSDs. This subset of affected patients present with some or all of the following neurologic symptoms: developmental regression, visual and hearing deficits, mental retardation, seizures, motor deficits, speech impairment, and other behavioral abnormalities (Hoffmann and Mayatepek, 2005; Sands and Haskins, 2008; Walkley, 1998). LSDs can affect patients as early as within the first year of life, or alternatively, they can present in adulthood. Regardless of onset, each disorder is progressive in nature, with a complex set of clinical maladies and ultimately premature death.

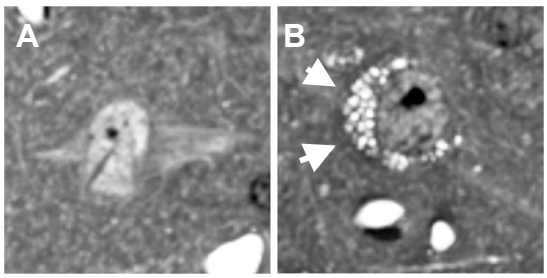

Figure 1. Lysosomal accumulation in a model of LSD. Notice the lysosomal accumulation and distension (arrows) in a diseased neuron (B) compared to a WT neuron (A).

Neuronal Ceroid Lipofuscinoses (NCLs)

Neuronal ceroid lipofuscinoses (NCLs), or Batten Diseases, are a group of autosomal recessive lysosomal storage disorders (LSDs) typified by prominent CNS involvement. As a class of disorders, the overall incidence is approximately 1:12,500 live births and represents the most common inherited pediatric neurologic disorders worldwide (Bennett and Hofmann, 1999; Goebel and Wisniewski, 2004; Hofmann and Peltonen, 2001). Classification of these disorders was historically based on the age of onset. Infantile (INCL), late-infantile (LINCL), and juvenile (JNCL) forms referred to cases affecting children; however, rare forms with an adult onset (ANCL) were also described. Recently, the use of modern genetic tools has led to a more accurate classification of the various forms of NCL. To date, there are eight different forms of Batten Disease resulting from mutations in separate genes, *CLN1* through *CLN8* (Cooper, 2003; Goebel and Wisniewski, 2004). Although the metabolic function of many of these gene products remains unclear, it is known that *CLN1*, *CLN2,* and *CLN5* encode soluble lysosomal enzymes while the remaining *CLN* genes encode lysosomal membrane proteins.

Although the age of onset, disease progression, and age of death vary in each form of NCL, there are characteristics common to all forms of NCL. The clinical course of disease is progressive and includes blindness, epilepsy, mental retardation, and motor deficits (Hofmann and Peltonen, 2001; Rider and Rider, 1988; Santavuori, 1988; Santavuori et al., 1974). A histological finding common to all the NCLs is the intracellular accumulation of autofluorescent substrates. To

date, the composition of this storage product remains largely unknown. The accumulation of storage material coincides with pathological changes such as widespread neuronal loss, retinal degeneration, cortical thinning, and overall brain atrophy (Wisniewski et al., 1988). More recently, astrocyte proliferation and microglia activation were described in both patients with NCL and animals models of disease. Although the CNS pathology and functional impairment is well documented in these diseases, it still remains unclear how the two are related.

Infantile Neuronal Ceroid Lipofuscinosis (INCL)

Of the eight distinct genetic variants currently described, infantile neuronal ceroid lipofuscinosis (INCL) is the most rapidly progressing form of NCL (Hofmann et al., 1999; Hofmann and Peltonen, 2001; Vesa et al., 1995). Clinically, patients with INCL appear asymptomatic at birth and development proceeds normally until 6-12 months of age. By 12 months of age, affected children begin to show signs of developmental regression, including mental retardation, microcephaly, and motor deficits (Hofmann et al., 1999; Hofmann and Peltonen, 2001; Santavuori et al., 1974; Vesa et al., 1995). Visual impairment is often the first clinical sign of INCL. Typically, visual defects emerge about one year of age, which lead to blindness by age 2. Myoclonic jerks appear between 16 to 24 months of age, which is concurrent with changes in electroencephalography (EEG). Specifically, there is decreased amplitude or flattening of background EEG activity by 2 years of age, which progresses to an

inactive EEG by 3-4 years of age (Haltia et al., 1973a; Haltia et al., 1973b; Haltia et al., 1995; Hofmann and Peltonen, 2001; Vanhanen et al., 1997). The average age of death is 6 years of age, but some children survive until adolescence.

At autopsy, the CNS pathology is remarkable (Haltia et al., 1973a; Haltia et al., 1973b; Haltia et al., 1995; Hofmann and Peltonen, 2001; Vanhanen et al., 1997). There is an overall brain atrophy, mostly due to thinning of the cerebral cortex. The cerebral cortex is denuded of neurons and replaced by macrophages, activated microglia and reactive astrocytes. The cerebellar cortex is also atrophic due to a loss of both granule cells and Purkinje cells. Neuronal cell loss is present in subcortical structures, with the thalamus most severely affected and the brain stem, hypothalamus, and subthalamus relatively spared. In addition to the neurodegeneration and astrocytosis in the cerebrum and cerebellum, there is a nearly complete loss of myelin at the end stage of disease, with myelin levels being 2% of normal.

The cellular pathology underlying the gross anatomical changes is severe as well. Like other forms of NCL, autofluorescent accumulation is a hallmark of INCL. The storage product, when examined by electron microscopy, is composed of granular osmiophilic deposits (GRODs) localized to the lysosome. Although the exact composition of GRODs is poorly understood, biochemical studies identified the storage material to be 43% protein and 35% lipid. Of the proteins extracted, three major products were identified- Saposins A and D (SAPs A and D) and glial fibrillary acidic protein (Haltia et al., 1995; Tayama et al., 1992; Tyynela et al., 1993). Interestingly, the major constituent of storage

accumulation in other NCLs, subunit C of mitochondrial ATPase (Palmer et al., 1992), is not found in GRODs from INCL patients. Although it is important to identify the storage products within disease cells, the role SAP A and D or GFAP plays in disease pathogenesis remains unknown.

Infantile neuronal ceroid lipofuscinosis is the result of mutations in the *CLN1* gene, which encodes the lysosomal enzyme, palmitoyl protein thioesterase 1 (PPT1; (Das et al., 1998; Hofmann et al., 2002; Mitchison et al., 1998; Mitchison et al., 2004; Vesa et al., 1995). The human cDNA encoding PPT1 consists of a 918 base pair open reading frame flanked by a short 14 base pair 5'-untranslated region and a 1388bp 3'-untranslated region (Camp et al., 1994; Hofmann and Peltonen, 2001). In the 306 amino acid residues of the human protein, the catalytic triad, consisting of serine, aspartine, and histine, at base pairs 115, 233, and 289, respectively, is necessary and sufficient for enzymatic activity (Calero et al., 2003; Schriner et al., 1996). Two isoforms of human PPT1 exist as monomers with molecular weights of either 37kDa or 35kDa, depending on glycosylation. Functionally, PPT1 is a soluble lysosomal hydrolase that cleaves fatty acid side chains from lipid-modified proteins. More specifically, PPT1 acts at the thioesterase cleavage site of membrane bound, palmitoylated proteins once targeted for degradation by the lysosome. The optimum pH for PPT1 is quite broad and depends upon the substrate. PPT1 is ubiquitously expressed throughout the CNS and viscera with the highest levels present in brain and testes. Within the CNS, *in situ* hybridization experiments demonstrated that PPT1 expression is both developmentally and spatially regulated (Haltia et

al., 1973a). High levels of enzyme are present in the cerebral cortex, CA1-CA3 of the hippocampus, dentrate gyrus, and the hypothalamus. Not surprisingly, these regions are the ones most severely affected by disease pathogenesis in INCL. It is hypothesized that without the removal of fatty acid residues from palmitoylated proteins, small peptides become resistant to degradation and form large aggregates, a process similar to that found in Prion and Alzheimer's Diseases.

Infantile neuronal ceroid lipofuscinosis is a debilitating, neurologic disease with a complex set of psychomotor dysfunctions due to widespread neurodegeneration. Besides supportive care for patients, there is currently no therapy or cure for INCL. Further work needs to be done to increase our understanding of disease progression in INCL in order to identify appropriate targets for therapeutic intervention.

PPT1-deficient mouse

Recently, a mouse model of INCL, the PPT1-deficient (PPT1-/-) mouse, was created by disrupting the PPT1 gene (Gupta et al., 2001). A neomycin resistance cassette was introduced into exon 9 of the murine PPT1 gene introducing a premature stop codon in the PPT1 protein. Immunoblot analysis coupled with enzymatic assays demonstrated the absence of both PPT1 protein and activity, respectively, making a functionally null mutant. The PPT1 mutation was subsequently backcrossed onto the C57Bl/6 brain for 10 generations to develop a congenic model of INCL (Griffey et al., 2005).

The phenotype of PPT1-/- mice mirrors the clinical course of INCL. PPT1-/- mice have a decreased life span compared to littermate controls where 50% of mice die by 7 months of age and 100% mice are dead by 10 months (Bible et al., 2004; Griffey et al., 2004; Gupta et al., 2001). Initial studies were performed to characterize the pathology and behavioral deficits at 7 months, an end stage of disease. These studies demonstrated that the mice develop similar cognitive, motor, visual, and physiological deficits as patients with INCL. Initial characterization studies described gait abnormalities in PPT1-/- mice at 4-5 mos. of age, which progressed to hind limb paralysis by 7 mos. Seizure activity, largely myoclonic jerks, was observable at an end stage of disease. EEGs of 7-month PPT1-/- mice demonstrated an abnormal background (interictal) pattern of activity in addition to seizures (Griffey et al., 2006). Electroretinograms (ERGs), a surrogate test for visual function, were abnormal as early as 2-3 mos. and worsened with age, demonstrating retinal deficits within the PPT1-/- mice. Taken together, these data demonstrate that PPT1-/- mice show similar functional deficits as those observed in patients with INCL (Griffey et al., 2005).

In addition to functional changes, the underlying pathology in the PPT1-/- mouse is similar to that seen in affected patients at a terminal stage of disease (Bible et al., 2004; Griffey et al., 2004; Gupta et al., 2001). Overall, brains of PPT1-/- mice were significantly smaller than normal littermates. Differential atrophy of various brain regions was observed with cortical areas most severely affected. On a cellular level, widespread accumulation of autofluorescent material, specifically GRODs, was observed in PPT1-/- mice There is variation in

the temporal and spatial accumulation of GRODs, but by 7 months the entire brain was grossly affected (Galvin et al., 2008). Widespread neurodegeneration was observed throughout the neuraxis. In addition to changes observed in the neuronal population of PPT1-/- brains, abnormalities in the glia were also described. Astrocyte reactivity and microglial activation was remarkable by 7 months of age (Bible et al., 2004).

Although INCL is considered primarily a neurodegenerative disease, the accumulation of GRODs is present in systemic tissues of the mouse, such as liver, kidney, and heart (Galvin et al., 2008). Contrary to other LSDs, the clinical consequences of systemic accumulation of GRODs appear to be mild. However, there are significant cardiac changes such as left ventricular hypertrophy and dilation of the ascending aorta. These changes are consistent with the visceral symptoms observed in children with INCL.

Taken together, the PPT1-/- mouse is an authentic murine model of INCL. Given the behavioral and physiological abnormalities observed, disease progression in the PPT1-/- mice mirrors that of the human course of disease. Similarly, the cellular pathology in the PPT1-/- mice at an end stage of disease is similar to the pathology described at autopsy in patients with INCL.

Goals of thesis

Given the similarities between the murine model and human form of INCL, it is possible to further investigate the cellular pathology and functional deficits in the PPT1-/- mice to gain insights into the course of human disease. The goals of

this thesis were to utilize the PPT1-/- mouse to obtain a better understanding of the disease progression associated with INCL and ultimately, develop novel therapies for the treatment of this disorder.

Thus, the first aim of this thesis was to investigate the temporal and spatial progression of CNS disease in the congenic PPT1-/- mouse. Based on the findings at autopsy in INCL patients as well as the preliminary data from the PPT1-/- mouse, we hypothesized that the progression of disease in the CNS involves both the neuronal and glial populations throughout the neuraxis. We hypothesized that the cellular pathology would correlate both spatially and temporally with the functional changes associated with INCL. Thus, characterization studies need to include not only the forebrain of PPT1-/- mice but also the hindbrain, where movement centers are located. Furthermore, we sought to evaluate the time course of functional deficits in the PPT1-/- mouse, specifically in regards to physiology (seizure activity) and behavior (motor deficits).

Based on the findings from our characterization studies (outlined in Chapter 2), we identified astrocyte activation, as defined by GFAP upregulation, as an early and prominent feature of this disease. More specifically, our studies demonstrated that astrocyte activation is the first pathological change observed in the PPT1-/- brains, prior to any signs of neurodegeneration or functional deficits. Therefore, the second aim of this thesis was to investigate the role of astrocyte activation in the disease progression of INCL.

Chapter Two

Characterization of the forebrain & hindbrain pathology in the PPT1-/- mouse, a mouse model of INCL

This chapter is adapted from the following manuscripts:

Macauley SL, Wozniak D, Kielar C, Tang Y, Cooper JD, and Sands M. Cerebellar pathology and motor deficits in the palmitoyl protein thioesterase 1 deficient mouse. *Exp. Neurol*. 2009 May; 217(1):124-35.

Kielar C., Maddox L, Bible E, Pontikis CC, **Macauley SL**, Griffey MA, Wong M, Sands MS, and Cooper JC. Neuron loss occurs in the thalamus before the cortex in a mouse model of infantile neuronal ceroid lipofuscinosis. *Neurobiol Dis.* 2007 Jan; 25(1):150-62.

Introduction

Infantile neuronal ceroid lipofuscinoses (INCLs), or Batten Disease, is an inherited neurodegenerative lysosomal storage disorder affecting the central nervous system (CNS) during infancy or childhood (Bennett and Hofmann, 1999; Goebel and Wisniewski, 2004; Hofmann and Peltonen, 2001). INCL is the result of mutations in the *CLN1* gene leading to a deficiency in the lysosomal enzyme, palmitoyl protein thioesterase 1 (PPT1; (Das et al., 1998; Hofmann et al., 2002; Mitchison et al., 1998; Mitchison et al., 2004; Vesa et al., 1995). Hallmark pathological changes in the CNS include accumulation of autofluorescent material, neuronal loss, cortical thinning, and brain atrophy, which ultimately lead to cognitive deficits, motor dysfunction, seizure activity, and blindness (Hofmann et al., 1999; Hofmann and Peltonen, 2001; Santavuori et al., 1974; Vesa et al., 1995) (Haltia et al., 1973a; Haltia et al., 1973b; Haltia et al., 1995; Hofmann and Peltonen, 2001; Vanhanen et al., 1997). The neurodegeneration associated with INCL in humans is well documented; however, it remains unclear how the cellular pathology, in either neurons or glia, within the CNS contributes to physiological deficits and behavioral impairment. Further investigation into the specific cellular pathology of neurons and astrocytes is necessary to better understand INCL and develop effective therapies for this disorder.

Initial characterization studies

A mouse model of PPT1-deficiency was created by a targeted disruption in the *CLN1* gene (Gupta et al., 2001). The initial characterization was

performed at an end stage of disease and demonstrated that the PPT1-deficient mouse (PPT1-/-) shares many of the histological and clinical features of INCL (Bible et al., 2004; Griffey et al., 2004; Griffey et al., 2005; Kielar et al., 2007). Although mice develop normally from birth, premature death occurs by 8.5-9 months. Phenotypically, these mice suffer from blindness (Griffey et al., 2005), seizures (Griffey et al., 2006; Kielar et al., 2007), cognitive deficits, and motor dysfunction (Griffey et al., 2004; Griffey et al., 2006) at the end stage of disease. These behavioral deficits are mirrored in children affected by INCL.

Upon gross examination of the PPT1-/- brains, Bible et al. (2004) described an overall brain atrophy at 7 mos. of age. The affected mice have a 20-25% decrease in brain weight (Bible et al., 2004; Griffey et al., 2004) compared to wildtype (WT) controls. Although an overall decrease in brain mass occurs in the PPT1-/- mouse, the extent to which certain areas are affected differs from region to region. For example, a significant decrease in brain mass was present in the cortex, thalamus, striatum, and hippocampus of PPT1-/- mice; areas similarly affected in patients with INCL. The greatest volumetric change was observed in the thalamus (i.e. 46% decrease), while the cortex and striatum suffered a 35% and 30% reduction, respectively. Furthermore, decreases in cortical thickness varied based on the region of cortex investigated. Although decreases in cortical thickness were apparent in numerous cortical areas (i.e. motor, visual, somatosensory, and entorhinal cortex), the visual cortex and somatosensory cortex were the most severely affected.

Similar to patients with INCL, the CNS atrophy described is the result of neuronal loss throughout the neuraxis of PPT1-/- brains. There is a significant decrease in neuron number in both the cortex and hippocampus, most notably within the interneuron population. Concurrent with the neuronal loss, there is an increase in autofluorescent accumulation in the cortex, striatum, and cerebellum of PPT1-/- brains. Although autofluorescent accumulation is a hallmark of INCL, there is no causal link between neuronal hypertrophy due to autofluorescent accumulation and neuronal death in the PPT1-/- mouse.

Concurrent with the characterization of the neuronal pathology, initial studies investigated glial reactivity as well. In a 7 mo. PPT1-/- mouse, there is a significant increase in both astrocyte activation (i.e. GFAP upregulation) and microglial reactivity (i.e. F4/80 upregulation) in the cortex, hippocampus, and striatum. This demonstrates that neuroinflammation plays a role in the pathogenesis of INCL, a phenomenon similarly described in human patients.

Initial characterization studies demonstrated that the phenotype of the PPT1-/- mouse mirrored the behavioral deficits and cellular pathology described in INCL patients at the end stage of disease. Based on these findings, we believe the PPT1-/- mouse is a valuable tool for investigating the disease pathogenesis of INCL. Although the pathology of INCL patients at autopsy is well described, it remains unclear how a genetic mutation, such as a *CLN1* mutation, can evolve into such a debilitating, neurologic disease. Thus, studies investigating the temporal-spatial progression of cellular pathology and behavioral deficits should be employed to gain a better understanding of INCL.

Aims of temporo-spatial characterization studies

The research aims seeking to further characterize the PPT1-/- mice were two fold. First, our primary goal in these studies was to investigate the disease progression in the cerebellum. Although profound motor deficits and cerebellar pathology is described in patients with INCL, the initial characterization studies in the PPT1-/- mouse did little to investigate the underlying pathology in the hindbrain. Apart from a brief description of gait abnormalities and qualitative reports of Purkinje cell loss in the PPT1-/- mouse, no additional investigation of cerebellar pathology or motor deficits was performed. In addition to the autopsy information from INCL patients, gene therapy studies in PPT1-/- mice demonstrated that the most efficacious gene therapy strategy for the treatment of INCL occurred when viral vectors were targeted to the cerebellum in combination with the forebrain. Again, these data suggests the disease is not restricted to the forebrain and further investigation of cerebellar pathology is warranted. Thus, our primary goal was to perform a time course investigating the cellular pathology and functional deficits associated with the cerebellar disease. In this study, we determined the temporal changes in cellular pathology in both neurons and glia. Concurrently, we quantified the progression of motor dysfunction. Taken together, these studies provide insight into the disease pathogenesis of INCL cerebellum and its relationship to motor function (Macauley et al., 2009).

The second aim of our characterization studies focused on expanding the initial descriptions of pathology and behavioral deficits localized to the forebrain.

This study was carried out in collaboration with Catherine Kielar and other members of Dr. Jonathan Cooper's laboratory at Kings College, London (Kielar et al., 2007). Although the descriptions of forebrain pathology at an end stage of disease in the PPT1-/- mice were thorough, a temporal investigation of pathology and functional deficits would provide insight into the evolution of disease in INCL. A summary of results from this study is also included in Chapter 2.

Methods

PPT1-/- Mice

PPT1-/- mice were created as previously described on a mixed background (Gupta et al., 2001). Subsequently, the mice were bred to C57Bl/6 mice for 10 generations to produce a congenic strain (Griffey et al., 2004). Wildtype (+/+) or PPT1- deficient (-/-) mice were generated by either heterozygous (+/-) or homozygous (-/-; +/+) matings at Washington University School of Medicine by M.S.S. Mouse genotype was determined by a PCR-based assay. Both male and female PPT1-/- mice and normal littermates (+/+) were used in this study. Animals were housed under a 12:12 hour light:dark cycle and were provided food and water *ad libitum*. All procedures were carried out under an approved IACUC protocol from Washington University School of Medicine.

Cerebellar Weights

Seven month PPT1-/- (n=6) and wildtype littermates (n=5) were sacrificed via CO_2 asphyxiation and the brains harvested by a researcher blinded to genotype and age. A sharp knife was inserted coronally into the transverse sinus

to separate the cerebellum from the forebrain. Similarly, a coronal cut was made immediately posterior to the cerebellum, separating the cerebellum from the medulla and spinal cord. Care was taken to ensure that the cut was flush with the back of the cerebellum. Each cerebellum was weighed using an analytical balance and group differences in weights were analyzed using an independent groups *t* test.

Quantification of Purkinje cells

Congenic PPT1-/- mice (n=3-6 per time point) and wildtype littermates (n=3-4 per time point) at 1, 3, 5, 6, and 7 mo. of age were used in this study. Briefly, mice were sacrificed via CO_2 asphyxiation, brains removed and post-fixed for 48 hours in 4% paraformaldehyde in phosphate buffered saline (PBS). Cerebella were separated from the forebrain and bisected in the sagittal plane about 1 mm off midline. The larger piece was embedded sagittally in paraffin and sectioned at 5μm through the midline. Sections were stained with hematoxylin & eosin (H&E). Counts of surviving Purkinje cells were made from midsagittal sections through the vermis for each lobe. Purkinje cells were counted if they possessed a well-defined cytoplasm and nucleus with the presence of a distinct nucleolus. Purkinje cells undergoing degeneration possessed a shrunken, pyknotic appearance with irregular margins and were not counted. The number of healthy Purkinje cells was recorded for each lobule (I through X) of the PPT1-/- and wild type cerebellum. For statistical analysis, data from wild type mice at the various ages counted (1-7 mos.) were collapsed and treated as a single wild type group. Previous work as (Macauley et al., 2008b)

well as data from this study demonstrated that Purkinje cell counts do not differ significantly over this age range. The Purkinje cell count data were analyzed by a repeated measures ANOVA model containing one between-subjects variable (groups) and one within-subjects variable (lobes), and subsequent pairwise comparisons. Bonferroni correction was used to maintain alpha levels at 0.05 when multiple comparisons were conducted.

Quantification of the Granular cell layer

To examine granule cell survival within lobule IV/V of the cerebellum, we used *StereoInvestigator* software (MicroBrightField Bioscience, Williston, VT) to obtain unbiased optical fractionator estimates of granule cell number from H&E stained sections. Cells were sampled using a series of counting frames distributed over a grid superimposed onto the section, with a random starting section chosen, followed by every fourth section thereafter. The sizes of the 'sampling grid' and of the 'dissector frame' used in this study were 250x160μm^2 and 20x20μm^2 respectively. Only clearly identifiable cells that fell within the dissector frame were counted, using a x100 oil objective.

The statistical significance of differences between genotypes of all quantitative data was assessed using a one-way ANOVA (SPSS 11.5 software, SPSS Inc, Chicago, IL), with statistical significance considered at $p \leq 0.05$. The mean coefficient of error (CE) for all individual optical fractionator and Cavalieri estimates was calculated according to the method of Gundersen and Jensen (1987) and was less than 0.08 in all analyses.

Immunohistochemistry for neuronal, astrocytic, & microglial markers

PPT1-deficient mice and wildtype littermates were sacrificed via CO_2 aphyxiation for immunohistochemistry at 1, 3, 5, 6 and 7 months of age. The brains were removed, fixed in 4% paraformaldehyde in phosphate buffer, and cryoprotected with 30% sucrose in tris-buffered saline (TBS). Brains were sectioned in the sagittal plane through the vermis (20µm) using a freezing cryostat. Adjacent, free floating sections were stained with the following antibodies: rabbit anti-glial fibrilllary associated protein (GFAP; 1:200 ImmunoStar, Inc.), rabbit anti-S100ß (1:200; Abcam), rat anti-F4/80 (1:100; Serotec), mouse anti-calbindin (1:1000; Sigma), guinea pig anti-GLAST (1:2000; Chemicon) rabbit anti-GLT1 (1:100; Santa Cruz), and rabbit anti-glutamine synthetase (GS; 1:200 Santa Cruz). Briefly, sections were washed in tris-buffered saline (TBS), incubated in 1% H_2O_2 (Sigma) to quench endogenous peroxidase activity, and rinsed thoroughly in TBS. The tissue was blocked for 1 hour in 10% normal goat serum (NGS; Sigma), 0.25% Triton X-100 in TBS. Sections were incubated overnight at 4˚C in primary antibodies in 5% NGS, 0.2% Triton X-100 in TBS. The following day the sections were rinsed in TBS and incubated in secondary antibodies (1:200; Vector Labs) in 10% NGS, 0.1% Triton X-100 in TBS for 75 minutes. The tissue was rinsed in TBS and then incubated in a peroxidase conjugated avidin-biotin complex (1:200; Vectastain Elite ABC kit from Vector Labs) for 1 hour at RT. Antibody immunoreactivity was visualized with 3'-3' diaminobenzidine and H_2O_2 (DAB kit; Vector Labs) in TBS. Sections were dehydrated and coverslipped.

DeOlmos Cupric Silver Staining

Six, 7 and 8 mo. old PPT1-/- mice (n=2 per time point) and wildtype littermates (n=1-2 per time point) were deeply anesthetized with euthasol and transcardially perfused with 4% paraformaldehyde in sodium cacodylate buffer. The brains were removed and post-fixed for 48 hours. Each brain was embedded in a gelatin-based matrix (Switzer, 2000) and serial coronal sections (35 μm) were cut on a freezing microtome by Neuroscience Associates (Knoxville, TN). Neuronal degeneration was visualized by staining with a modified cupric silver method of DeOlmos (DeOlmos & Ingram, 1972; Switzer, 2000). A matrix of PPT1-/- and WT brains at identical levels in the coronal plane were stained simultaneously. Every sixth section (210 μm interval) was stained with the silver method and adjacent sections stained with H&E.

Luxol Fast Blue & PAS Stain

Seven-month-old PPT1-/- and wildtype littermates were sacrificed and sectioned at 20μm as described above. Every 12th section throughout the vermis was stained with luxol fast blue and Periodic-acid Schiff stain.

TUNEL Staining

TUNEL staining was performed on sagittal sections throughout the cerebellum of PPT1-/- mice and wildtype littermates at 1, 3, 5, 6, and 7 months of age using the Apoptag Apoptosis Detection Kit (Milipore Corp) per the manufacturers instructions. Briefly, sections were warmed to room temperature (RT) and treated with proteinase K (20μg/ml) for 15 minutes at RT. Immediately following, endogenous peroxide was quenched with 1% hydrogen peroxide in

methanol. After sections were incubated in equilibration buffer for 1 minute, working strength terminal deoxynucleotidyl transferase (TdT) enzyme was added to the tissue and incubated in a humidified chamber at 37˚C. After a 60-minute incubation, the reaction was stopped by the addition of working strength stop/wash buffer for 10 minutes. An anti-digoxigenin conjugate was placed on each specimen for 30 minutes and the reaction visualized with DAB substate. The tissue was counterstained with nuclear fast red.

Rotarod Testing

Congenic PPT1-/- mice (n=11-14 mice per group) and wildtype littermates (n=11-14 mice per group) were tested on the constant speed rotarod (2.5 rpms) at 1, 3, 5, 6, and 7 months of age. Latency to fall served as the dependent variable and trials lasted a maximum of 60 s. At each age, mice received three test sessions where each session included a pretest trial on a stationary rod, followed by two test trials on the constant speed rotarod. To combat the effects of training, only the last test session was used in computing statistical differences with the previous two trials treated as training. A repeated measures ANOVA, including one between-subjects variable (genotype) and one within-subjects variable (age), was the main analysis conducted on monthly performance. Additional analyses (independent groups and paired *t* test, respectively) were performed on 1- and 7- month time points due to smaller sample sizes at these ages.

Seizure Activity

C57Bl/6 controls (n = 4) and PPT1−/− mice at 6 (n = 4), 6.5 (n = 6), 7 (n =

6) and 7.5 (n = 7) months of age were monitored for seizure activity and interictal EEG activity using simultaneous video and EEG recordings (Griffey et al., 2006). Briefly, each mouse was implanted with four epidural screw electrodes two days prior to monitoring. Each monitoring session consisted of a continuous 48-hour period. During each session, mouse behavior was captured via video monitoring while EEGs were recorded using a computer interface and *AxoScope* software (Molecular Devices, Sunnyvale, CA). Seizures were identified using both behavioral and EEG recordings. The number of animals with seizures, the number of seizures per animal, and seizure duration will be counted for each animal during each monitoring period. Statistical analysis was performed using Kruskal–Wallis non-parametric ANOVA. Additionally, the background EEG was scored by a board certified neurologist blinded to genotype. For analysis of the interictal EEG back- ground, one-minute segments obtained from every 4 h of the 48 h EEG record were randomly selected and graded with a previously described scale (Griffey et al., 2006) comprising: Grade 1 (normal)—normal background theta rhythm with no spikes, Grade 2 (mildly abnormal)—mostly normal background with some epileptiform spikes, Grade 3 (moderately abnormal)—mostly abnormal background with frequent epileptiform spikes, Grade 4 (severely abnormal)—burst-suppression pattern. A mean interictal EEG grade was calculated for each genotype, and statistical comparisons were made using ANOVA with Tukey–Kramer multiple comparison post hoc test.

Results from Cerebellar Study

Cerebellar Weights

Upon gross inspection at 7 mo. of age, the PPT1-/- cerebella appeared smaller than aged matched wildtype littermates (Figure 1A). The mean weight of PPT1-/- cerebella was 0.076g (SEM±0.0054) compared to 0.112g

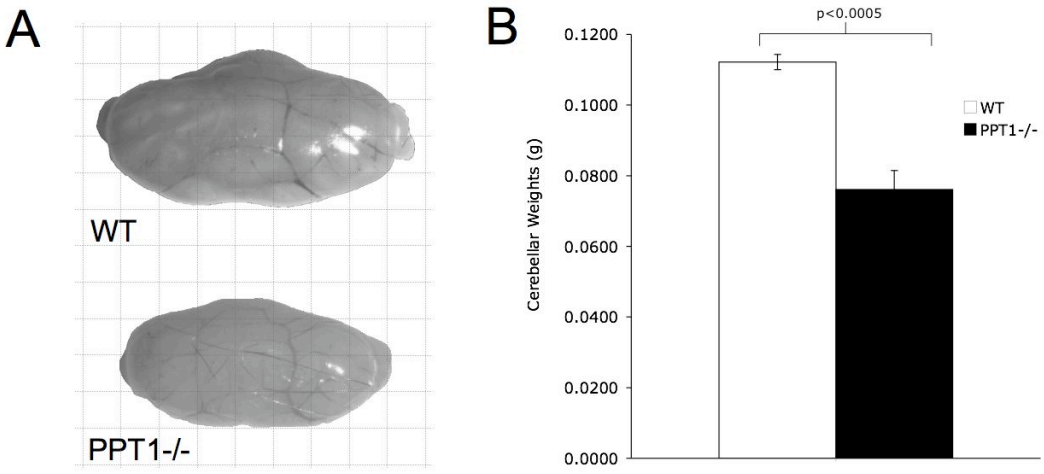

Figure 1. An overall atrophy is observed in the PPT1-/- cerebellum at 7 mo. of age. (A) Representative images of PPT1-/- and wildtype cerebella. Notice the size differential between the mutant and wildtype control. (B) Quantification of the cerebellar weights in PPT1-/- (n=5) and wildtype mice (n=5) revealed a statistically significant decrease in cerebellar mass in PPT1-/- mice compared to wildtypes ($p<0.002$).

(SEM±0.0022) for normal mice. At an end stage of disease (7 mo.), analysis of cerebellar weights (Figure 1B) demonstrated a significant loss of mass in the PPT1-/- mice, [$t(9) = 5.77$, $p < 0.0005$].

deOlmos Cupric Silver Staining

Silver staining was performed on 6, 7, and 8 mo. PPT1-/- mice and wildtype controls (Figure 2). Representative images of the anterior lobes of the cerebellum in the coronal plane are shown in Figure 2. As PPT1-/- mice aged,

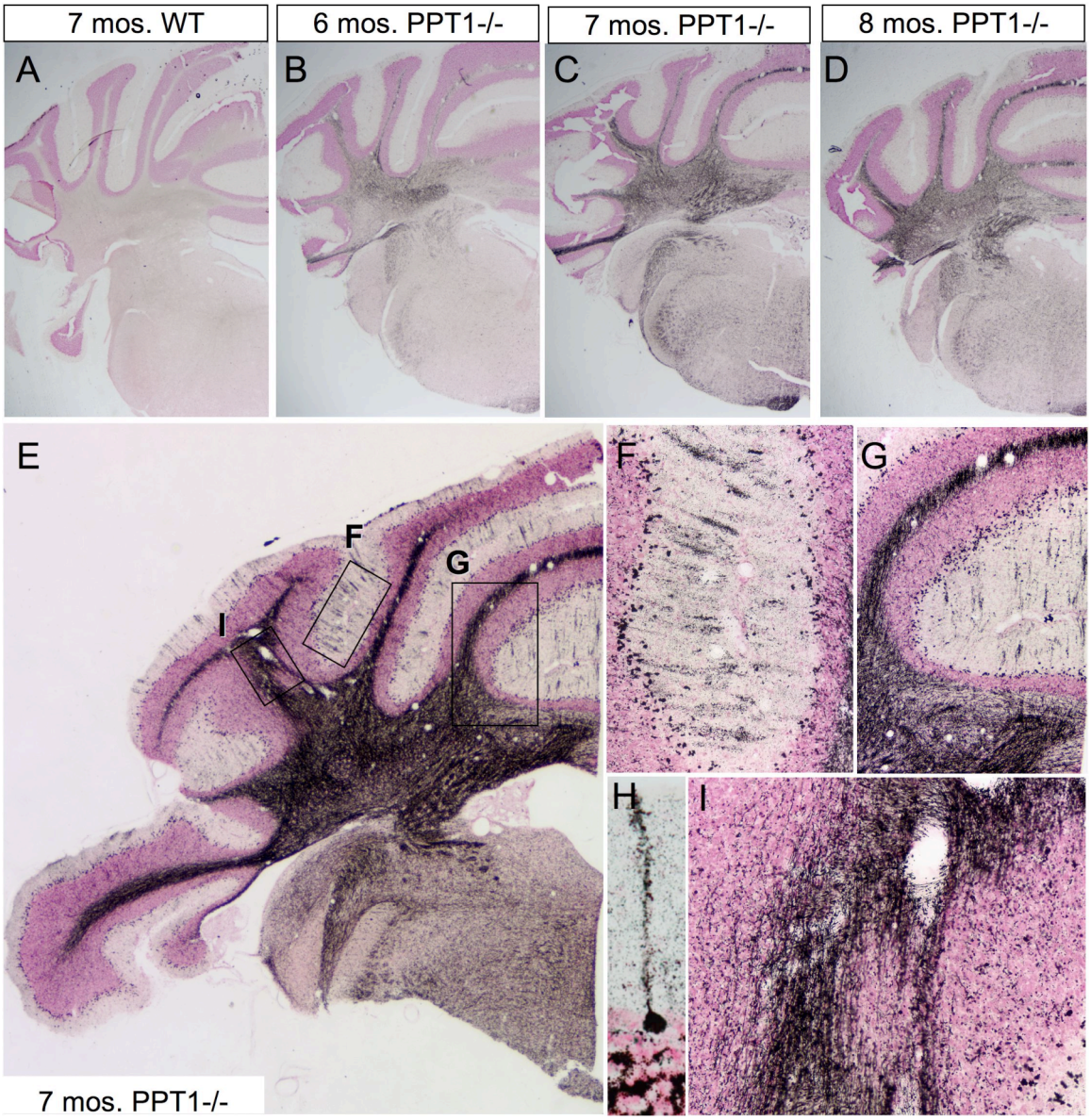

Figure 2. DeOlmos cupric silver degeneration staining in PPT1-/- mice. (A-D) Representative coronal images of silver staining in the anterior cerebellum of 7 mo. WT (A), 6 mo. PPT1-/- (B), 7 mo. PPT1-/- (C), and 8 mo. PPT1-/- mice (D). Notice the overall increase in silver staining as the PPT1-/- mice age, most notably within the cerebellar white matter. (E) Higher magnification image of the 7 mo. PPT1-/- cerebellum. In addition to the cerebellar white matter, silver stained parasagittal bands, or blackened stripes, are visualized in the molecular layer in the cerebellar cortex. Locator boxes identify the areas magnified in subsequent panels. (F & G) High magnification of parasagittal banding found in an individual folia of PPT1-/- mice at 7 mo. The banding seen in the molecular layer is staining of the dendritic arbors of diseased Purkinje cells. Blackened debris litters the Purkinje cell layer, most likely due to dying Purkinje cells. (H) High magnification of a degenerating Purkinje cell, with a blackened soma and dendritic arbor. (I) High magnification image of the cerebellar white matter tracts contains degenerating efferent and afferent projections to the cerebellar cortex. Degenerating axons represent the sole output of the PPT1-/- cerebellum.

there was a progressive increase in neurodegeneration as visualized by silver staining (Figure 2B, C, D; respectively) when compared to normal (Figure 2A). When the CNS undergoes neurodegeneration, neurons bind silver causing individual cells and processes to appear 'blackened' with this staining method. Thus, at low magnification, diffuse silver staining was appreciable in the cerebellum at 6 mo. of age, most notably in the white matter tracts throughout the vermis and lateral hemispheres. As the mice aged, the intensity and distribution of staining increased to include 'patches' throughout the Purkinje cell and molecular cell layers. At 8 mo. of age, widespread neurodegeneration was evident in the anterior lobes of the cerebellum, although the staining was of equal or lower intensity.

Higher magnification images of a 7 mo. old PPT1-/- brain show parasagittal bands of degenerating Purkinje cells in the cerebellar cortex of the vermis and lateral hemispheres (Figure 2E, F). The molecular layer was littered with fragmented dendritic arbors associated with dying Purkinje cell neurons (Figure 2H). In addition to their dendritic arbors, the cerebellar white matter tracts, composed of afferant and efferent fibers, displayed an intense silver staining (Figure 2G, I).

Purkinje cell degeneration

The Purkinje cell layer in wildtype mice consists of a one-cell-thick monolayer of contiguous Purkinje neurons nestled between the molecular and granular cell layers of the cerebellum (Figure 3B). In contrast, there was a clear disruption in the Purkinje cell layer in PPT1-/- mice (Figure 3B), immediately

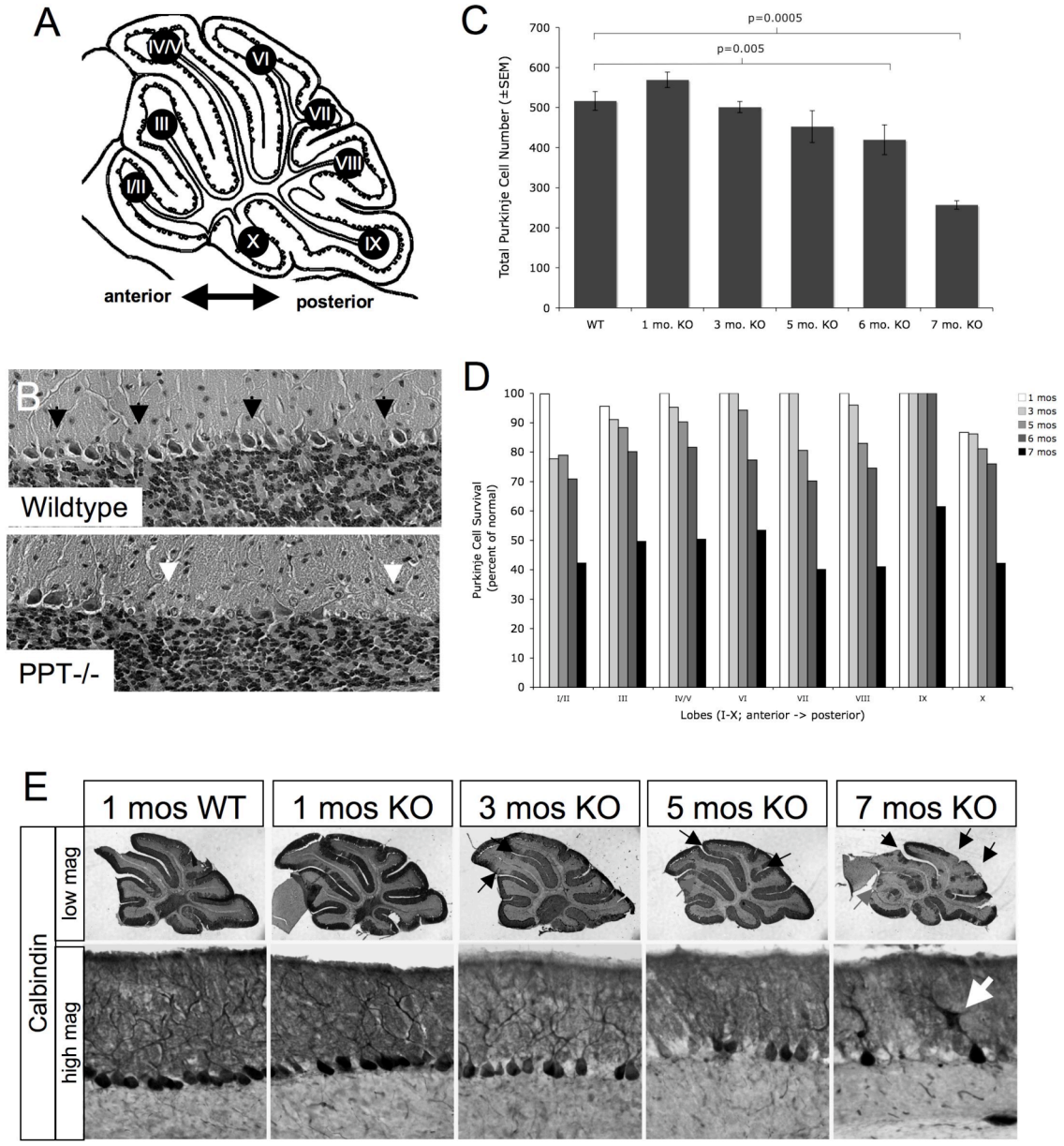

Figure 3. **Purkinje cell loss in the PPT1-/- cerebellum.** (A) Schematic representation of lobes I-X of the cerebellar vermis. (B) H&E stained cerebella from PPT1-/- and wildtype mice. Black arrows indicate a contiguous Purkinje cell monolayer present in WT cerebellum. In the PPT1-/- cerebellum, white arrows indicate patches of missing Purkinje neurons. (C) Graphical representation of Purkinje cell survival (total cell number±SEM) in PPT1-/- cerebella at 1, 3, 5, 6, and 7 mo. of age. (D) Purkinje cell survival by lobe (as a percent of normal) in 1, 3, 5, 6, and 7 mo. PPT1-/- mice. (E) Calbindin staining in the PPT1-/- cerebellum. At low magnification, there were comparable levels of staining in a 1 mo. WT and PPT1-/- cerebellum. By 3 mo. of age, loss of calbindin staining appeared in patches throughout the anterior cerebellum (arrows). By 7 mo. of age, nearly half of the cerebellum lacked calbindin immunoreactivity. At high magnification, the molecular and Purkinje cell layers of 1 mo. WT and PPT1-/- cerebella appeared normal with darkly stained Purkinje cell bodies and dendritic arbors. As the mice age, there was a decrease in the intensity of calbindin staining, a denudation of the Purkinje cell layer and pruning of the dendritic arbors. The white arrow identifies a swollen dendrite. Comparable levels of calbindin staining were observed in 1, 3, 5, 6, and 7 mo. wildtype mice.

illustrating cell loss at 7 mo. of age throughout both the anterior-posterior as well as the medial-lateral axis of the cerebellum. Additionally, remaining Purkinje cells appeared unhealthy, presenting with a shrunken cytoplasm and a foamy appearance characteristic of lysosomal distension. To further investigate this apparent neuronal loss, Purkinje cell counts were performed throughout the vermis on each lobe (I-X; Figure 3A) from wildtype and PPT1-/- brains at 1, 3, 5, 6, and 7 mo. of age. At 5 mo. of age, there was a trend towards a decrease in total Purkinje cell number (13% decrease in total number; $p=0.08$). By 6 months of age, there was a statistically significant decrease in total Purkinje cell number ($p=0.005$) and culminated in a 50% reduction in total number at 7 mo. of age ($p<0.0005$; Figure 3C). Regionally, loss of Purkinje cells began at 3 mo. of age in the most anterior lobes. Although there was only a 3% decrease in total Purkinje cell number at 3 mo., there was a 23% decrease in cell number in lobe I/II compared to normal littermates (Figure 3D). By 5 mo., Purkinje cell death increased in posterior lobes. At 6 mo. of age, pairwise comparisons conducted for each lobe showed significant cell loss (beyond Bonferroni correction) in lobes I/II ($p=0.039$), IV/V ($p=0.019$), VI ($p=0.001$), VII ($p=0.018$), and VIII ($p=0.003$), with lobes IX and X spared. All lobes suffer a ≥50% reduction in Purkinje cell number by 7 mo. of age ($p\leq0.001$). No change in Purkinje cell number is observed in PPT1-/- mice at 1 mo. of age.

In addition to quantifying neuronal loss, we investigated the morphology of the remaining neurons as an indicator of their general health. To examine any gross changes seen in Purkinje cell morphology, a time course of PPT1-/- and

wildtype control brains were stained with an antibody against the calcium binding protein, calbindin. At low magnification, calbindin-stained Purkinje cells from lobe IV/V appeared indistinguishable in PPT1-/- brains compared to age-matched normal littermates at 1 mo. of age (Figure 3E). A contiguous layer of calbindin-positive cell bodies occupied the Purkinje cell layer, while the molecular layer was filled with a network of darkly stained dendritic arbors (black arrows). In addition, axonal projections from the Purkinje cell layer were observed transversing the granular cell layer. At 3 mo., gaps in calbindin-positive staining were appreciable at low magnification in the anterior lobes (I-V) of the PPT1-/- cerebellum, consistent with our counts of Purkinje cell number. At higher magnification, there was a decrease in the density of staining within the molecular layer demonstrating a pruning of dendritic arbors of the Purkinje cell neurons. By 5 mo. of age, numerous disruptions in calbindin staining throughout the anterior-posterior axis of the cerebellum were seen at low magnification. At higher magnification, the molecular layer appeared disorganized while the axonal projections through the granular cell layer looked fractured and swollen. By 7 mo. of age, Purkinje cell loss was widespread, with large gaps in staining throughout the cerebellar vermis. In addition, frank cell loss was appreciable in the lateral hemispheres of the cerebellum similar to the vermis (data not shown). On closer inspection, the soma of Purkinje neurons often displayed irregular margins with little to no dendritic arborization observed. Where arbors remained, swollen dendrites in Purkinje cells were observed (Figure 3E; white arrow). In addition to the profound Purkinje cell death that occurs in the PPT1-/-

cerebellum, the remaining Purkinje cells, even at an early time point, appeared unhealthy.

Apoptosis and Assessment of Granular Cell Loss

Although widespread Purkinje cell loss occurs at a variety of ages, the only TUNEL-positive profiles were observed within the granular cell layer on PPT1-/- mice at 7 mo. of age (Figure 4A). To investigate granule cell loss, cell

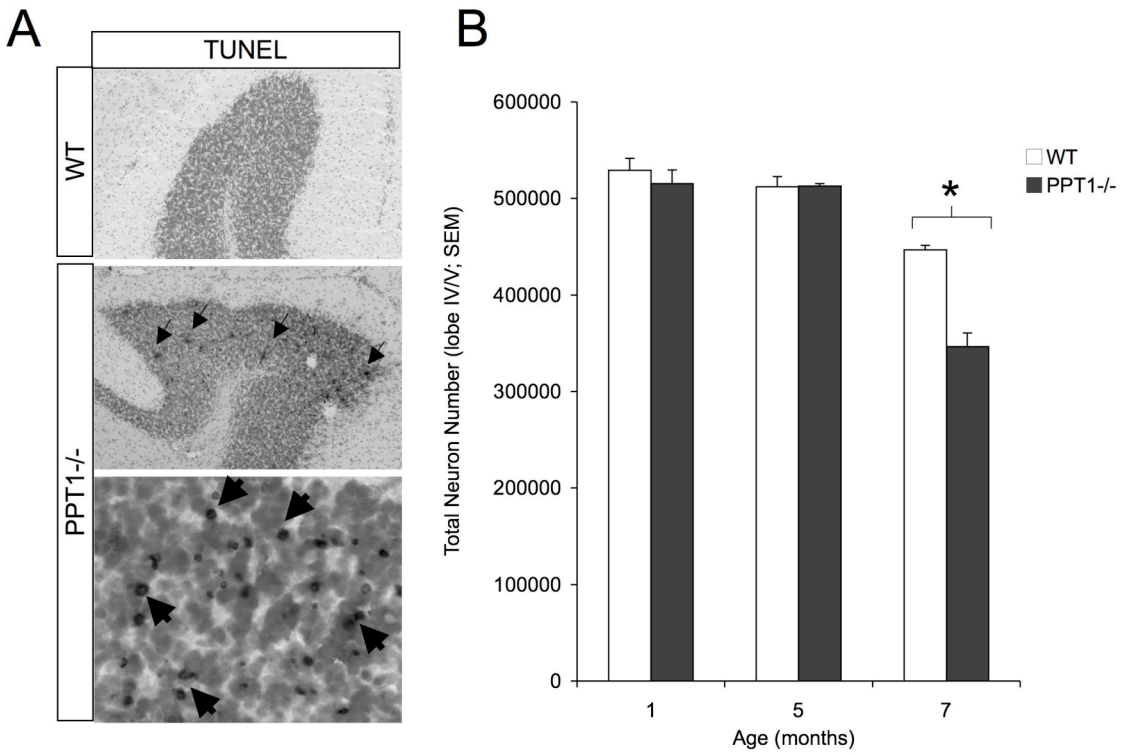

Figure 4. Cell loss in the granular cell layer. (A) TUNEL-positive cells were found in the granular cell layer (GCL) of the 7 mo. PPT1-/- cerebellum. Nuclear fast red staining identified cells within the granular cell layer at low magnification. At high magnification, numerous darkly stained, TUNEL + profiles were observed throughout the GCL (dark staining; arrows). (B) Quantification of the granular cell number demonstrated a statistically significant ($p<0.05$; asterisk) cell loss at 7 mo. of age, with no changes in total cell number evident before this age. No TUNEL positive cells were observed in 1, 3, 5, 6, and 7 mo. wildtype mice.

counts in the granular cell layer were performed throughout the vermis of lobe IV/V in wildtype and PPT1-/- brains at 1, 5 and 7 mo. (Figure 4). At 7 mo. of age,

there was a statistically significant [$F(1,4) = 44.37$, $p = 0.003$] decrease in total number of cells within the granular cell layer in PPT1-/- mice. Total cell number was estimated to be 3.46×10^5 within lobe IV/V of mutant mice compared to 4.47×10^5 in age-matched wildtype controls (Figure 4B). This represents a 23% percent cell loss in the granular cell layer at 7 mo. of age. At earlier time points investigated, there was no decrease in the number of granule cells in lobe IV/V, suggesting this loss of neurons is a later stage phenomenon.

Astrocyte activation

Astrocyte activation, visualized by glial fibrillary associated protein (GFAP) upregulation, began at an early age (Figure 5A). At 1 mo. of age, there was a slight increase in GFAP staining in PPT1-/- mice compared to wildtype controls. By 3 mo., the Bergmann glia (Golgi epithelial cells) displayed a clear increase in GFAP immunoreactivity both at the cell body and within their processes. At low magnification, this staining appeared 'patchy' throughout the A-P axis of the cerebellum. Astrocyte activation continued to increase at 5 mo. of age, and by 7 mo., the entire molecular layer throughout the vermis of lobes I-X was strongly immunoreactive for GFAP. At high magnification, there was an increase in number of GFAP-stained Bergmann glial processes in the molecular layer as well as an apparent hypertrophy of individual glial processes.

Astrocyte Dysfunction

In an effort to quantify astrocyte cell number, S100ß staining, a calcium binding protein largely localized to astrocytes, was performed on cerebella from PPT1-/- and wildtype littermates (Figure 5B). As the PPT1-/- mice aged, there

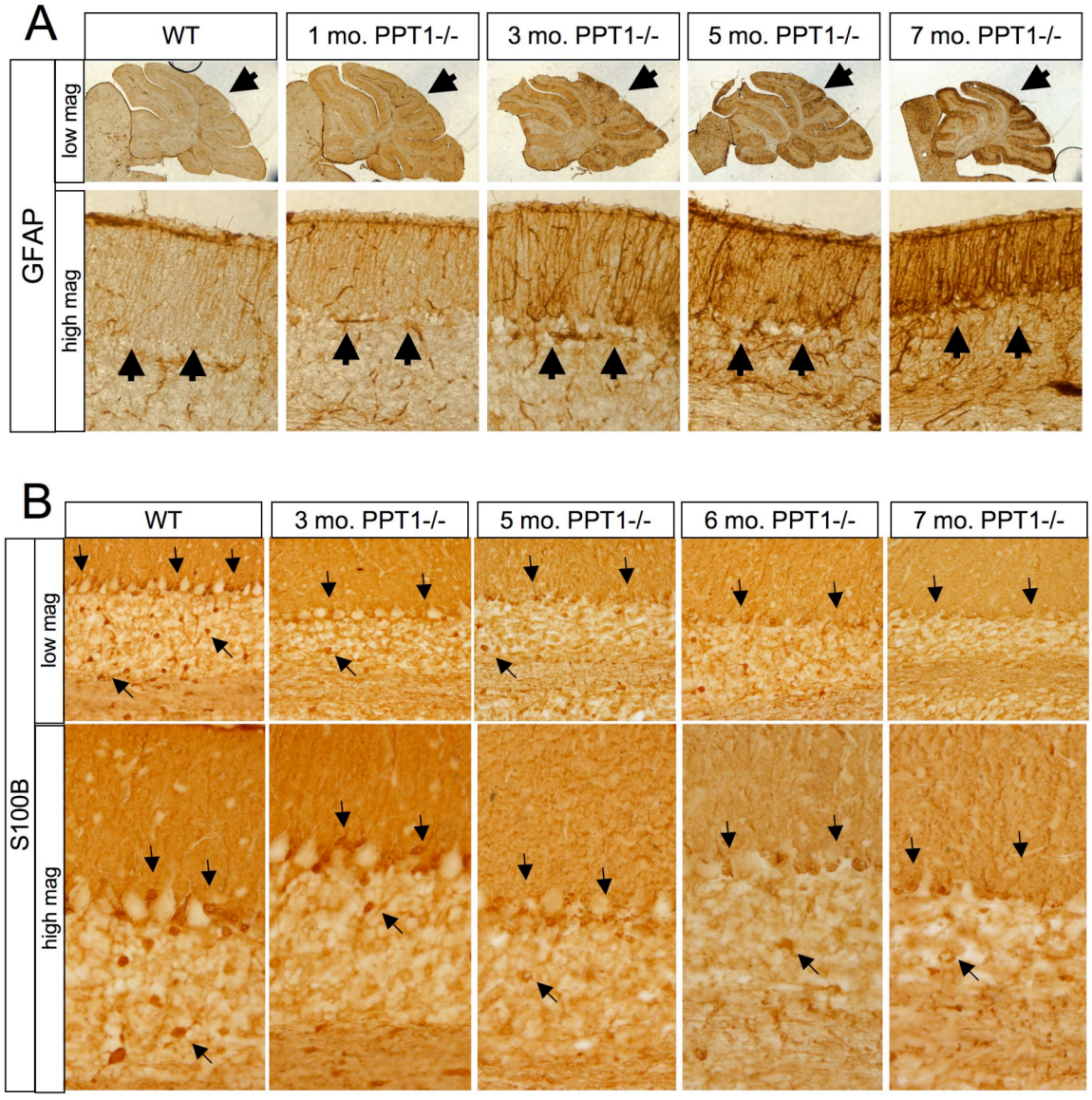

Figure 5. Astrocyte changes in the PPT1-/- cerebellum. (A) GFAP staining was performed on 1, 3, 5, and 7 mo. PPT1-/- cerebella. Astrocyte activation was found in PPT1-/- mice as early as 1 mo. of age, with a diffuse increase in GFAP immunoreactivity. By 3 mo. of age, there was a hypertrophy of astrocytic processes and patches of GFAP upregulation through the PPT1-/- cerebellum (black arrows). This phenomenon continues as the mice age. Comparable levels of GFAP staining were observed in 1, 3, 5, 6, and 7 mo. wildtype mice. (B) Astrocyte dysfunction in the PPT-/- mouse. S100ß staining was performed on 1, 3, 5, 6, and 7 mo. PPT1-/- cerebella. Compared to WT, there was an overall decrease in S100ß by 5 mo. of age (black arrows). Most notably, there was a progressive loss of immunoreactivity in the Bergmann glia and astrocytes of the granular cell layer.

was an overall decrease in S100ß staining throughout the cerebellum. In the wild type control, S100ß-positive cell bodies were mostly localized within the granular and Purkinje cell layers. Diffuse staining of Bergman glial fibers was also apparent within the molecular layer. By 3 mo. of age, the PPT1-/- cerebella showed a decrease in the intensity of S100ß immunoreactive cell bodies, most notably within the granular cell layer. As the mice age, the S100ß -positive Bergman glia, with their cell bodies intermixed with Purkinje neurons in the Purkinje cell layer, demonstrated a loss of immunoreactivity. In addition, there was a diffuse loss of S100ß staining within all layers of the 7 mo. PPT1-/- cerebellum. S100ß -positive cell bodies were absent from both the Purkinje cell and granular cell layers.

Glutamine Synthetase (GS), GLAST, & GLT-1 Immunohistochemistry

To further investigate whether the loss of S100ß immunoreactivity was due to changes in protein expression or due to a loss of astrocytes, we used a second astrocyte marker, glutamine synthetase (GS), to stain 7 mo. old wildtype and PPT1-/- mice (Figure 6). There was a decrease in GS staining in the 7 mo. PPT-/- cerebellum compared to normal controls. Although there was an appreciable loss of neuropil in the PPT1-/- cerebellum at 7 mo., the remaining cells in the granular cell layer stained for GS. Qualitatively, the number of GS-positive cell bodies in the molecular layer seemed less than the wild type control. Importantly, there was a considerable decrease in the number of GS-immunoreactive cell bodies in the Purkinje cell layer, suggestive of a loss of Bergman glia at 7 mo. of age.

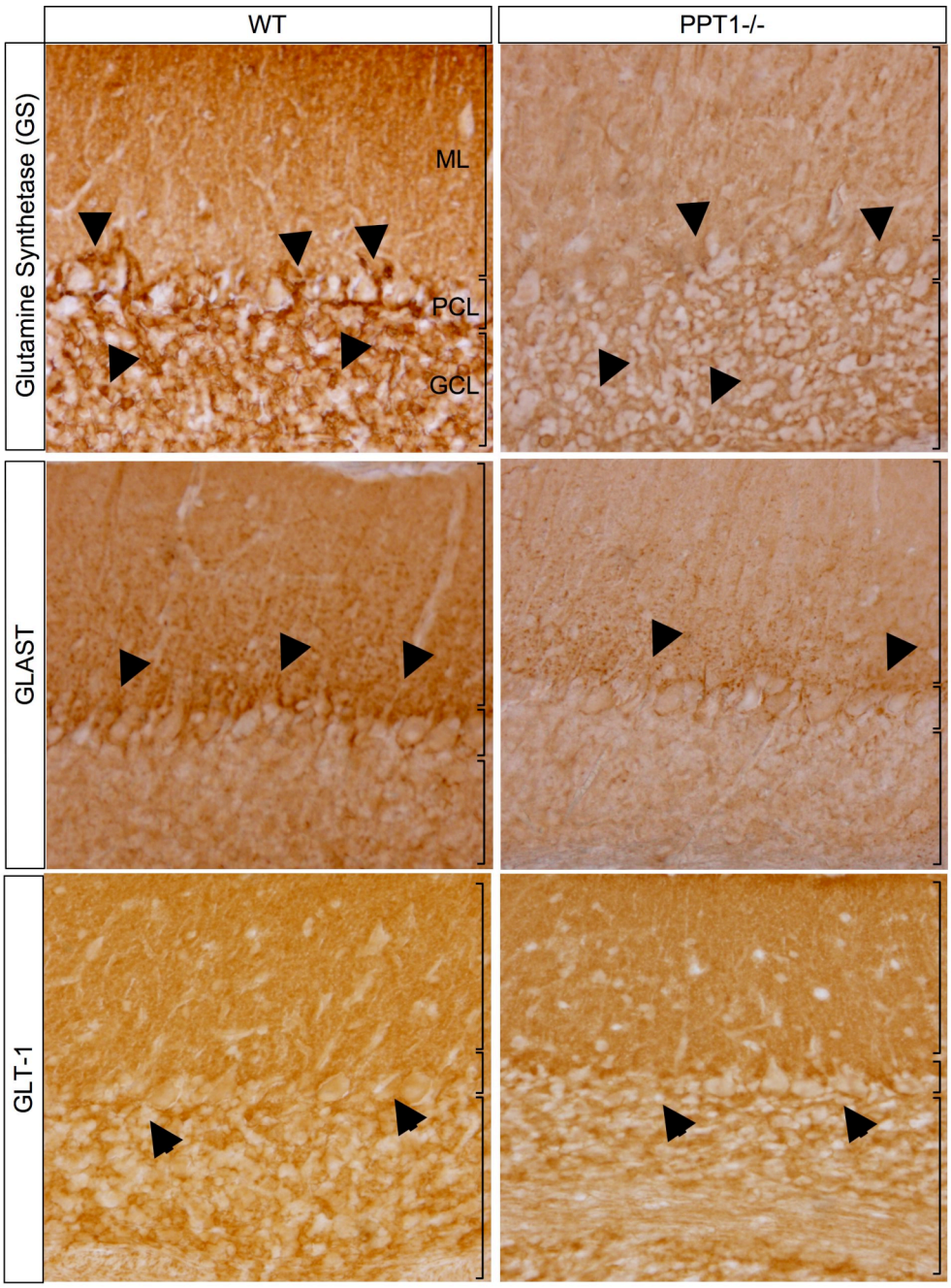

Figure 6. Glutamine synthetase (GS), GLAST, and GLT-1 staining in 7 mos. PPT1-/- and WT mice. An apparent loss of GS staining was observed in the cerebellar cortex of 7 mos. PPT1-/- mice. Most notably, there was a loss of staining within the cell bodies of the Bergmann glia (black arrows). GLAST staining in PPT1-/- mice demonstrated a diffuse, overall reduction in immunoreactivity compared to WT. A decrease in GLAST expression in the Bergmann glia (arrows) and the molecular layer was also apparent. In contrast, GLT-1 staining was comparable in WT and PPT1-/- mice. A notable exception is the intensity of staining in the Purkinje cell layer, which was markedly reduced in the PPT1-/- mice.

Given the number of changes observed in PPT1-/- astrocytes, we performed immunohistochemistry staining for several astrocyte specific glutamate transporters, GLAST and GLT-1, in PPT1-/- and wild type mice (Figure 6). At low magnification, the wild type-Bergman glia were largely immunoreactive for GLAST, with punctate staining present in the Purkinje cell and molecular layers. In contrast, the PPT1-/- cerebellum at 7 mo. of age suffered an overall decrease in GLAST immunoreactivity. At higher magnification, this change in protein expression was most notable in the Bergmann glial processes in the molecular layer, with a near complete loss of staining at 7 mo. of age.

Although GLAST expression was altered in the PPT1-/- mice, GLT-1 staining in the cerebellar folia seemed relatively unchanged when compared to wildtype littermates. The major change in GLT-1 staining in mutant mice coincided with a loss of Purkinje cells at 7 mo. of age. The normal pattern of GLT-1 staining circumscribes the Purkinje cell bodies and in their absence in mutant mice, this staining is lost. Otherwise, comparable patterns and levels of GLT-1 staining were apparent in both PPT1-/- and wildtype cerebella in the granular cell and molecular layers.

Microglial Reactivity

PPT1-/- and wildtype brains were stained for F4/80, a marker for microglia and macrophages (Figure 7). Prior to 5 mo. of age, there was no detectable F4/80 staining within the brains PPT1-/- mice or wildtype littermates. At 5 mo. of age, an increase in F4/80 staining was evident in the PPT1-/- cerebellum. The F4/80-positive cells, mostly comprised of small-ramified cells, were evenly

dispersed throughout the molecular, Purkinje cell, and granular cell layers. As the mice age, there was a progressive increase in the number of positively

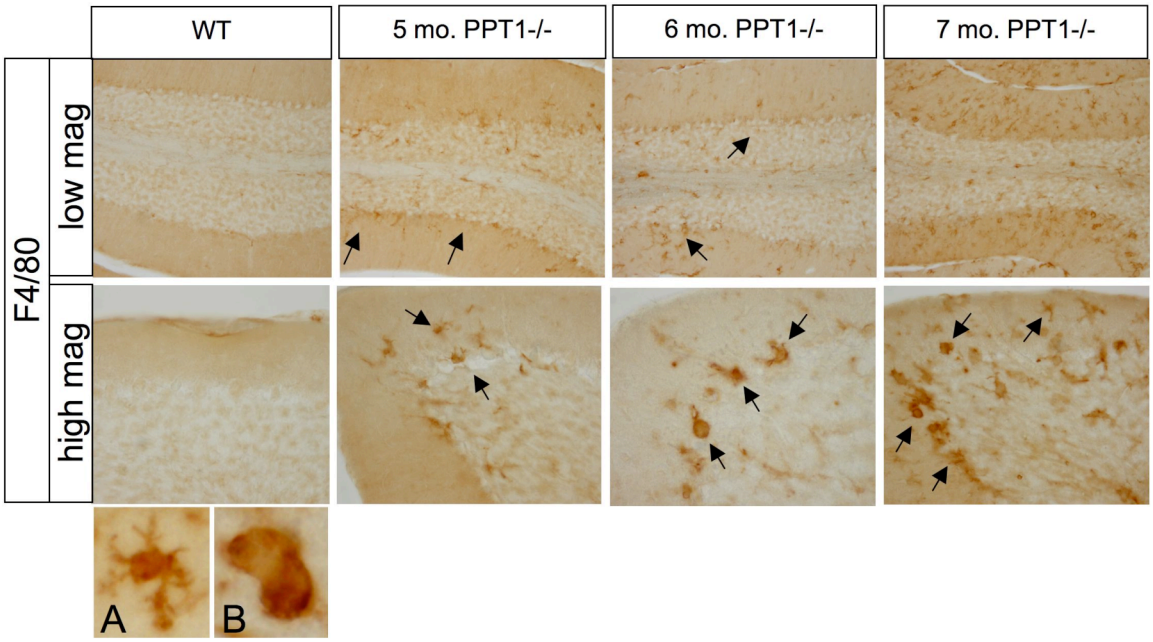

Figure 7. F4/80 staining, a monocyte marker, in PPT1-/- and wildtype mice. PPT1-/- mice showed an increase in the number of monocytes starting at 5 mos. of age. As the mice age, there was an increase in monocytes at 6 and 7 mos. (black arrows). In addition, there was a change in the morphology of the F4/80 positive cells from small, ramified cells with a microglial morphology (A) to larger rounded brain macrophage-like cells (B). Comparable levels of F4/80 staining were observed in 1, 3, 5, 6, and 7 mo. wildtype mice.

stained cells in the PPT1-/- cerebellum. In addition, the morphology of the positive cells changed from small-ramified cells (A) to large, round cells with brain macrophage-like morphology (B) as the mice age.

Luxol Fast Blue and Periodic acid Schiff staining

Luxol Fast Blue (LFB) and Periodic acid Schiff (PAS) staining were performed on 7 mo. old PPT1-/- mice and normal littermates (Figure 8). Upon gross examination, the white matter tracts, as visualized by LFB, appeared thinner in PPT1-/- mice (arrows) compared to normal littermates. At higher magnification, LFB staining revealed an array of densely stained myelinated

fibers traversing through the white matter in the wildtype mouse. In contrast, the PPT1-/- cerebellar white matter appeared disorganized, less intensely stained

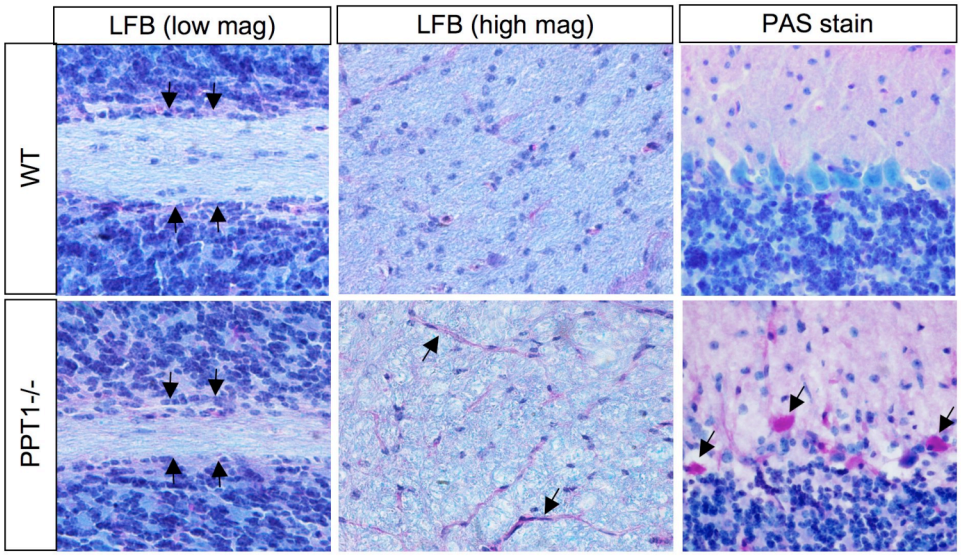

Figure 8. Luxol Fast Blue (LFB) and Periodic acid-Schiff (PAS) staining in the PPT1-/- cerebellum. Staining for the myelin marker, luxol fast blue, was markedly decreased in PPT1-/- mice at 7 mo. At low magnification, there was a thinning of the cerebellar white matter tracts in the PPT1-/- mice compared to WT. At high magnification, the intensity of staining and organization of the white matter was disrupted in the PPT1-/- cerebellum. PAS staining (red) demonstrated glycogen inclusions in the molecular layer and Purkinje cell layers of PPT1-/- mice. In addition, the vasculature in the white matter tracts was PAS positive (arrows).

and littered with 'holes'. Furthermore, the number of densely stained cell bodies in the white matter was decreased and the morphology of the remaining cell bodies appeared shrunken and irregular in PPT1-/- mice. These densely stained cells are glia, most likely oligodendrocytes, given their localization and organization in the cerebellar white matter.

PAS staining, a marker of glycogen storage was performed on 7 mo. PPT1-/- mice. There was a noticeable increase in the intensity of PAS staining in the vasculature of the white matter tracts (black arrows). In addition, PAS-

positive cells were present in the molecular layer and Purkinje cell layers of the PPT1-/- cerebellum, but only at a late stage of disease (5-7 mo.).

Rotarod Testing

PPT1-/- mice and normal littermates were tested on the rotorod at 1, 3, 5, 6 and 7 mo. of age and latency to fall was recorded (Figure 9). At 1 mo. of age, the performance of PPT1-/- mice and normal littermates was indistinguishable on the rotorod (54.9s v. 54.7s; respectively). The latency to fall began to decrease

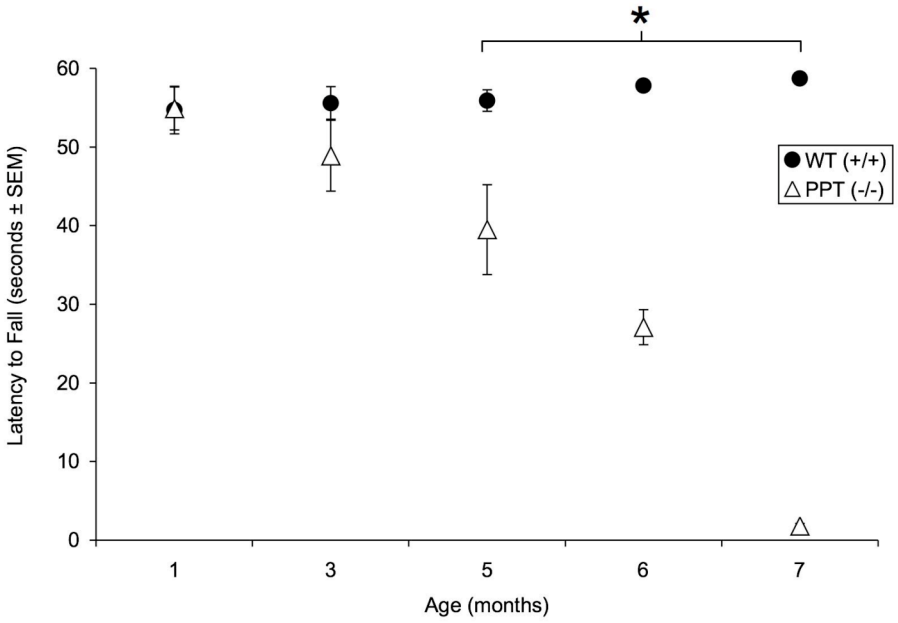

Figure 9. Constant speed rotarod testing in the PPT1-/- mice. PPT1-/- mice display significant motor deficits ($p<.0.0005$) on the rotarod test beginning at 5 mo. of age, and continuing through 6 ($p<.0.0005$) and 7 ($p\leq0.001$) months of age. The asterisk denotes statistical significance. WT mice performed at criterion for the entire task.

in PPT1-/- mice compared to WT mice at 3 mo. of age (55.6s v. 48.9s; respectively), although this was not a significant change. By 5 mo. of age, the ability of the PPT1-/- mice to stay on the rotorad was significantly impaired (39.5s; $p\leq0.0005$), while wildtype littermates continued to perform near criterion

(55.9s). The performance of PPT1-/- mice continued to decrease at 6 mo. (27.1s; $p<0.0005$) and reached a nadir at 7 mo. of age (1.8s; $p\leq0.001$). Repeated measures ANOVA revealed a significant main effect of group, [$F(1,26) = 68.75$, $p < 0.0005$], a significant effect of age, [$F(2,52) = 24.16$, $p < 0.0005$], and a significant group by age interaction, [$F(2,52) = 27.84$, $p < 0.0005$].

Results from Forebrain Study

Astrocyte activation is an early stage phenomenon

Astrocyte activation, as identified by GFAP upregulation, is one of the first pathological changes observed in the PPT1-/- brains (Figure 10). The forebrains

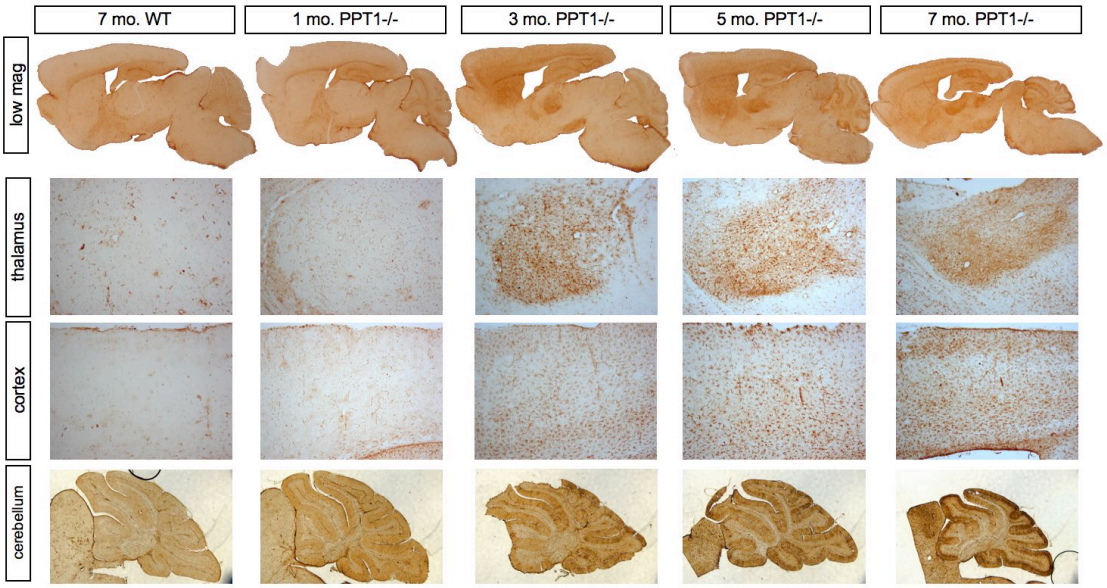

Figure 10. Early astrocyte activation precedes neuronal loss. GFAP staining in 1, 3, 5, and 7-month-old PPT1-/- and 7-month-old WT brains. Focal areas of GFAP upregulation occur in the PPT1-/- brain beginning at 1-3 months of age. Specifically, there is a notable increase in GFAP staining in the cortex, thalamus, and cerebellum of PPT1-/- mice. The intensity and distribution of GFAP increases as the PPT1-/- mice age.

from PPT1-/- and WT mice at 1, 3, 5, and 7 mos. of age were stained with GFAP. By 3 mos. of age, a statistically significant increase in GFAP staining was present

in the PPT1-/- forebrain, most notably within the cortex and thalamus (Figure 11A). Initially, diffuse staining was present across all cortical laminae, in multiple regions of the cortex (i.e. motor, somatosensory, visual). As the mice aged, the intensity and distribution of GFAP staining increased. In contrast to the cortex, GFAP staining in the thalamus was more localized to individual thalamic nuclei. By 3 mos. of age, the lateral geniculate (LGN), medial geniculate (MGN), ventral posterior (VPM/VPL), mediodorsal (MD), central medial (CM), and reticular thalamic (Rt) nuclei were all densely stained. As the mice aged, GFAP staining increased in intensity but also spread to include adjacent thalamic regions. By 7 mos. of age, the entire forebrain in the PPT1-/- mouse contained astrocyte activation.

Neuronal loss in the thalamus

In the PPT1-/- forebrain, the thalamus is one of the first areas to undergo neuronal loss. Neuronal loss in the thalamus is progressive in nature and specific to individual nuclei. The LGN, part of the visual center, is the first nucleus to degenerate at 3 mos of age. Neuronal loss in the remainder of the thalamic nuclei, including the MGN, VPM/VPL, and Rt, did not begin until 5 mos. of age. Thus, these data indicate that neuronal loss in the thalamus is a later stage phenomenon beginning at 5 mos. of age.

Cortical atrophy and neuronal loss

Although cortical thinning is one of the key elements of disease in INCL, this pathological change is a later stage phenomenon. A statistically significant decrease in cortical thickness is not present until 5-7 months of age (summarized

in Figure 11B). Also, cortical atrophy is not uniform but varies depending upon the region assayed. For example, cortical thinning was present in the motor,

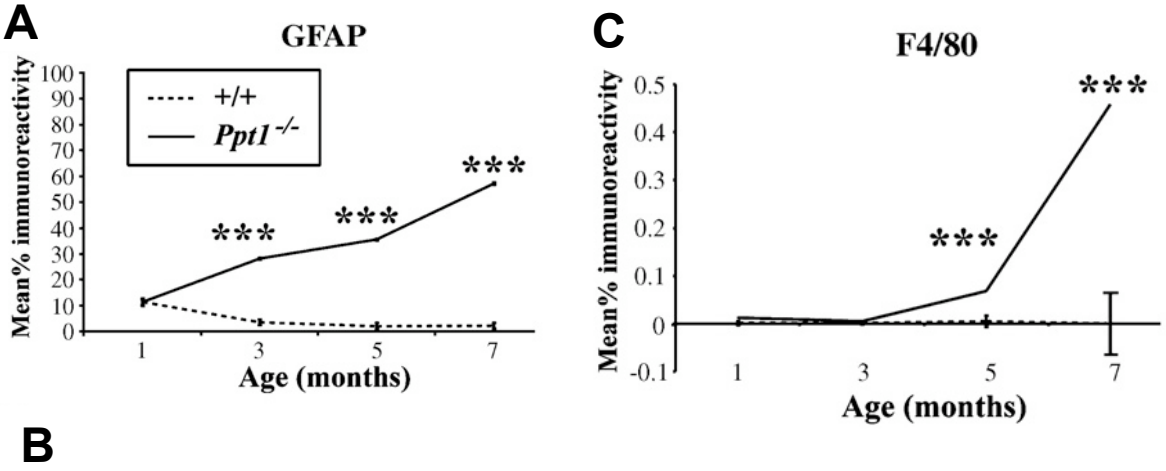

B

Thalamus		
Region	**Function**	**Neuronal Loss**
Lateral Geniculate Nucleus (LGN)	Visual	3 mos
Ventral Posterior Thalamic Nucleus (VPM/VPL)	Somatosensory	5 mos
Medial Geniculate Nucleus (MGN)	Auditory	5 mos
Reticular Thalamic Nucleus (Rt)	Inhibitory input to thalamus	5 mos
Cortex		
Region	**Function**	**Neuronal Loss**
Visual Cortex (V1)	Visual	5 mos
Somatosensory Cortex (S1BF)	Somatosensory	7 mos

Figure 11. Summary of Forebrain Pathology in the PPT1-/- mouse. (A) Threshold analysis of GFAP stained images in the S1BF cortex demonstrates a quantitative increase in staining as the PPT1-/- mice age. By 3 mos. of age, this is a significant increase when compared to WT brains. (B) A summary of the time course of significant neuronal loss ($p<0.05$ level) in the forebrain. Neuronal loss is first observed in the thalamus, with neuronal death occurring in cortical relays later. (C) F480 threshold analysis demonstrates that microglia activation is a late stage phenomenon in the S1BF cortex. A significant increase in F480 staining begins at 5 mos. in the PPT1-/- mice but steadily increases as the mice age.

visual, and auditory cortex, where no statistically significant change in cortical thickness was found in the somatosensory or entorhinal cortex. Furthermore, the

visual cortex is the first region to demonstrate atrophy at 5 mos. of age, while the motor and auditory cortex do not degenerate until 7 mos. of age.

Quantitation of neuronal number reinforced the finding that cortical degeneration is a late stage phenomenon. Neuronal loss is first seen in the visual cortex at 5 mos. of age. However, neuronal loss occurs in the somatosensory cortex at 7 mos. of age. These data demonstrate that cortical atrophy and neuronal loss occur subsequent to neuronal loss in their thalamic relays.

Microglial reactivity is a late stage phenomenon

While astrocyte activation is an early stage phenomenon, microglial activation occurs during the later stage of disease (Figure 11C). Microglial reactivity, as visualized by F4/80 staining, was not significantly elevated until 5 mos. of age. Prior to that time, little or no reactive microglia were present in the brain suggesting that microglia reactivity occurs in response to neurodegeneration. Furthermore, the number of activated microglia increased in both the thalamus and cortex as the mice age.

Seizure Activity

PPT-/- and WT mice at 6, 6.5, 7 and 7.5 mos. of age were monitored by EEG recordings and video surveillance for spontaneous seizure activity (Figure 11). No seizure activity was present in PPT1-/- mice prior to 7 mos. of age. At 7 mos. of age, only 50% of all PPT1-/- mice had seizures while 100% of 7.5 mos. old mice had seizures. There was no change in seizure duration or frequency in the 7 or 7.5 mos. old mice. The interictal EEG tracings were scored for all

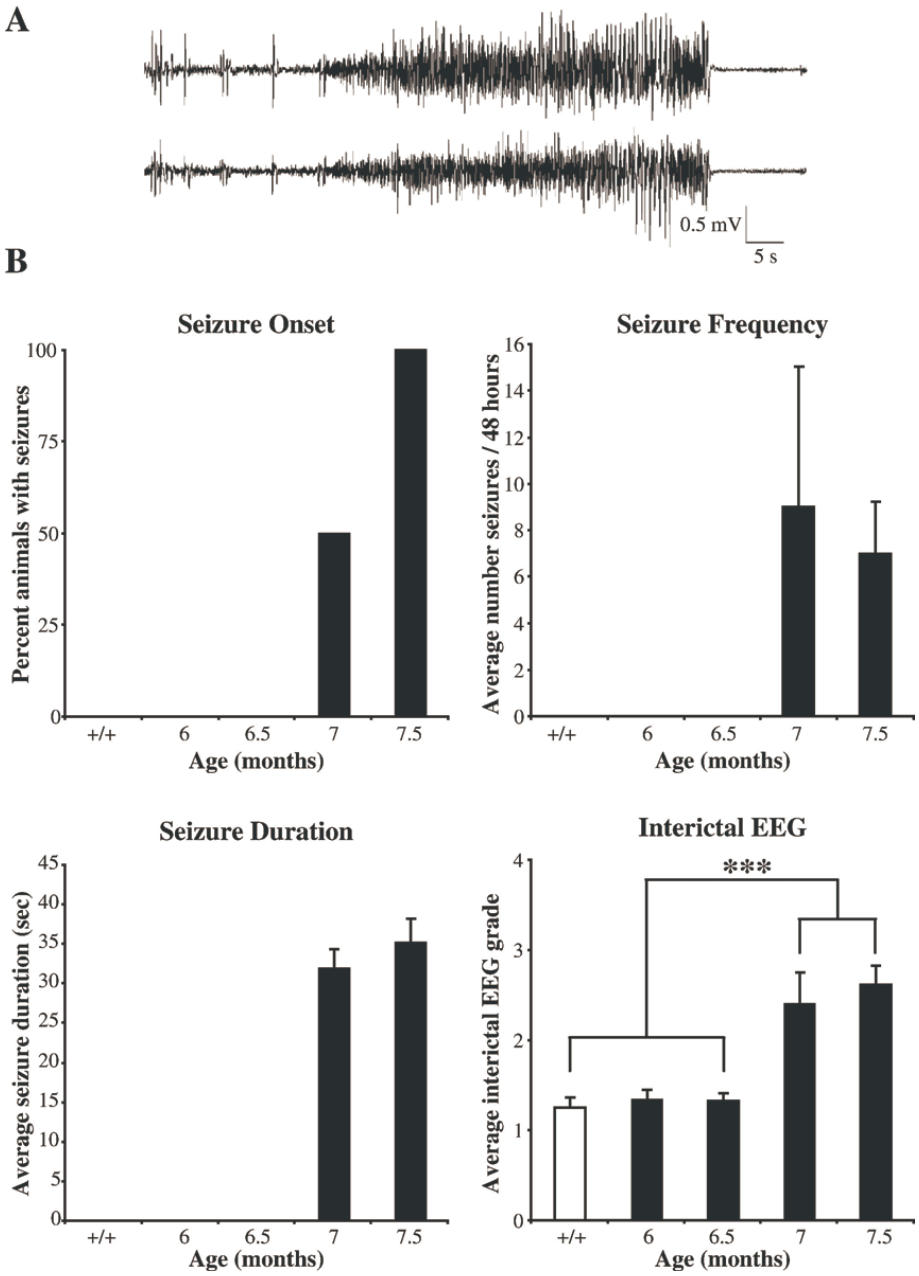

Figure 12. Progressive development of the seizure phenotype in PPT1-/-mice. (A) Representative example of a seizure recorded in a PPt1−/− mouse by two channel EEG. (B) Seizures were not evident in PPT1−/− mice until 7 months of age and were present in all mutant mice by 7.5 months of age, but were not present in age-matched controls (+/+). There was no significant difference between mutant mice in the frequency or duration of seizures at 7 and 7.5 months of age. Graded scoring of EEG recording traces also revealed a significant worsening of the interictal background EEG in mutant mice above 7 months of age, compared to mutant mice at 6 and 6.5 months of age and age-matched controls (***$p < 0.001$, ANOVA with post hoc Tukey–Kramer multiple comparisons).

animals tested. There were no significant differences in the interictal EEG tracings of 6 and 6.5 months PPT1-/- mice when compared to WT. However, with the onset of seizure activity, the background EEG patterns were abnormal by 7-7.5 mos. of age.

Discussion

Although pathological changes within the PPT1-/- forebrain at an end stage of disease were described in detail (Bible et al., 2004; Griffey et al., 2004), little is known about the morphological and functional changes localized to the hindbrain. Since reports of INCL patients describe profound cerebellar pathology (Haltia et al., 1973a; Haltia et al., 1973b) and motor deficits (Santavuori et al., 1974), a complete characterization of the disease progression within the PPT1-/- cerebellum is essential. Our findings demonstrate that substantial pathology exists within the PPT1-/- cerebellum, consistent with the human course of disease. At an end stage of disease, there was significant cerebellar atrophy, suggesting profound cell loss in the PPT1-/- cerebella. We performed silver degeneration staining to investigate which aspects of the cerebellum were most affected. Staining of the cerebellar white matter was first observed, suggesting the major afferent and efferent projections were undergoing widespread degeneration. Similarly, the molecular and Purkinje cell (PC) layers were argyrophillic, identifying 'patches' of degenerating PC bodies and dendritic arbors. As described by Sarna and Hawkes (2003), PCs in the cerebellum are highly organized into parasagittal bands (based on zebrin II immunoreactivity),

which carry their own molecular fingerprint, and are differentially susceptible to toxic insults. Silver staining suggests that specific classes of PPT1-/- PCs are more susceptible to cell death than others.

Quantification of the PC layer showed a trend towards early neuronal loss. As described above, the death of PCs throughout each lobe was not random but rather a stereotyped wave of cell death beginning in the anterior lobes of the cerebellar vermis and later affecting the posterior lobes. Although an increased sensitivity of certain classes of Purkinje cells is described in cerebellar mutants, lysosomal storage diseases (LSDs) with a cerebellar involvement preferentially affect the anterior lobes. Other LSDs such as Nieman Pick Type A/B (Macauley et al., 2008a; Macauley et al., 2008b; Sarna et al., 2001), Nieman Pick Type C (Sarna and Hawkes, 2003), and late infantile neuronal ceroid lipofuscinosis (Chang et al., 2008; Sleat et al., 2004) detail a vulnerability of the PCs in the anterior lobes to cell death. Some have postulated that increased levels of metabolic enzymes (Slemmer et al., 2007), increased glutamate transporter expression (EAAT4) (Welsh et al., 2002) and the presence of small heat shock proteins (Armstrong et al., 2000, 2001) is thought to be neuroprotective for PCs in the posterior lobes.

Although some PCs are initially more resistant to toxic insults in INCL, the posterior lobes still become affected later in disease progression. This phenomenon is consistent with other LSDs, but dissimilar to other cerebellar mutants (reviewed in (Sarna and Hawkes, 2003). Even if a subset of PCs survives longer than others, we hypothesize that their function is compromised

based on the morphological changes observed (Figure 3). Electrophysiology experiments are needed to evaluate surviving PCs.

Consistent with PC loss in the PPT1-/- cerebellum, there was an age dependent decline in rotarod performance. As PCs begin to die at 3 mo. of age, there is a concurrent decrease, although not significant, in PPT1-/- performance on the rotarod, which worsens with age. Significant performance deficits ($p \leq 0.05$) on the constant speed rotarod are seen at 5 mos. of age, which coincides with a trend towards Purkinje cell loss that becomes significant by 6 mos. of age. These data demonstrate a strong relationship between cerebellar pathology and motor function, a phenomenon seen in other LSDs (Macauley et al., 2008). Furthermore, these findings correlate with the loss of neurons within motor pathways in the basal ganglia and thalamus (Kielar and Cooper, unpublished observations), which may also contribute to this phenotype.

In contrast to PC loss, apoptotic cell death in the granular cell layer is a later stage phenomenon. These data illustrate a selective vulnerability of cerebellar neurons to cell death, an important consideration for therapeutic delivery and timing.

Recent reports on the NCLs (Bible et al., 2004; Chang et al., 2008; Kielar et al., 2007; Pontikis et al., 2005) demonstrate that gliosis occurs early in disease pathogenesis (reviewed in (Cooper et al., 2006). Similarly, activation of the PPT1-/- Bergmann glia was the first cerebellar change. Gliosis is a common component of many neurodegenerative disorders, yet it remains unclear whether this process is helpful or harmful to a chronically diseased CNS. GFAP

upregulation is used as a marker of gliosis, yet its exact role in CNS disease remains uncertain. We hypothesize that an early stage gliosis occurs for several reasons. First, astrocyte activation is occurring in response to altered neuronal-glial interactions (see below). In response to neuronal or glial stress, astrocytes shift roles from a quiescent to a reactive astrocyte early in INCL. We hypothesize this shift stabilizes glutamatergic synapses to maintain the health of the CNS. Thus, we hypothesize that activated Bergman glia are modulating neuronal-glial interactions in an effort to prevent CNS damage. Secondly, we hypothesize that early stage astrocyte activation occurs as an anti-inflammatory mechanism within the CNS and at the gliovascular unit. We postulate reactive astrocytes restrict access of systemic immune cells to the CNS via modulation of the blood brain barrier and/or chemokine signaling.

Although INCL is described as a neurodegenerative disorder, there is prominent astrocyte pathology in the PPT1-/- cerebellum, a phenomenon likely independent of astrocyte activation. As previously reported, normal astrocytes express PPT1 (Haltia, 2003; Margraf et al., 1999), and PPT1-deficient astrocytes accumulate GRODs (Galvin et al., 2007). Our studies demonstrate a decrease in S100ß staining at early stages in PPT1-/- mice, most notably in the Bergman glia, suggesting a primary pathology in astrocytes. Interestingly, S100ß staining is typically upregulated, not down regulated in CNS injury (i.e. neurodegenerative disorders, traumatic brain injury, etc.), (Goncalves et al., 2008; Griffin et al., 1995; Mrak and Griffinbc, 2001; Rothermundt et al., 2003; Wainwright et al., 2004). This reduction of S100ß in astrocytes could be due to the secretion of

S100ß into the extracellular space, a neurotoxic event in the adult brain (reviewed in Donato, 2003). Alternatively, the loss of S100ß staining may represent astrocytic cell loss. To investigate this, we stained PPT1-/- cerebella for glutamine synthetase, an astrocyte specific enzyme important for glutamate-glutamine recycling. GS staining in the Bergman glia was decreased or largely absent in the PPT1-/- cerebellum, suggesting that astrocyte dysfunction or cell loss is a prominent feature in disease pathogenesis.

GLAST staining further illustrated pathological changes in astrocytes. GLAST, an astrocyte specific glutamate transporter, is responsible for glutamate clearance at the synaptic cleft. An overall decrease in GLAST expression was observed in the aged PPT1-/- cerebellum. Furthermore, specific loss of GLAST is observed in the Bergman glia circumscribing PCs. Although comparable levels of GLT-1 were observed in the PPT1-/- cerebellum, GLAST is the main glutamate transporter in Bergman glia, thus demonstrating a potential disruption in glutamate recycling in the PPT1-/- cerebellum. Furthermore, localized changes in the expression of glutamate and both astrocytic and neuronal glutamate transporters are also evident in the thalamus, basal ganglia and hippocampus (Kielar and Cooper, unpublished observations), suggesting that altered glutamate/glutamine cycling may be an important feature of INCL pathogenesis.

Although changes in astrocytes and neurons occur at an early stage in INCL, changes in microglia and oligodendrocytes occur later. As the mice age, there is an increase in F4/80+ cells in the CNS as well as changes in their morphology (Figure 7A,B). We hypothesize that microglial activation is initially

mounted in the PPT1-/- cerebellum to clear cellular debris. As the mice age, there is a secondary macrophage infiltration in INCL where circulating immune cells invade the PPT1-/- CNS. It will be important to determine the relationship between these events, neuron loss, and blood brain barrier permeability.

Demyelination is seen in the aged PPT1-/- cerebellum. At autopsy, patients with INCL suffer a near complete loss of myelin in the CNS (Haltia, 2003). Not surprisingly, we found atrophy of the cerebellar white matter tracts as well as a loss of myelin components, such as CNPase (data not shown), in the PPT1-/- cerebellum. Whether this demyelination is due to the axonal death of PCs or a primary oligodendrocyte dysfunction needs further investigation.

The temporal-spatial characterization of the cerebellum successfully identified a time line for cellular pathology in the PPT1-/- brain (Figure 12). The first pathological change observed in the PPT1-/- cerebellum is astrocyte activation at 1-3 months of age. This change preceded neuronal loss, in either the Purkinje cell or granular cell layers. By 5-7 mos. of age, there was a significant neuronal loss throughout the cerebellum concurrent with other changes in the glial population. Specifically, by 7 mos. of age, there appears to be loss of the Bergmann glia, frank demyelination in the cerebellar white matter, and late stage microglial reactivity. Interestingly, the motor deficits observed in the PPT1-/- mouse correlated with neuronal loss as a mid to late stage event.

A similar time line occurred regarding studies performed on the PPT1-/- forebrain (Figure 13). Similar to the cerebellum, the first pathologic change observed was astrocyte activation in both the cortex and thalamus of PPT1-/-

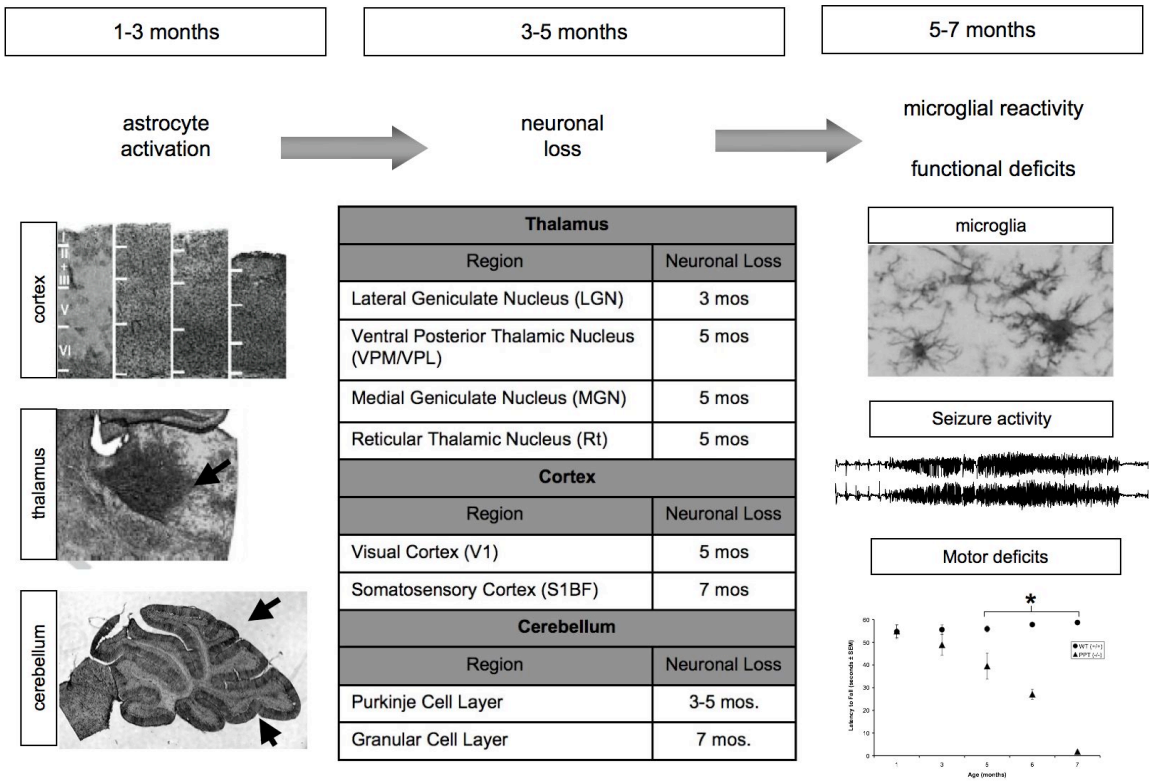

Thalamus	
Region	Neuronal Loss
Lateral Geniculate Nucleus (LGN)	3 mos
Ventral Posterior Thalamic Nucleus (VPM/VPL)	5 mos
Medial Geniculate Nucleus (MGN)	5 mos
Reticular Thalamic Nucleus (Rt)	5 mos
Cortex	
Region	Neuronal Loss
Visual Cortex (V1)	5 mos
Somatosensory Cortex (S1BF)	7 mos
Cerebellum	
Region	Neuronal Loss
Purkinje Cell Layer	3-5 mos.
Granular Cell Layer	7 mos.

Figure 13. Summary of disease progression in the PPT1-/- mouse. Disease progression is broken down into 3 stages- early (1-3 mos.), mid (3-5 mos.), and late (5-7 mos.). During the early phase of disease, the first pathological change observed is astrocyte activation, delineated by GFAP upregulation. Neuronal loss within the thalamus begins during the mid stage of disease, with neuronal loss in the cortex to follow. Finally, at an end stage of disease, there is microglial activation and functional deficits in the PPT1-/- mice.

mice at 3 mos. of age. Subsequently, there was localized neuronal loss in thalamic nuclei were astrocyte activation had occurred. Following neuronal loss in the thalamus, cortical atrophy and neuronal loss occurred in the PPT1-/- brains at 5-7 mos. of age. Neurodegeneration correlated with an increase in microglia reactivity in both the cortex and thalamus. The onset of seizure activity and changes in the interictal EEG pattern occurred at 7 mos. of age, coinciding with neuronal loss in cortex and thalamus.

These studies provide a comprehensive characterization of cellular pathology and its relationship to behavioral dysfunction in INCL. We demonstrate that cellular pathology is not restricted to neurons, and that a

concurrent glial involvement, most notably in astrocytes, exists. We demonstrate that astrocyte activation is one of the first pathological changes observed in either the forebrain or hindbrain of PPT1-/- mice. With a better understanding of how the disease progresses in INCL, we can identify possible avenues for intervention in future therapy studies. Since clinical trials for LINCL and INCL are ongoing (Sondhi et al., 2008; Sondhi et al., 2005; Taupin, 2006; Worgall et al., 2008; Zhang et al., 2001), our studies identify the need to target therapies not only to the forebrain of patients suffering from INCL, but also to the hindbrain. It also provides evidence of profound glial involvement and thus necessitates the development of therapies aimed at treating both neuronal and glial dysfunctions.

Chapter Three

The role of astrocyte activation,
as defined by GFAP upregulation,
in a mouse model of INCL

Introduction

Characterization studies in the PPT1-/- mice yielded valuable insights into the progression of CNS disease in INCL (Kielar et al., 2007; Macauley et al., 2009). Previous studies demonstrated that localized areas of astrocyte activation, as defined by an increase in glial fibrillary acidic protein (GFAP) expression, are the first pathological changes observed in the PPT1-/- brains. By 1-3 months of age, there is a significant increase in GFAP staining in the thalamus, cortex, and cerebellum. Interestingly, the thalamus, cortex, and cerebellum also suffer the greatest neuronal loss and regional atrophy subsequent to this early astrocyte activation. Thus, we hypothesize that astrocyte activation, in particular GFAP upregulation, plays an active role in the pathogenesis of INCL, given its temporal-spatial association with future sites of neurodegeneration. By investigating the role of astrocyte activation and GFAP upregulation, we will determine whether gliosis is protective or harmful to the underlying neurodegeneration and functional deficits associated with INCL.

GFAP Upregulation and Astrocyte Activation

Astrocyte activation, or reactive gliosis, although often described, is a poorly understood phenomenon in CNS injury and disease (Kalman, 2004; Pekny and Nilsson, 2005; Sofroniew, 2005). Although GFAP upregulation is the classic biomarker of gliosis, the relationship between increased GFAP expression and functional changes remains unclear. This ambiguity is partly because the role of GFAP as a key intermediate filament protein in astrocytes remains poorly understood (Messing and Brenner, 2003; Pekny, 2001). As

important components of astroglial cells, intermediate filament proteins, such as GFAP, vimentin and nestin, are thought to regulate the shape, structure, and motility of astrocytes (Eng et al., 2000; Potokar et al., 2007). More specifically, GFAP is also responsible for stabilizing astrocytic processes, organizing organelles within cytoplasm, as well as anchoring glutamate transporters (i.e. GLAST) to the plasma membrane (Sullivan et al., 2007). Studies from GFAP-null mice infer that the GFAP protein is involved in the maintenance of the blood brain barrier, myelin, and neuronal synapses. Beyond these generalized or inferred functions, the biological role of GFAP remains elusive. Moreover, the role of GFAP in astrocyte activation, specifically, is unclear.

Although the function of GFAP is poorly understood, the correlation between GFAP upregulation and astrocyte activation is clear and well described (Bates et al., 2002; Hafiz and Brown, 2000; Haltia, 2003; Kobayashi et al., 2002; Levine and Hoenig, 1972; Li et al., 2008; Murphy et al., 1992; Murray et al., 2006; Oberheim et al., 2008; Pekny and Nilsson, 2005; Renkawek et al., 1999; Vajda, 2002). When the CNS is subjected to an insult or injury, there is an increase in GFAP expression, which coincides with a shift from a quiescent astrocyte to an activated astrocyte. In a healthy CNS, quiescent astrocytes are responsible for a variety of functions, beyond providing structural integrity to the brain. Most notably, astrocytes maintain neuronal synapses via metabolic support, neurotransmitter uptake, and glutamate recycling (Mazzanti et al., 2001; Nedergaard et al., 2003; Perea et al., 2009; Ransom et al., 2003; Schousboe et al., 1997; Volterra and Meldolesi, 2005; Walz, 2000). Astrocytes also form the

gliovascular unit and modulate the blood brain barrier (BBB)(Goldstein, 1987; Nedergaard et al., 2003). In addition to neuron-glial and gliovascular interactions, astrocytes are joined via gap junctions to create an astrocyte syncytium responsible for the propagation of intracellular signals (Kielian and Esen, 2004). In response to injury, quiescent astrocytes become “activated” or “reactive” and adopt a secondary set of functions (Aschner, 1998a, b; Daginakatte et al., 2008; Eddleston and Mucke, 1993; Heales et al., 2004; Maragakis and Rothstein, 2006). Morphologically, reactive astrocytes upregulate intermediate filament proteins like GFAP, vimentin (vim), and nestin resulting in astrocyte hypertrophy (Pekny, 2001; Pekny and Nilsson, 2005). Both the number and thickness of astrocytic processes increases giving these cells their star shaped, or more accurately, “bushy” appearance (Wilhelmsson et al., 2006). Beyond structural modifications, reactive astrocytes are transformed functionally; they clear cellular debris, form glial scars, express cytokines, and promote inflammation.

Although the process of gliosis is well described, it is often debated whether these structural and functional changes in astrocytes are helpful or harmful to the injured CNS. Reactive gliosis has largely been studied in models of acute trauma or injury (Pekny and Pekna, 2004; Sofroniew, 2009; Sofroniew et al., 1999). Findings from these studies demonstrate that although reactive astrocytes form glial scars that contain a site of injury, these cells also limit regeneration of the CNS via both a physical (i.e. glial scar) and molecular (i.e. cytokines) barrier (Daginakatte et al., 2008; Ridet et al., 1997; Voskuhl et al.,

2009). Given the dichotomous nature of reactive astrocytes in acute injury, there is an inherent need to gain a better understanding of this phenomenon, specifically in chronic, neurodegenerative diseases.

The GFAP-/-, Vimentin-/-, PPT1-/- (3KO) mouse

Recently, a mouse model lacking the intermediate filament proteins (IFs), GFAP and vimentin, was created and can be utilized to address the relationship between structural alterations (i.e. GFAP upregulation) and functional changes (i.e. cytokine production, neurodegeneration, etc.) associated with astrocyte activation in CNS injury and disease (Pekny et al., 1999). When left unchallenged, the GFAP-/-, Vim-/- double knockout (2KO) mice breed, develop normally and live a normal lifespan. However, when the 2KO mice are exposed to CNS injury, the outcomes are rather complex. In the case of mechanical stress (i.e. traumatic brain injury, retinal detachment, stroke, etc.), the 2KO mice showed a decreased structural stability in the absence of IFs resulting in more damage (Kinouchi et al., 2003; Lane and Pekny, 2004; Li et al., 2008; Lundkvist et al., 2004; Nakazawa et al., 2007; Pekny, 2001; Pekny and Pekna, 2004; Verardo et al., 2008). Although the glial scar was less organized in these models of CNS trauma resulting in larger infarct volumes, several of these models report positive outcomes such as greater axonal sprouting, synaptic regeneration and faster wound healing. In a model of retinal detachment, the 2KO demonstrated a reduction in monocyte infiltration, cytokine expression, and photoreceptor cell death. Taken together, results from studies using 2KO mice help elucidate both

the positive and negative outcomes associate with reactive gliosis in models of CNS injury.

Goals of Chapter 3

To further our understanding of the role of astrocyte activation in INCL, we crossed the 2KO mouse to the PPT1-/- mouse, thus creating the GFAP-/-, Vimentin-/-, PPT1-/- triple knockout (3KO) mouse. By knocking out GFAP and Vimentin, we hypothesized we would alter how astrocytes react to injury in a model of INCL. In this study, we investigated the effects of altered gliosis in the PPT1-/- brain. We determined that astrocyte activation plays a protective role in INCL and in its absence disease pathogenesis is accelerated. In the 3KO brains, the hallmark characteristics associated with INCL, such as premature death, brain atrophy, cortical thinning, and neurodegeneration, are exacerbated compared to the PPT1-/- mice and controls. Furthermore, the underlying mechanisms responsible for this accelerated phenotype include immune cell infiltration, cytokine upregulation, and a compromised gliovascular unit. Taken together, the 3KO mouse provides valuable information concerning the role of astrocyte activation in INCL.

Methods

GFAP-/-, Vimentin-/-, PPT1-/- Mice

The GFAP-/-, Vimentin (Vim) -/- double knockout (2KO) and PPT1-/- mice were created through standard genetic techniques as previously reported. The GFAP-/-, Vim-/- mice (a kind gift from Milos Pekny, University of Goteborg,

Goteborg, Sweden) were crossed to the PPT1-/- mice (Griffey et al., 2005; Gupta et al., 2001) to create the GFAP-/-, Vim-/-, PPT1-/-, or triple knockout (3KO), mice. For the purposes of these studies, 3KO, 2KO, PPT1-/-, and wildtype (WT) mice were generated and maintained at Washington University School of Medicine as an outbred colony. Mouse genotypes were determined by PCR-based assays. Both male and female mice from each genotype were used in this study. Animals were housed under a 12:12 hour light:dark cycle and were provided food and water *ad libitum*. All procedures were carried out under an approved IACUC protocol from Washington University School of Medicine.

Brain Weights

Six-month-old 3KO, 2KO, PPT1-/-, and WT mice (n=5-6 mice per genotype per age) were sacrificed via a lethal injection of euthasol and the brains harvested by a researcher blinded to both genotype and age. A razor blade was inserted coronally between the forebrain and olfactory bulbs to remove the olfactory bulbs from the remainder of the brain. Similarly, a coronal cut was made immediately posterior to the cerebellum, separating it from the medulla and spinal cord. Care was taken to ensure that the cuts were flush with the front of the cerebrum and back of the cerebellum. Each brain was weighed using an analytical balance. Group differences in weights were analyzed using a repeated measure ANOVA with one between subjects' variable (genotype), one within-subjects variable (age), and subsequent pairwise comparisons. Bonferroni correction was used to maintain alpha levels at 0.05 when multiple comparisons were conducted.

Autofluorescent Accumulation

Six-month-old 3KO, 2KO, PPT1-/-, and WT mice (n=3 mice per group) were used to quantify autofluorescent accumulation in the somatosensory barrel field (S1BF) cortex using epifluorescent microscopy (Bible et al., 2004; Kielar et al., 2007). Briefly, mice were given a lethal injection of euthasol, the brains removed, and fixed for 48 hrs in 4% PFA in phosphate buffer. Following fixation, the brains were cryoprotected in 30% sucrose, embedded in OCT, and sectioned coronally on a freezing cryostat at 20μm thickness. Images from 3 serial sections through S1BF for each group were captured via a 20x objective and FITC filter on a Nikon microscope with a SPOT camera attached. All variables associated with image capture, including exposure time, binning, and gain, were held constant for all groups. Using ImageJ software, threshold analysis was performed to determine which pixels contained autofluorescent accumulation in a given image. The percentage of pixels containing autofluorescent material was calculated for each image and reported as the *area fraction*. Three sets of *area fraction* measurements were captured for each of the 3 sections through S1BF in each of the 4 groups. The average for each group was calculated. Statistical significance was assessed using an ANOVA followed by Bonferrini correction post-hoc test.

Nissl Staining

Nissl staining was performed on six-month-old 3KO, 2KO, PPT1-/-, and WT mice (n=3 mice per group). Briefly, mice were given a lethal injection of euthasol, the brains removed, and fixed for 48 hrs in 4% PFA in phosphate

buffer. Following fixation, the brains were cryoprotected in 30% sucrose, embedded in OCT, and sectioned coronally on a freezing cryostat at 20μm thickness. Sections throughout the primary visual (V1) cortex were mounted on glass slides, placed on a warming plate for 1 hr. and allowed to thoroughly dry overnight at room temperature. Sections were briefly rinsed in dH_20, incubated in 0.5% cresyl violet for 2 mins., and rinsed with dH_20. The sections were then dehydrated via a series of alcohols and xylenes and coverslipped.

Cortical Thickness

Cortical thickness measurements were performed on Nissl stained tissue from 3KO, 2KO, PPT1-/- and WT brains (n=3 brains per group). Images throughout V1 were captured at 10X magnification using an Olympus BX41 microscope and Olympuis DP 20 camera. Cortical thickness measurements were made from the boundary of the white matter to the pial surface for each brain, as delineated by Paxinos and Franklin and as previously described(Bible et al., 2004; Kielar et al., 2007). A series of 10 individual measurements were made for each of 3 sections for each mouse (n=3 mice per group). The mean cortical thickness measurement for each mouse was determined. Statistical significance was assessed using an ANOVA followed by Bonferrini correction post-hoc test.

DeOlmos Cupric Silver Staining

5-month-old 3KO, 2KO, PPT1-/-, and WT mice (n=2 per time point) as well as a time course of 3KO mice at 3, 5, and 6 mos. of age (n=2-3 per time point) were processed for deOlmos silver staining. Briefly, the mice were deeply

anesthetized with euthasol and transcardially perfused with 4% paraformaldehyde in sodium cacodylate buffer. The brains were removed and post-fixed for 48 hours. Each brain was embedded in a gelatin-based matrix (Switzer, 2000) and serial coronal sections (35 μm) were cut on a freezing microtome by Neuroscience Associates (Knoxville, TN). Neuronal degeneration was visualized by staining with a modified cupric silver method of DeOlmos (DeOlmos & Ingram, 1972; Switzer, 2000). A matrix of PPT1-/- and WT brains at identical levels in the coronal plane were stained simultaneously. Every sixth section (210 μm interval) was stained with the silver method and adjacent sections stained with H&E.

Blood Brain Barrier Permeability

Blood brain barrier (BBB) permeability was assessed in 7 mos. PPT1-/-, 7 mos. WT, and 5.5 mos. 3KO (n=4 mice per group) using an Evan's blue assay (Belayev et al., 1996; Young et al., 2004). PPT1-deficient mice receiving a middle cerebral artery occlusion (MCAO), or stroke, served as a positive control. Mice were injected with 2% Evan's blue in saline via a tail vein injection (4μl/ g of body weight). After 30 minutes, the mice were transcardially perfused with PBS until both the perfusate and liver were clear (approximately 1-2 minutes). The brains were removed, bisected, and weighed. One hemisphere was placed in 500μl of 50% trichloroacetic acid (TCA) solution and homogenized for 1 minute. Following centrifugation, the dye was extracted and diluted 1:3 in ethanol (ETOH). To determine the concentration of Evan's blue dye in samples, the fluorescence of each sample was read on a fluorescent spectrophotometer

(Hitachi F-2000; excitation of 620nm and emission at 680nm) and the concentration calculated based on external standards (100-500 ng/ml) per gram of tissue. A one-way ANOVA was performed to determine statistical significant at the $p<0.05$ level, with Tukey's Multiple comparison's post-hoc test.

Cytokine Assays

To estimate the concentration of cytokines within the brain parenchyma, a Bio-Plex multiplex cytokine assay kit was used on 3mos. 3KO, PPT1-/-, 2KO, and WT mice (Bio-Rad laboratories, Hercules, CA). The ELISA-based cytokine assay uses fluorescently labeled beads coated with cytokine-specific antibodies to detect cytokine levels in tissues (Hulse et al., 2004). The 23-plex sample kit includes standards and antibodies for the following cytokines: IL1α, IL-1β, IL-2, IL-3, IL-4, IL-5, IL-6, IL-9, IL-10, IL-12(p40), IL-12(p70), IL-13, IL-17, Eotaxin, G-CSF, GM-CSF, IFN-γ, KC, MCP-1, MIP-1α, MIP-1β, RANTES and TNF-α. Briefly, mouse brains were transcardially perfused with PBS and homogenized in a solution consisting of 10 mM Tris, 150 mM NaCl, 1 mM Dithiotreitol, 0.2% Triton and 20 l/ml of Protease Inhibitor Cocktail (#P8340, Sigma, St. Louis, MO). The supernatant from brain homogenates was diluted to obtain a protein target concentration of 0.5-1.0 mg/ml and stored at -70 C. For the multiplex assay, the samples were processed as per the manufacturer's instructions. The fluorescent beads were incubated with the brain homogenates, washed and then incubated with biotin-labeled antibody cocktail. The samples were then incubated with streptavidin-PE and the fluorescence values were read and analyzed by the flow cytometry based Bio-Plex 2200 system (Bio-Rad laboratories, Hercules, CA).

The concentration of the cytokine in each sample was estimated by using the standard curve generated for each cytokine by the standards supplied in the kit.

Immunohistochemistry

Triple KO, 2KO, PPT1-/- and WT mice were sacrificed via a lethal injection of euthasol and transcardially perfused with phosphate buffered saline (PBS) until the liver was clear. The brains from 1, 3, 5, and 6 and 7 months old mice were removed and fixed in 4% paraformaldehyde in phosphate buffer for 48 hours. Subsequently, the brains were cryoprotected with 30% sucrose in tris-buffered saline (TBS) and imbedded in OCT. Brains were sectioned in the coronal plane throughout rostral-caudal axis using a freezing cryostat. Adjacent, free floating sections were stained with the following antibodies: rat anti-CD31 (PECAM; 1:50, BD Pharmingen), rat anti-CD45 (1:50, BD Pharmingen), rat anti-CD3 (1:200; Abcam), and rabbit anti-Aquaporin 4(1:1000; Chemicon). Briefly, sections were washed in tris-buffered saline (TBS), incubated in 1% H_2O_2 (Sigma) to quench endogenous peroxidase activity, and rinsed thoroughly in TBS. The tissue was blocked for 1 hour in 10% normal goat serum (NGS; Sigma), 0.25% Triton X-100 in TBS. Sections were incubated overnight at 4˚C in primary antibodies in 5% NGS, 0.2% Triton X-100 in TBS. The following day the sections were rinsed in TBS and incubated in secondary antibodies (1:200; Vector Labs) in 10% NGS, 0.1% Triton X-100 in TBS for 75 minutes. The tissue was rinsed in TBS and then incubated in a peroxidase conjugated avidin-biotin complex (1:200; Vectastain Elite ABC kit, Vector Labs) for 1 hour at RT.

Antibody immunoreactivity was visualized with 3'-3' diaminobenzidine and H_2O_2 (DAB kit; Vector Labs) in TBS. Sections were dehydrated and coverslipped.

Results

Longevity

While WT mice live a normal lifespan, the 3KO and PPT1-/- mice experience a premature death mimicking a clinical feature of disease in INCL

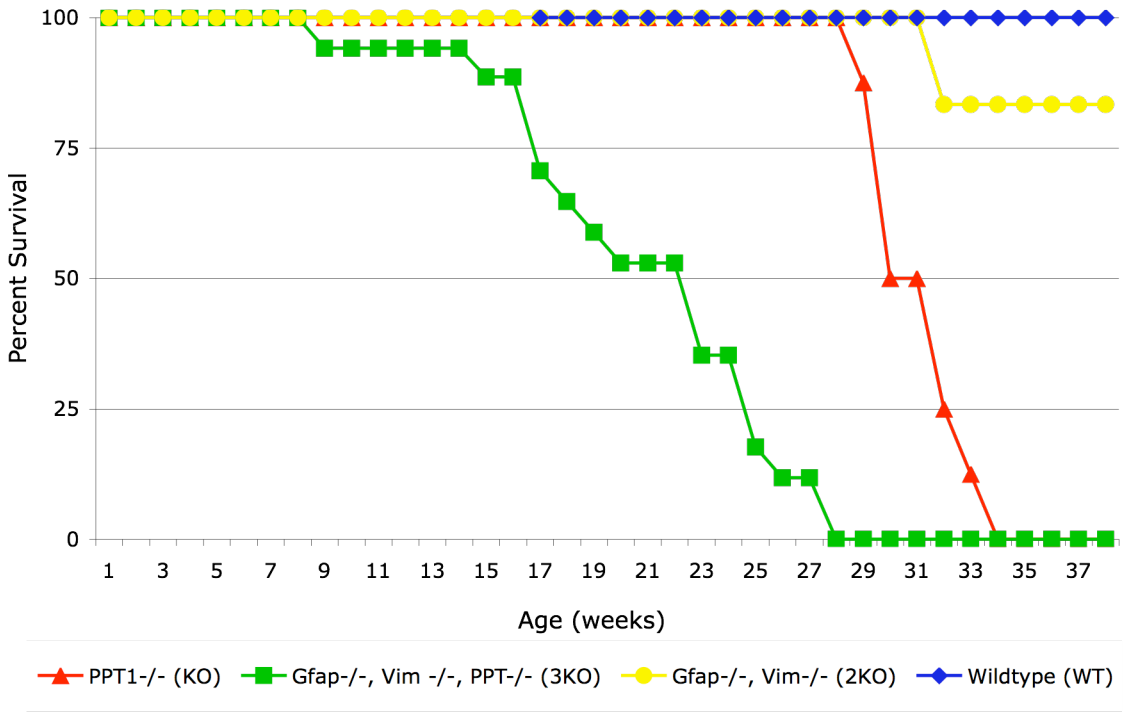

Figure 1. Lifespan of the GFAP-/-, Vimentin-/-, PPT1-/- (3KO) mice. The 3KO mice die earlier than the 2KO, PPT1-/-, or wild type mice. The 3KO and PPT1-/- die by 27 weeks and 33 weeks, respectively. Furthermore, the 50% mortality rate for 3KO averages 20 wks while the PPT1-/- mice is 30 wks.

(Figure 1). All 3KO and PPT1-/- mice die by 27 weeks and 33 weeks, respectively. Furthermore, the 50% mortality for the 3KO is 20 weeks of age compared to 30 weeks for the PPT1-/- mice. Thus, the 3KO mice die earlier than

the PPT1-/- mice, in addition to the WT and 2KO mice. This demonstrates an accelerated disease course in the 3KO mice compared to the PPT1-/- mice.

Brain atrophy

Brain weights were used as a marker of overall brain atrophy. Brains from 3KO, 2KO, PPT1-/-, and WT mice were weighed at 3, 5, and 6 mos. of age (Figure 2). At 3 mos. of age, there was no significant difference in brain weights among the groups tested ($p<0.30$). Conversely, there was a significant decrease in brain weight at 5 mos. of age in the 3KO mice ($p<0.027$) compared to the either PPT1-/-, 2KO, or WT mice. On average, the 3KO brains weighed 13.6%

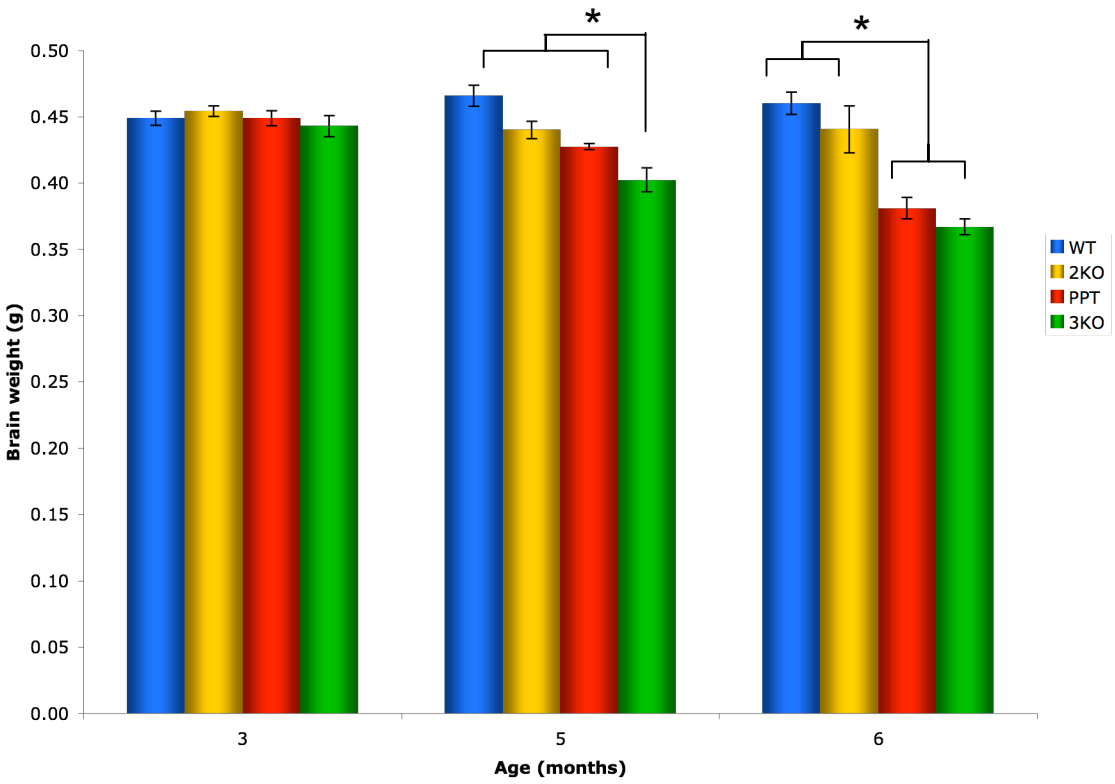

Figure 2. Brain atrophy in the GFAP-/-, Vimentin-/-, PPT1-/- (3KO) mice. At 3 mos. of age, there is no significant difference in the brain weights between 3KO, 2KO, PPT1-/-, and WT mice. However, the 3KO brains weigh significantly less than PPT1-/-, 2KO, and WT mice at 5 mos. of age suggesting atrophy occurs at this time. By 6 mos. of age, both the 3KO and PPT1-/- brains weigh significantly less than WT and 2KO brains (* = $p<0.05$).

less than WT brains at 5 mos. By 6 mos. of age, there was a significant decrease in the brain weights of both the 3KO and PPT1-/- mice compared to WT and 2KO mice ($p<0.001$). The 3KO and PPT1-/- brains decreased in weight by 20% and 17%, respectively, when compared to WT brains. These data demonstrate an overall brain atrophy in 3KO mice beginning at 5 mos. of age, which precedes the atrophy seen in the PPT1-/- brain at 6 mos. of age.

Cortical Thinning

Upon gross examination, the primary visual cortex (V1) of 3KO and PPT1-/- mice appeared atrophied in comparison to 2KO and WT brains (Figure 3A).

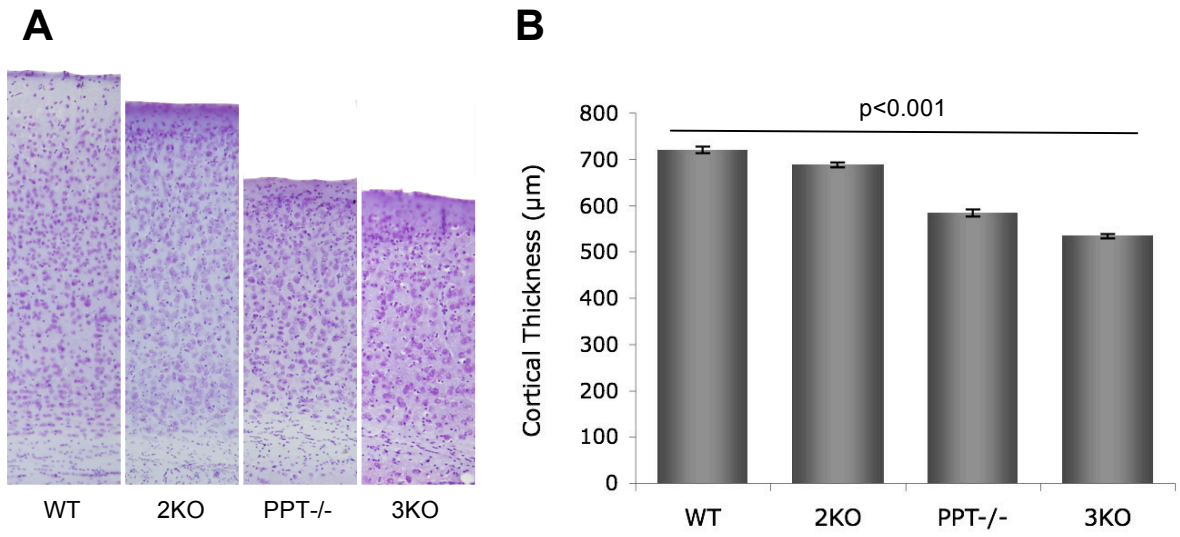

Figure 3. Cortical thinning in the GFAP-/-, Vimentin-/-, PPT1-/- mice. (A) Representative images from the visual cortex (V1) of WT, 2KO, PPT1-/-, and 3KO mice. Upon gross examination, V1 of 3KO and PPT1-/- mice appeared atrophied in comparison to 2KO and WT brains. (B) Quantification of cortical thickness in the WT, 2KO, PPT1-/-, and 3KO mice. There is a significant difference in cortical thickness between all groups ($p<0.0001$). The visual cortex of 3KO mice is thinner than the V1 cortex of PPT1-/-, 2KO, and WT mice.

Therefore, we measured cortical thickness in V1 at 6 mos. of age in the 3KO, 2KO, and WT mice (Figure 3B). There was a significant difference in cortical thickness between all groups measured ($p<0.001$). At 6 months of age, the 3KO

mice had a mean cortical thickness of 533.2μm, compared to WT, 2KO, and PPT1-/- brains, which were 719.6μm, 687.8μm, and 583.2μm, respectively. Thus, there was a 25.9% decrease in cortical thickness of 3KO brains compared to WT, while the PPT1-/- brains only suffer an 18.9% loss. Therefore, cortical thinning in the 3KO is more severe than in the PPT1-/- or 2KO brains when compared to WT.

Autofluorescent Accumulation

Accumulation of an autofluorescent substrate throughout the neuraxis is a hallmark of INCL. Therefore, we investigated whether the 3KO brains had a demonstrable load of autofluorescent material. Qualitatively, the 3KO and PPT1-/- brains both contained autofluorescent storage material throughout the brain at 6 mos. of age. Autofluorescent substrate accumulated intracellularly in the 3KO brain in a pattern similar to the PPT1-/- mouse (Figure 4A). A low level of autofluorescent material was detected in the WT and 2KO, largely due to the presence of autofluorescent red blood cells contained within the vasculature. To determine the level of storage material in the CNS, we quantified autofluorescence in the S1BF cortex of 3KO, 2KO, PPT1, and WT brains (Figure 4B). There was a significant increase ($p<0.001$) in autofluorescent accumulation in both the PPT1-/- and 3KO brains compared to WT and 2KO. Furthermore, there was a significant difference ($p<0.0023$) in the levels of autofluorescent substrate in PPT1-/- and 3KO mice. More specifically, there was a 21% increase in autofluorescence in the S1BF cortex of PPT1-/- mice compared to the 3KO mice.

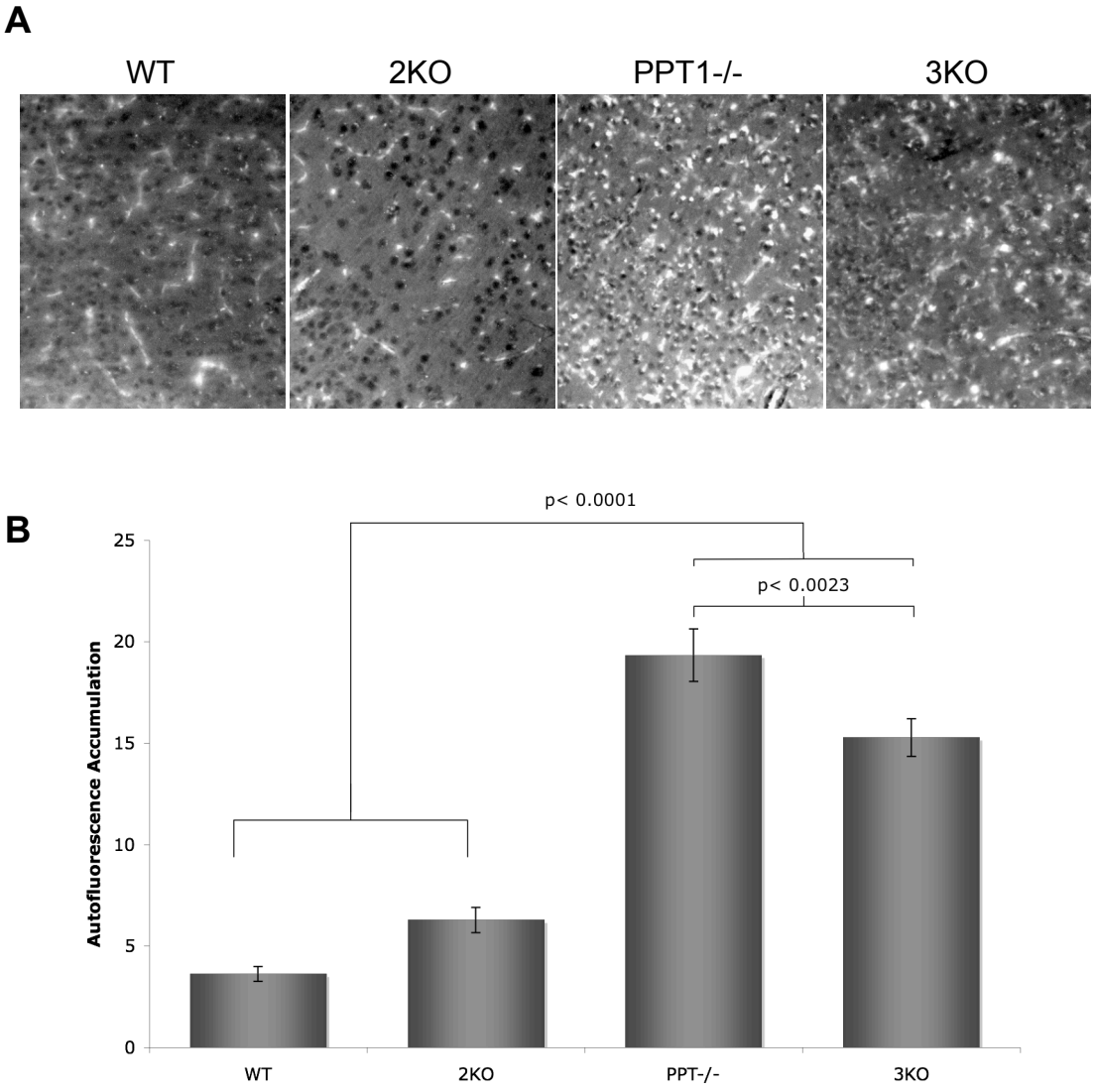

Figure 4. Autofluorescent accumulation in the GFAP-/-, Vimentin-/-, PPT1-/- mice. (A) Representative images of the somatosensory barrel field (S1BF) cortex in WT, 2KO, PPT1-/-, and 3KO mice. Autofluorescent accumulation is present in both the 3KO and PPT1-/- mice compared to the 2KO and WT brains. (B) There is a significant increase ($p<0.0001$) in autofluorescent material in the PPT1-/- and 3KO mice compared to WT and 2KO mice. Interestingly, there is a significant decrease in autofluorescent load in the 3KO mice compared to PPT1-/- mice ($p<0.0023$).

Neurodegeneration

Given that neuronal loss is a hallmark feature of INCL, de Olmos cupric silver staining was performed to assess the levels of neurodegeneration present in the 3KO brains (Figure 5). When neurons undergo degeneration in the CNS, they have a high binding affinity for silver causing both cell bodies and processes to appear 'blackened' with this staining method. Thus, we first examined the distribution of silver staining in the 3KO brain. Previous studies in the PPT1-/- mice demonstrated the neuronal loss was largely found within the thalamus, cortex, cerebellum, and hippocampus of aged mice (Griffey et al., 2005; Griffey et al., 2006). In fact, the distribution of neurodegeneration in the 3KO brains mirrored the pathology observed in the PPT1-/- brains. Globally, degenerating neurons were present within the cortex, thalamus, hippocampus, and cerebellum at 5 mos. of age (Figure 5A). In the cortex, 'blackened' cell bodies of dying neurons are primarily localized to layers II & V while degenerating axons litter the cortex. Diffuse staining throughout the thalamus is present, most notably in the afferent and efferent fibers associated with thalamic nuclei. Intense staining is found the cerebellum, with the cerebellar white matter densely stained. Additionally, darkened cell bodies are found within the Purkinje cell layer demonstrating degeneration in the 3KO cerebellum similar to the PPT1-/- brain. Darkly stained profiles were also found in the CA1 field of the hippocampus as well as degenerating processes filling the stratum radiatum. Based on these findings, the distribution of neurodegeneration within the 3KO brains mimics the observations found in the PPT1-/- mice.

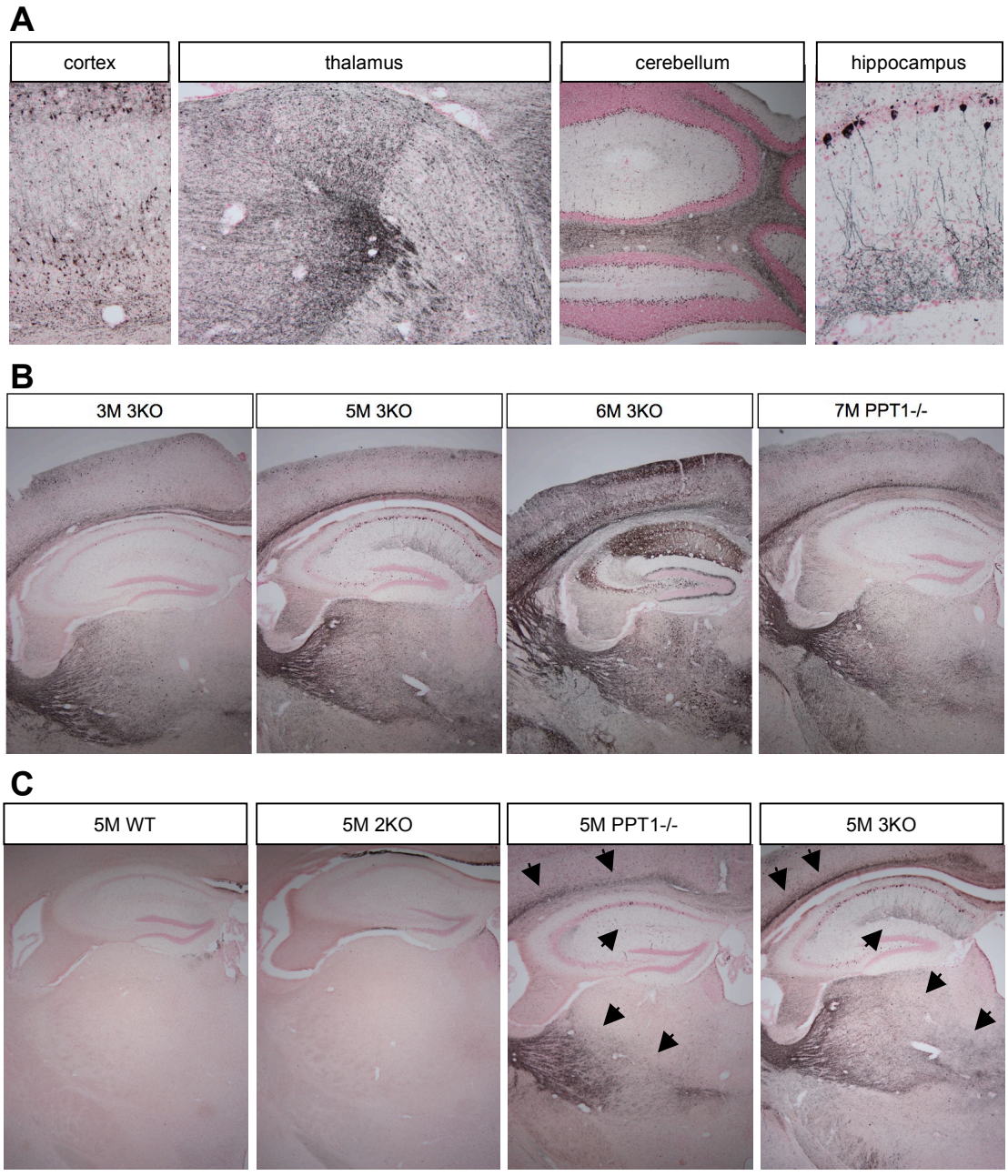

Figure 5. Neurodegeneration, as visualized by silver degeneration staining, in the GFAP-/-, Vimentin-/-, PPT1-/- mice. (A) Representative images from the cortex, thalamus, cerebellum, and hippocampus of 5 mo. old 3KO mice. Darkly stained cell bodies are present in the cortex and CA1 field of the hippocampus, while degenerating axons are present in the thalamus and cerebellar white matter tracts. (B) Time course of neurodegeneration in the 3KO mouse. As the 3KO mice age, the intensity and distribution of silver staining increases demonstrating an increase in neurodegeneration. Interestingly, the level of degeneration in a 7 mos. PPT1-/- brain appears comparable to the 3KO at 5 mos. of age. (C) Comparison of silver staining at 5 mos. of age in the WT, 2KO, PPT1-/-, and 3KO mice. At 5 mos. of age, there is no staining within the WT or 2KO brains. Staining in the PPT1-/- brain is localized to the corpus callosum, hippocampus, and thalamus. In the 3KO brain, staining in these regions appears more intense, suggesting an accelerated disease course in the 3KO brains.

In addition to the regional distribution of neurodegeneration, we also investigated the temporal progression of disease in the 3KO at 3, 5, and 6 mos. (Figure 5B). As the 3KO mice age, there is increase in silver degeneration staining throughout the thalamus, hippocampus, and cortex. Although silver staining is present in the cortex and thalamus at 3 mos. of age, the hippocampus is relatively spared. As the mice age, darkly stained profiles are apparent in the hippocampus as well as the cortex. Similarly, staining in the corpus callosum increases in intensity by 5 mos. By 6 mos. of age, the entire 3KO brain appears blackened. In areas where individual degenerating axons were easily reconciled (i.e. pyramidal neurons from the CA1 field of the hippocampus), the 6 mos. 3KO brains now appear densely stained and indiscernible. The neurodegeneration occurring in the 6 mos. 3KO is more advanced than a PPT1-/- brain at 7 mos. of age (Figure 5B), again illustrating the accelerated disease phenotype in the 3KO mice.

In addition to characterizing the distribution and progression of pathology in the 3KO, we sought to compare the relative severity of pathology in the 3KO mouse to the PPT1-/-, 2KO, and WT mice (Figure 5C). Little or no silver staining was present within either the 2KO or WT brains. In the PPT1-/- brain, blackened cellular profiles were apparent within the cortex and CA1 field of the hippocampus. In addition, blackened axonal projections filled the thalamus and corpus callosum. Qualitatively, the same pattern of staining was present in the 3KO mice but it appears to be stained more intensely. In particular, the corpus callosum and statum radiatum appeared more densely stained in the 3KO

compared to PPT1-/- mice. Furthermore, the distribution and intensity of staining increased in the 3KO cortex and thalamus. Overall, the level of neurodegeneration in the 3KO brains seems greater than that of the PPT1-/- brains.

Immune cell infiltration

H&E stained sections of 3KO brains displayed a small cell infiltrate not present in either the PPT1-/-, 2KO, or WT brains (data not shown). Hypothesizing the small cell infiltrate was composed of blood-derived leukocytes, we performed CD45 staining, a pan-leukocyte marker, in the 3KO, 2KO, and WT brains (Figure 6). At 5 mos. of age, the 3KO brains had a qualitative increase in the number of CD45-positive profiles throughout the neuraxis compared to PPT1-/- and controls (Figure 6A). Although some CD45-positive profiles were present within the PPT1-/- brains, the staining was considerably less than that of the 3KO brains. Furthermore, CD45+ staining was absent from the WT controls.

At higher magnification, it was clear that the CD45-positive cells within the 3KO brains were morphologically diverse (Figure 6B, C, D). Some of the cells resembled microglia (Figure 6B), granulocytes or macrophages (Figure 6C), and lymphocytes (Figure 6D). To ascertain what CD45 population was invading the brain parenchyma, we stained for different cell lineages with lineage specific markers. Using Iba-1 staining for microglia or brain macrophages, we demonstrated a large number of Iba-1 positive cells in both the PPT1-/- and 3KO brains (Figure 6E). The intensity of staining per cell appeared qualitatively increased in the 3KO brains, although no overt increase in the number of cells

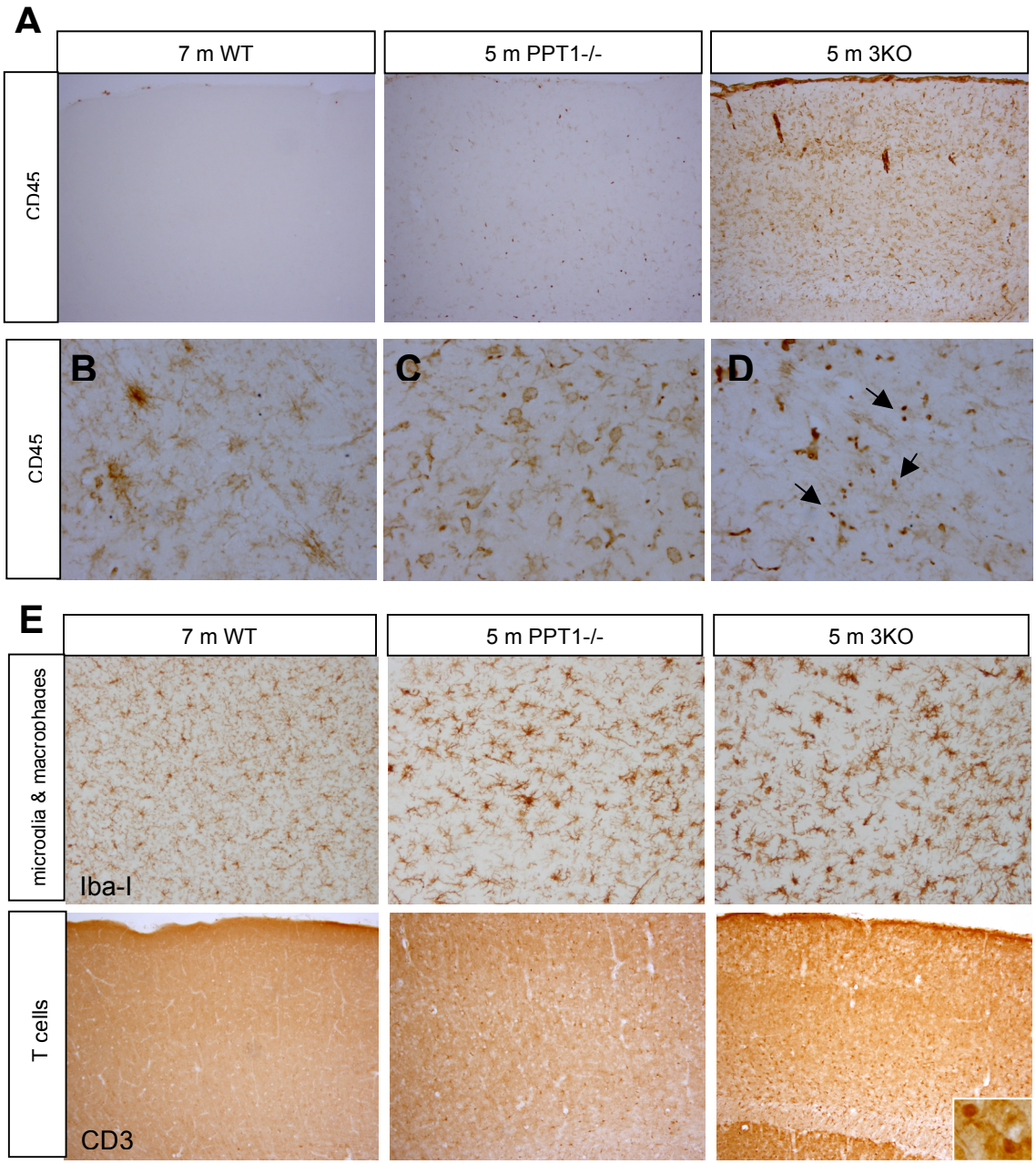

Figure 6. Immune cell infiltration into the 3KO CNS. (A) CD45, a leukocyte marker, staining in the 5 mo. 3KO, 5 mo. PPT1-/-, and 7 mo. WT cortex. Notice the large number of CD45+ cells within the 3KO cortex in comparison to either the PPT1-/- or WT brains. At higher magnification, the CD45+ cells appeared to be morphologically similar to microglia (B), granulocytes or macrophages (C), and lymphocytes (D). (E) Staining with lineage-specific markers demonstrated a large population of Iba-1+ microglia and macrophages within the PPT1-/- and 3KO brains. Interestingly, there was a large population of CD3+ T cells (small intensely staining foci) within the 3KO brains, when compared to PPT1-/- and WT.

stained was appreciable. Interestingly, CD3 staining, a T cell marker, demonstrated a marked increase in the number of CD3+ cells within the 3KO brains compared to either PPT1-/- or WT (Figure 6E). Although CD3+ cells were present in low amounts in the PPT1-/- brain, the number of CD3+ profiles in the 3KO was considerably higher than in PPT1-/- mice.

Blood brain barrier permeability and the gliovascular unit

To detect possible perturbations in the blood brain barrier (BBB), a quantitative Evan's blue (EB) assay was employed (Figure 7). When delivered intravenously, EB binds albumin and circulates throughout the blood stream. If the BBB is disrupted due to an insult or injury, the EB/albumin complex will cross the BBB into the brain parenchyma and the levels of EB within the brain can be quantified. PPT1-/-, 3KO, and WT mice were injected intravenously with EB dye and the concentration in the brain was analyzed. To serve as a positive control for BBB permeability, WT mice were given middle cerebral artery occlusions (MCAO), a procedure known to disrupt the BBB (Belayev et al., 1996). There was a significant ($p<0.001$) increase in EB concentration within the MCAO brain compared to the 3KO, PPT1-/-, or WT. Interestingly, there was no significant difference ($p< 0.1798$) in EB concentration in either 3KO or PPT1-/- brains compared to WT mice, suggesting no overall perturbation of the BBB in the 3KO mice.

Although no gross disruption of the BBB was detected in the 3KO, we investigated the structural integrity of the gliovascular unit. We immunostained 6 mo. old 3KO and WT mice for aquaporin 4 and CD31 (PECAM). Qualitative

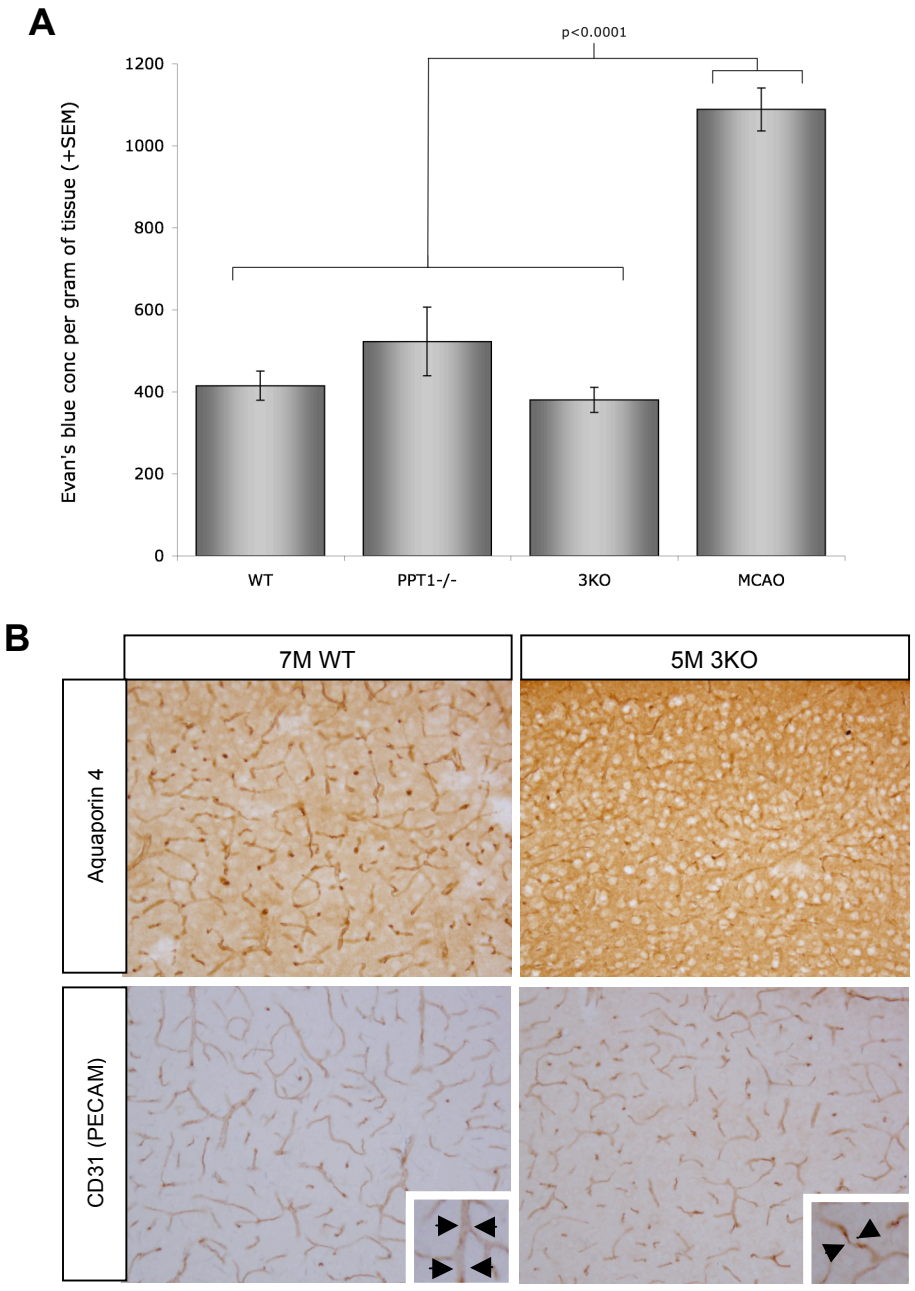

Figure 7. BBB integrity in the 3KO mouse. (A) An Evan's blue assay was performed to assess BBB permeability in the 3KO, PPT1-/-, and WT mice. There was no significant difference in the amount of Evan's blue detected in the brains of 3KO compared to PPT1-/-, or WT mice. A middle cerebral artery occluded (MCAO) mouse served as a positive control for the assay. (B) Alterations in the gliovascular unit of 3KO mice was evident with aquaporin 4 (AQP4) and CD31 (PECAM) staining. There was a redistribution in AQP4 staining in the 3KO mice compared to WT. Similarly, the PECAM staining illustrated changes in the vascular in 3KO brains.

differences in aquaporin 4 staining, a water channel localized to the endfeet of astrocytes, were apparent in the 3KO mice compared to WT (Figure 7B). In the WT cortex, aquaporin staining appears to outline the vasculature and localizes to the junction of the astrocytic endfeet and blood vessels. In the 3KO mice, however, this intimate junction between the astrocytic endfeet and vasculature appears disrupted and is replaced by a more diffuse pattern of aquaporin 4 staining throughout the cortex. It remains unclear whether there is an actual decrease in the amount or merely an altered distribution of aquaproin 4 in the 3KO brains. Alterations in CD31 (PECAM) staining were also appreciable in 3KO brains compared to WT. In the WT brains, CD31 demarcated the vascular bed traversing through the CNS. Although the size of vessle differed from vessel to vessel, the diameter of individual blood vessels appeared uniform in the WT brains (Figure 6B; inset). Conversely, regions of CD31+ vessels in the 3KO mice appeared either shrunken, dysmorphic or “pinched” (Figure 7B; inset). Together, CD31 and aquaporin 4 staining demonstrates changes in the gliovascular unit of 3KO mice.

Cytokine Levels

A panel of 23 cytokines was simultaneously evaluated in 3 mos. old 3KO, PPT1-/-, 2KO, and WT brains using a Bio-Plex cytokine assay system (Bio-Rad). Out of the 23 cytokines assayed, 13 analytes displayed increased expression in both 3KO and PPT1-/- mice compared to WT (Figure 8). In all cases, cytokine elevation in the 3KO mice was greater than the PPT1-/- mice. Many of the upregulated molecules (i.e. IL-3, IL-5, IL-6, IL-13, etc.) are traditionally secreted

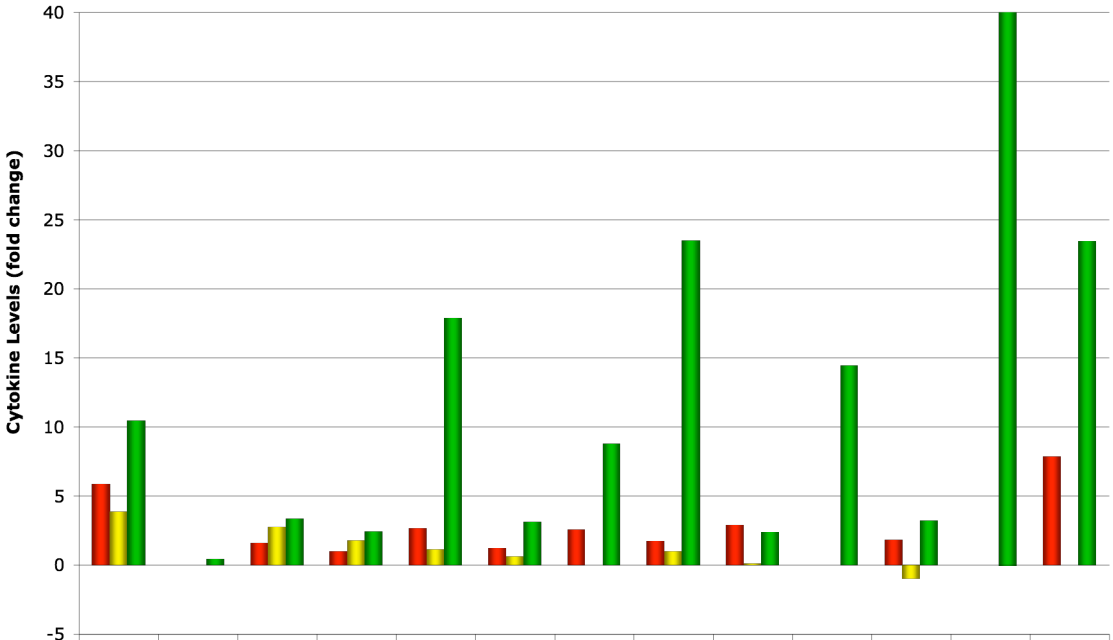

	IL-3	IL-5	IL-6	IL-13	IL-17	Eotaxin	GM-CSF	IFN-g	KC	MCP-1	MIP-1a	MIP-1b	RANTES
PPT1-/-	5.86	0.00	1.57	1.01	2.63	1.19	2.57	1.73	2.89	0.00	1.83	0.00	7.86
2KO	3.86	0.00	2.75	1.79	1.16	0.61	0.00	1.01	0.09	0.00	-1.00	0.00	0.00
3KO	10.43	0.40	3.34	2.44	17.88	3.11	8.79	23.46	2.39	14.43	3.22	131.67	23.43

Figure 8. Elevated cytokine levels in the 3KO brains. The brains from 3 mos. old 3KO, 2KO, PPT1-/-, and WT mice were simultaneously assayed for 23 different cytokines. Of those assayed, 13 cytokines were upregulated in the 3KO (green) and PPT1-/- (red) brains normalized to WT. The 3KO brains contained elevated levels of cytokines in comparison to PPT1-/-. IL-17, IFN-g, MIP-1β, and RANTES demonstrated greater than 15-fold higher cytokine levels than WT.

by T cells and stimulate additional immune cell activation. In addition, a number of the cytokines, such as MCP-1, MIP-1α, and MIP-1β, are secreted by monocytes and activate both monocytes as well as other immune cells. There were 4 cytokines with greater than a 15-fold change in levels compared to WT brains. These molecules include IL-17, IFN-g, MIP-1β, and RANTES, all of which a pro-inflammatory molecules.

Discussion

Previous research demonstrated that the first histopathological change observed in the mouse model of INCL is astrocyte activation. Astrocyte activation, as defined by GFAP upregulation, is present as early as 1-3 mos. of age in the thalamus, cortex, and cerebellum of PPT1-/- mice (Kielar et al., 2007; Macauley et al., 2009). Subsequent to this early stage gliosis, there is significant neuronal loss in the same regions. Therefore, we hypothesized that astrocyte activation plays a role in the disease pathogenesis of INCL. However, one question remained: was astrocyte activation a helpful or harmful process in INCL?

To investigate the role of astrocyte activation in INCL, we created the GFAP-/-, Vimentin-/-, PPT1-/- triple knockout (3KO) mouse. Since astrocytes first respond to injury by upregulating the intermediate filament proteins, GFAP and vimentin, increased GFAP expression is viewed as the classic sign of astrocyte activation or gliosis (Kalman, 2004; Pekny and Nilsson, 2005; Sofroniew, 2005). In addition, increased expression of IFs in activated astrocytes correlates with a change in the molecular profile and function of astrocytes. Typically responsible for homeostatic maintenance and structural support in the CNS (Ransom et al., 2003), astrocytes take on the additional role of an inflammatory-mediating cell responsible for cytokine secretion, scar formation, and the clearance of debris in the context of gliosis. Since there was a strong correlation between the upregulation of IFs and the functional shift in astrocytes, we hypothesized that by knocking out GFAP and its co-polymerizing IF protein,

vimentin, we would alter the manner in which astrocytes respond to injury. Thus, by creating the 3KO mouse, we could evaluate whether astrocyte activation is helpful or harmful in a mouse model of INCL.

Our first goal was to investigate whether the classic features of INCL were reproduced in the 3KO mice. Since the brains from INCL patients display an overall atrophy, cortical thinning, autofluorescent accumulation, and widespread neurodegeneration, we chose to investigate these pathological changes in the 3KO mouse. Interestingly, we found that the 3KO mouse displayed the same pathological features as the PPT1-/- mice and patients with INCL. The 3KO mice suffered premature death by 28 weeks of age compared to 2KO and WT mice. Similarly, there was both a global brain and regional atrophy observed in the 3KO mice compared to controls at an end stage of disease. Furthermore, the brains from 3KO mice displayed an increase in autofluorescent material, a hallmark of INCL. Most importantly, silver staining demonstrated that the regional distribution of neurodegeneration matched the pattern of pathology seen in the PPT1-/- or INCL brains. These findings demonstrate that in the absence of the IF proteins, GFAP and Vimentin, the pathological changes associated with INCL are reproduced in the 3KO mouse. Thus, the introduction of two novel mutations (i.e. GFAP and Vimentin deficiencies) onto the PPT1-/- background did not create a novel disease phenotype. Therefore, the 3KO mouse is an excellent model to investigate the effects of altered astrocyte activation on clinical features of INCL.

Although the hallmarks of INCL are recapitulated in the 3KO mice, the

progression of disease is altered compared to the PPT1-/- mice. In the absence of the IF proteins, GFAP and Vimentin, the time course of disease is accelerated compared to the PPT1-/- mice. On nearly every parameter measured, the 3KO mice displayed either an early onset of disease (i.e. premature death & brain atrophy) or an increased severity of disease at a particular time point (i.e. cortical thinning & neurodegeneration). This demonstrated that astrocyte activation is a protective feature of disease in INCL. In the absence of GFAP and Vimentin upregulation, the disease phenotype present in the PPT1-/- mice displays an early onset and increased severity.

The one notable exception to the accelerated disease course in the 3KO mouse is autofluorescent accumulation. Although both the 3KO and PPT1-/- brains demonstrate an increase in autofluorescent storage compared to 2KO and WT mice, the 3KO mice have significantly less material compared to PPT1-/- mice. This finding has several possible explanations. Most likely, there could be less autofluorescent material in the 3KO mice because there is greater neurodegeneration resulting in fewer cells to accumulate stored substrates. Conversely, it is plausible that the 3KO mice do not accumulate storage pathology as rapidly as PPT1-/- mice. Thus, the causal relationship between autofluorescent accumulation and neurodegeneration remains poorly understood and warrants further study.

In an effort to investigate the underlying mechanism causing the accelerated phenotype in 3KO mice, we investigated the presence of inflammatory cells within the 3KO brains. In fact, we detected the presence of

CD45-positive cells, or leukocytes, in the brains of 5-month-old 3KO mice, a phenomenon absent in the PPT1-/- brains at a comparable age. Interestingly, if PPT1-/- brains at 7 mos. of age are stained with a CD45 antibody, CD45+ leukocytes are present in the brain. Again, suggesting that the same disease processes are present in the 3KO but exacerbated when compared to the PPT1-/- mice. The CD45+ cells within the 3KO brains were morphologically diverse. Through cell lineage-specific markers, CD3 and Iba-1 staining, we showed a large T cell and monocyte population within the 3KO brains, respectively. We hypothesize that the infiltration of T cells and monocytes is contributing to the accelerated disease course observed in the 3KO mice. Other neurodegenerative disorders, such as multiple sclerosis (McCandless and Klein, 2007), Krabbe disease (Wu et al., 2001), and West Nile viral infection (Shrestha et al., 2003), demonstrate the presence of peripheral immune cells in the CNS and it is hypothesized that this phenomenon is playing an active role in disease pathogenesis (Chavarria and Alcocer-Varela, 2004; Lucas et al., 2006).

To examine the possible mechanisms for T cell and monocyte entry into the CNS, our work focused on the blood brain barrier in the 3KO mice. Interestingly, the astrocytes that first display an increase in GFAP immunoreactivity are cells in intimate contact with the vasculature (data not shown). Postulating that the integrity of the BBB was compromised in the 3KO mice, we investigated the ability of a large EB-albumin complex to cross the BBB. Interestingly, no gross perturbation of the BBB was appreciable in either the 3KO or PPT1-/-. We further examined the BBB integrity by investigating the structural

composition of the gliovascular unit. By staining the 3KO and WT brains with aquaporin 4 and CD31 (PECAM), we demonstrated both a redistribution in aquaporin 4 staining as well as dysmorphic blood vessels in the 3KO brain. This suggests that there are alterations in the gliovasucular unit in the 3KO mice when compared to WT. Changes in both aquaporin 4 and PECAM expression have been implicated in neurodegenerative diseases and disruptions in the BBB that facilitate leukocyte entry into the CNS (Chavarria and Alcocer-Varela, 2004; Nesic et al., 2006). Based on these observations, we hypothesize that IFs are necessary for maintaining the gliovascular unit during astrocyte activation. In the absence of intermediate filament proteins, the structural organization of the BBB becomes compromised and allows for leukocyte entry into the CNS, thus exacerbating disease.

Given that the BBB is not only a structural barrier but also a molecular barrier, we sought to investigate the molecular signals expressed by the CNS that are responsible for the influx of leukocytes. Therefore, we performed a Bio-Plex mouse cytokine assay, which screens the levels of 23 different cytokine simultaneously. At 3 mos. of age, there was a notable increase in 13 cytokines in both the 3KO and PPT1-/- brains. In all cases, cytokine evaluations in the 3KO mice were greater than those seen in PPT1-/- mice. In addition to changes in the gliovascular unit, this finding demonstrates that increased cytokine expression could be responsible for the influx of peripheral immune cells into the CNS.

Of the cytokines with increased expression levels, many of the molecules

(i.e. IL-3, IL-5, IL-6, IL-13, etc.) are traditionally secreted by T cells and responsible for the stimulation and activation of other immune cells (Doan et al., 2007; Dong and Benveniste, 2001; Rengarajan et al., 2000). Similarly, a number of the cytokines normally secreted by monocytes/macrophages, such as MCP-1, MIP-1α, and MIP-1β, are responsible for the activation of other immune cells (Cocchi et al., 1995). Given the large T cell and monocyte populations within the 3KO brains, it is not surprising that this set of cytokines is upregulated. Interestingly, several of the cytokines expressed in the 3KO and PPT1-/- brains are also routinely expressed by astrocytes during neuroinflammation, including IL-6, KC, GM-CSF, RANTES, and MCP-1 (Dong et al). Although it is unclear what cells types are responsible for the elevated cytokine levels, it is clear that a large neuroinflammatory response is occurring within the CNS of 3KO brains.

Of the cytokines upregulated, there were four cytokines with a greater than 15-fold increase in expression. These molecules include IL-17, IFN-g, MIP-1β, and RANTES. Not surprisingly, IL-17, a pro-inflammatory molecule responsible for the induction of numerous cytokines (e.g. IL-6, GM-CSF) and chemokines (e.g. IL-8, MCP-1) in a variety of cell types (e.g. endothelial cells, macrophages), demonstrated a 17.9-fold increase in cytokine levels in the 3KO brains. Similarly, interferon gamma (IFN-g), one of the most common pro-inflammatory cytokines in the CNS during disease or injury, displayed 23.4-fold change compared to WT. IFN-g is known to be a potent inducer of class II MHC expression in astrocytes, which is subsequently responsible for the activation of both T cells and macrophages. Furthermore, production of IFN-g can damage

the BBB due to cytotoxic effects on endothelial cells (Chavarria). Produced by macrophages, MIP-1β is a chemotactic cytokine responsible for the recruitment of granulocytes as well as the stimulation and release of additional cytokines by monocytes. Interestingly, RANTES, often expressed by astrocytes, is another chemotactic cytokine responsible for the recruitment of T cells and other leukocytes to sites of inflammation. Given the high level of expression of these four cytokines, it is not surprising that an invading leukocyte population was detected in the brains of the 3KO mice or that an increase in neurotoxic insults was appreciable in the CNS.

The goal of this study was to investigate the role of astrocyte activation, as defined by GFAP upregulation, in INCL. To do so, we created the GFAP-/-, Vimentin-/-, PPT1-/- triple knockout mouse and investigated the effects of knocking out the intermediate filament proteins on the disease progression associated with INCL. Although we found that PPT1-/- mice lacking GFAP and Vimentin displayed the classic features of INCL, the 3KO mice displayed a more accelerated course of disease compared to PPT1-/- mice alone. The 3KO mice displayed either an early onset of disease (i.e. premature death & brain atrophy) or an increased severity of disease at a particular time point (i.e. cortical thinning & neurodegeneration) when compared to PPT1-/- mice. To determine the underlying mechanisms contributing to this accelerated phenotype, we found a T cell and monocyte population in the brains of 3KO mice. Although there was no overt disruption in the BBB, there were alterations in the gliovacular unit that may be responsible for leukocyte infiltration. In addition to structural changes in the

BBB, we demonstrated increased cytokines are potentially responsible for the increased neuroinflammation in 3KO and ultimately the accelerated disease course. Taken together, these data suggest that astrocyte activation, as defined by GFAP upregulation, plays a protective role in a mouse model of INCL.

Chapter Four

Summary, Conclusions,
and Future Directions

Summary and Conclusions

Infantile neuronal ceroid lipofuscinosis (INCL) is a rare lysosomal storage disorder typified by prominent CNS involvement (Hofmann et al., 1999; Hofmann and Peltonen, 2001; Vesa et al., 1995). INCL is caused by an enzyme deficiency in the lysosomal hydrolase, palmitoyl protein thioesterase 1 (PPT1). In its absence, all cells throughout the CNS and viscera accumulate autofluorescent material (i.e. GRODs) to varying extents (Das et al., 1998; Hofmann et al., 2002; Mitchison et al., 1998; Mitchison et al., 2004; Vesa et al., 1995). Normally diagnosed by 1.5 years of age, patients with INCL present with clinical features such as blindness, seizures, motor deficits, retinal defects, and mental retardation. Underlying these clinical manifestations, pathological changes in the brain include an overall brain atrophy, cortical thinning, widespread neurodegeneration, astrocyte activation, and microglial reactivity. Invariably, INCL is fatal and leads to death by 6 years of age (Haltia et al., 1973a; Haltia et al., 1973b; Haltia et al., 1995; Hofmann and Peltonen, 2001; Vanhanen et al., 1997). Currently, there is no efficacious treatment available for INCL.

Gupta and colleagues (2001) created a mouse model of INCL, the PPT1-/- mouse. Initial characterization studies suggested that the mouse model of INCL recapitulates the human course of disease quite well(Bible et al., 2004; Griffey et al., 2004; Griffey et al., 2005; Griffey et al., 2006; Gupta et al., 2001). At an end stage of disease, the PPT1-/- mice suffered brain atrophy, cortical thinning, widespread neurodegeneration, glial activation, retinal defects, motor deficits, and seizure activity; features similar to those found in patients with INCL.

Based on these results, we believe the PPT1-/- mouse is a valuable tool for investigating the disease pathogenesis of INCL. Although the pathology of INCL patients at autopsy is well described, the underlying progression of pathology remains poorly understood. Thus, the first goal of this work was to investigate the temporo-spatial progression of cellular pathology and behavioral deficits in the PPT1-/- mouse. By gaining a better understanding of disease pathogenesis in a mouse model of INCL, we will be able to identify possible areas of therapeutic intervention for treatment of the human course of disease.

Summary of characterization studies

The goals of the characterization studies in the PPT1-/- mice were two-fold. The initial characterization studies in the PPT1-/- mouse investigated the pathology of the forebrain and demonstrated that many of the pathological changes seen in patients with INCL were mirrored in the PPT1-/- mice. Therefore, the first goal of the characterization studies was to expand the forebrain characterization to investigate the temporal changes as they occur during disease progression. These studies were carried out in collaboration with Jonathon Cooper's Lab at Kings College – London (Kielar et al., 2007).

The first pathologic change observed was astrocyte activation in both the cortex and thalamus of PPT1-/- mice at 3 mos. of age. Subsequently, there was localized neuronal loss in thalamic nuclei that coincide with the regions where astrocyte activation occurred. Beginning at 3-5 months of age, the thalamic regions affected by neuronal loss include the LGN, VPL/VPM, MGN, and Rt. Following neuronal loss in the thalamus, cortical atrophy and neuronal loss

occurred in the cortical relays of PPT1-/- mice at 5-7 mos. of age. These regions included both the visual and somatosensory cortex, which receive reciprocal input from the thalamus. Neurodegeneration within both the thalamus and cortex correlated with an increase in microglia reactivity beginning at 5 mos. of age. Similarly, the onset of seizure activity and changes in the interictal EEG pattern occurred at 7 mos. of age, coinciding with neuronal loss and glial activation within the cortex and thalamus. When taken together, this study identified a timeline for pathological changes within the forebrain. First, astrocyte activation occurs followed by neuronal loss in thalamic nuclei. Surprisingly, neurodegeneration and atrophy occur secondarily in the cortex to the thalamus. Finally, widespread microglial activation and functional deficits occur in the PPT1-/- brain.

The main goal of our characterization studies was to focus attention on the cerebellum (Macauley et al., 2009). Motor deficits (Santavuori et al., 1974) and cerebellar atrophy (Haltia et al., 1973a; Haltia et al., 1973b) are well documented in patients with INCL, but no work was done to characterize the time course of pathology within the PPT1-/- mouse. Therefore, we investigated the time course of cerebellar disease progression and motor deficits in the PPT1-/- mouse.

Similar to the findings from the forebrain studies, the first pathological change observed in the PPT1-/- cerebellum was astrocyte activation. As early as 1 month of age, there was an increase in GFAP staining throughout the vermis. The intensity and distribution of GFAP staining increased as the mice aged.

Subsequent to astrocyte activation, there was neuronal loss in the PPT1-/- cerebellum. At 3 mos. of age, degenerating Purkinje cells were present within

the anterior lobes of the cerebellum. There was a trend towards a decrease in total Purkinje cell number at 5 mos. with a significant loss in this population by 6 mos. of age. By 7 mos. of age, only 50% of all Purkinje cells remained in the PPT1-/- cerebellum. Similarly, a significant decrease in granule cell number was also seen at 7 mos. of age, but not prior to this late stage time point.

The scope of neurodegeneration occurring within the PPT1-/- cerebellum was visualized by silver degeneration staining. In a 7 mo. old PPT1-/- brain, parasagittal bands of degenerating Purkinje cells filled the cerebellar cortex of the vermis and lateral hemispheres. The molecular layer was littered with fragmented dendritic arbors associated with dying Purkinje cell neurons. In addition to their dendritic arbors, the cerebellar white matter tracts displayed an intense staining suggesting the afferant and efferent fibers of the cerebellum were undergoing neurodegeneration.

In addition to astrocyte activation and widespread neurodegeneration at 7 mos. of age, there were pathological changes within the glial population of the PPT1-/- mouse. There are numerous changes in the Bergmann glia suggestive of astrocyte dysfunction or death. There are decreases or losses in markers like S100β and glutamine synthetase. Furthermore, there are decreases in glutamate transporter staining, such as GLAST and to a lesser degree, GLT-1. The loss of these markers demonstrates a primary pathology intrinsic to the astrocyte that occurs in addition to early stage astrocyte activation. In addition to the astrocytes, there is microglia activation beginning at 5 mos. of age as visualized by F4/80 staining. The number, intensity and distribution of F4/80

stained cells increase as the PPT1-/- mice age. Moreover, there is a shift in the morphology of F4/80+ monocytes, from small, ramified microglia to larger, more amoeboid shaped macrophages. Finally, a decrease in myelin is appreciable at 7 mos. of age in the cerebellar white matter tracts of PPT1-/- mice. The staining for myelin appears less intense and patchy at an end stage of disease. Taken together, these findings demonstrate that pathology within the PPT1-/- cerebellum is not limited to the neuronal population. Rather, there is considerable pathology localized to the glial population, including the astrocytes, microglia, and oligodendrocytes, in the PPT1-/- mice.

Finally, we sought to investigate how the changes in the underlying pathology correlated with motor deficits in the PPT1-/- mice. A constant speed rotorod paradigm demonstrated significant motor deficits in the PPT1-/- beginning at 5 months of age. The performance of the PPT1-/- mice further declined as the mice aged, with a nadir in performance by 7 months of age. The alterations in motor function mirrored the Purkinje cell loss in the PPT1-/- mice.

Conclusions from characterization studies

The characterization studies provide a comprehensive time course of disease progression in the PPT1-/- mice. These findings cause a shift in how we view the pathogenesis of INCL. Historically, work performed on INCL patients at autopsy brought focus to certain pathological changes within the brain, including brain atrophy, cortical thinning, neuronal loss, and autofluorescent accumulation. Although these pathological changes are rightfully hallmarks of INCL, our work

demonstrates that many of these features occur at the end stage of disease and provide little insight into the evolution of pathology in this disorder.

First, the dogma surrounding this disease is very neuro-centric and gives little attention to the profound glial involvement in this disease. Our studies demonstrate that not only is astrocyte activation the first pathological change observed in INCL, but prominent glial involvement, including astrocytes, microglia, and oligodendrocytes, is a key component to this disease. Thus, understanding the relative contributions of each cell type to disease pathology is important for the development and direction of therapies (see Future Directions).

Secondly, given the data at autopsy and the functional deficits experienced by INCL patients, much of the focus for therapeutic intervention has centered on targeting the cortex. Since neurodegeneration and atrophy in the cortex is a rather late stage phenomenon, intervention should occur earlier to prevent the disease progression and in areas affected at the onset of disease. Thus, interventions targeting astrocyte activation or the pathological changes in the thalamus would be better suited for early interventions to maximize therapeutic outcomes (see Future Directions).

Finally, these characterization studies demonstrate both the extent and severity of disease in INCL. Patients with INCL suffer from a complex set of clinical features, with extensive underlying pathology, which involves the majority of the CNS. Thus, in order to properly treat these disorders, one form of targeted therapy will not be sufficient. To provide patients with a therapeutic benefit,

multiple therapies aimed at a variety of disease pathologies and targets must be employed (see Future Directions).

Summary of findings from the GFAP-/-, Vimentin-/-, PPT1-/- mice

Based on the finding that the first pathological change observed in the PPT1-/- mouse was GFAP upregulation, therefore, we investigated whether astrocyte activation and GFAP upregulation was helpful or harmful to the CNS in INCL. To accomplish this, we created the GFAP-/-, Vimentin-/-, PPT1-/- triple knockout (3KO) mouse by breeding the GFAP-/-, VImentin-/- double (2KO) mouse to the PPT1-/- mouse (Gupta et al., 2001; Pekny et al., 1999). First, we investigated the effects of knocking out GFAP and Vimentin on disease parameters specific to INCL. Interestingly, we found that PPT1-/- mice lacking GFAP and Vimentin displayed similar clinical features of INCL, but an accelerated time course when compared to PPT1-/-, 2KO, or WT mice. The 3KO mice died earlier than the PPT1-/-, 2KO, and WT mice. Moreover, the 3KO brains atrophied quicker than PPT1-/- mice and controls. Both cortical atrophy and neurodegeneration was more severe in 3KO mice compared to PPT1-/- mice. Thus, lacking the intermediate filament proteins, GFAP and Vimentin, increased the pervasiveness of the INCL phenotype in the PPT1-/- mouse.

One possible explanation for this accelerated phenotype is due to the influx of peripheral immune cells into the CNS of the 3KO mice. Normally absent from the brain parenchyma, we found CD45-positive cells, or leukocytes, littering the neuraxis of the 3KO brains. Staining with cell lineage specific markers illustrated the presence of CD3+ T cells and Iba-1+ macrophages and microglia

in the 3KO brains, cells normally absent from a healthy CNS. Postulating that the trafficking of leukocytes into the CNS is due to a perturbation of the BBB, we investigated BBB integrity in the 3KO mice. We found no gross disruption in the BBB of 3KO mice when compared with PPT1-/- or WT mice. However, we did find structural alterations in the gliovascular unit of 3KO mice. There was a redistribution of aquaporin 4 staining suggesting changes at the endfeet of 3KO astrocytes. Furthermore, changes in PECAM staining demonstrated dysmorphic blood vessels in the 3KO brain. Together, these changes demonstrated alterations in the gliovascular unit of 3KO mice. Since the BBB is both a physical and molecular barrier in the CNS, we investigated the cytokine profiles in the 3KO brains in comparison to PPT1-/-, 2KO, and WT brains. In total, there were 13 cytokines upregulated in the 3KO and PPT1-/- brains. In every case, the cytokines elevation was greater in the 3KO brains in comparison to the PPT1-/- brains, in some cases up to a 40-fold increase compared to WT. The molecules that were upregulated were largely pro-inflammatory molecules, chemokines for lymphocyte and monocyte chemotaxis, as well as stimulatory molecules for immune cell activation (Dong and Benveniste, 2001). Thus, in the absence of the intermediate filament proteins, GFAP and Vimentin, there are signals within the PPT1-/- mouse brains that actively recruit peripheral immune cells into the CNS. We hypothesize this leukocyte infiltration exacerbates disease, specifically the key features of INCL, in the 3KO mouse.

Conclusions from the 3KO mice

Our studies in the 3KO mice show that astrocyte activation, as defined by GFAP upregulation, is a protective process in INCL. In the absence of GFAP and its copolymerizing IF, vimentin, the clinical features of INCL are the same in the PPT1-/- and 3KO mice, but increase in severity causing the mice to suffer an accelerated time course of disease. Thus, we hypothesize that early stage astrocyte activation is protecting the CNS from injury. Furthermore, our findings suggest that the upregulation of IFs is necessary to maintain the structural integrity of the blood brain barrier. And in their absence, leukocyte infiltration from the periphery can occur and exacerbate CNS disease.

Although we described changes in the 3KO mice at an end stage of disease, a thorough characterization of disease progression in the 3KO brains should be performed (See Future Directions). By investigating temporal changes in the 3KO mice, we could more thoroughly dissect the role astrocyte activation plays in INCL. Specifically, if we are able to elucidate the function of astrocyte activation at early time points, we might be able to gain a better understanding of why astrocyte activation is the first change observed in INCL.

Beyond the role of astrocyte activation in INCL, these studies begin to help elucidate the function of IF upregulation and its relationship to the function of activated astrocytes in a model of chronic neurodegeneration. To date, little is known about how IF upregulation and changes in the astrocyte's morphology relates to changes in cell function. Increased GFAP expression is always used to demonstrate the presence of gliosis in CNS injury and disease, but little has been done to show the functional significance of GFAP upregulation in the

context of astrocyte activation. Studies in the 3KO mice demonstrate a correlative role between IF upregulation and the functional changes associated with astrocyte activation.

By using the PPT1-/- mouse as our model of disease, we are also investigating the role of astrocyte activation in a chronic, neurodegenerative disorder of the CNS. Contrary to most of the work in the field, gliosis is normally studied in response to an acute injury, including models of tramautic brain injury, spinal cord lesion, acute infection, stroke, etc. It is most likely that the manner with which the CNS responds to a focal, acute injury differs from its response to a disease that is chronic, progressive, and widespread. Therefore, the 3KO mouse provides us with an excellent tool to study the mechanisms by which reactive astrocytes respond to a persistent, widespread disease (See Future Studies).

Finally, the 3KO mouse illustrates the dualistic nature of astrocyte activation. Although astrocyte activation is overall a protective process in INCL, there are aspects of this inflammatory process that are harmful to the CNS. For example, we demonstrated in the PPT1-/- mouse that cytokines responsible for leukocyte trafficking into the CNS are upregulated, while the 3KO model illustrated how leukocyte entry into the CNS correlates disease severity. Although gliosis is a process that adds protection to an injured brain (i.e. PPT1-/- brain), there are aspects of gliosis that are suboptimal (i.e. cytokine production) and can be targeted for therapeutic intervention (see Future Directions).

Future Directions

Cell-specific contributions to INCL

Findings from the characterization studies performed in the PPT1-/- mice chronicled the scope of pathology observed within the PPT1-/- brains. Although neurodegeneration was a widespread, pervasive phenomenon in the PPT1-/- brains, the extent of glial pathology had largely gone unappreciated until now. We demonstrated that astrocytes, microglia, and oligodendrocytes are all involved in the disease pathology of INCL. Given that PPT1-deficiency is a global phenomenon in INCL and that glial cells are reported to express PPT1, perhaps it is not surprising that these cell types are equally as affected as neurons within the CNS. However, to move towards a treatment of INCL, it would be beneficial to investigate the relative contribution of each cell type to disease pathology. This would allow us to better target therapies to the correct cell lineage.

Investigating the specific effects of cell lineages on INCL pathology is not easy to accomplish. Attempting to isolate cell-specific effects in any disorder is difficult but there are unique benefits and problems when studying lysosomal storage diseases. The main difficulty comes from the principle of "cross-correction". "Cross-correction" refers to the phenomenon in which lysosomal enzymes are expressed within the target cell as well as secreted and taken up by adjacent cells (Neufeld and Fratantoni, 1970). This allows for one cell to act as an enzyme depot for all cell types within a microenvironment. Although the

principle of “cross-correction” is beneficial for treatment of INCL and other LSDs, it complicates studying the cellular pathology in disease. Therefore, traditional approaches using cell-specific promoters, transgenic technology, and the native PPT1 protein are not suitable for investigating the cellular mechanisms of disease in INCL.

One way to circumvent the principle of “cross-correction” is to develop a means of sequestering lysosomal enzymes to prevent secretion. This would allow for the specific correction of a target cell while keeping the diseased milieu intact. Guarnieri and his colleagues (Guarnieri et al., 1993) identified a 35 amino acid peptide sequence, containing the transmembrane domain and cytoplasmic tail of lysosome-associated protein, LAMP-1, that is both necessary and sufficient for lysosomal trafficking and retention. Therefore, it is possible to fuse a short LAMP1 peptide sequence to the carboxyl terminus of PPT1 to effectively create a lysosomal enzyme that is properly targeted to and retained by the lysosome (Marathe et al., 2000). In fact, this approach was successfully used by Marathe et al (2000) to create a mouse model of Niemann-Pick Type B disease.

Using this approach to sequester the PPT1 enzyme within a specific cell type can then be used in concert with other standard gene transfer or transgenic approaches to investigate cellular mechanisms of disease. By sequestering PPT1 within neurons or glia, it is possible to investigate the effects of selectively restoring function to a specific cell lineage on both the pathological and functional changes that occur in INCL. This will provide valuable insights into the process

of disease pathogenesis as well as provide valuable targets for treatment of INCL.

Further characterization of the 3KO mice

Our initial characterization studies in the 3KO mice provided insight into the role of astrocyte activation in INCL. However, further work needs to be done to investigate the temporal changes in the 3KO mice. Specifically, by clarifying the function of astrocyte activation at early time points, we can gain a better understanding of why astrocyte activation is the first change observed in INCL. Determining the timeline for the structural and molecular changes in the BBB would also provide insight into the role of activated astrocytes in INCL. We demonstrated that increased expression of cytokines leads to an influx of peripheral immune cells into the CNS. However, we failed to demonstrate what initial factors were responsible for cytokine upregulation and immune cell entry in the CNS. By studying the 3KO pathology at earlier stages, we can uncover the true functions of activated astrocytes and work towards a better definition of what this process entails.

Effective targeting of therapeutics in INCL

Our characterization studies in the PPT1-/- mouse established a time line of CNS pathology that challenged the current dogma in the field (Kielar et al., 2007; Macauley et al., 2009). First, we showed that astrocyte activation occurs early in the INCL, not later as was first hypothesized. Secondly, we demonstrated that the thalamus is the first area to undergo neuronal loss, with degeneration in the cortex occurring secondarily. Lastly, we illustrated that

pathological changes in INCL are not limited to a neuronal population, but also include glia. Based on these findings, we need to alter the framework by which we develop and target therapies for INCL.

One of the most promising options for the treatment of LSDs is CNS-directed gene therapy (Daly and Sands, 1998; Macauley and Sands, 2009a; Sands and Davidson, 2006; Sands and Haskins, 2008). Since INCL and most other LSDs are due to a single enzyme deficiency, the simplest therapeutic approach is enzyme replacement therapy (ERT). One way to ensure long-term, CNS-directed enzyme replacement therapy is through the use of viral vectors. Currently, adeno-associated virus (AAV) and lenti-viral vectors are touted as the best options for CNS-directed therapy due to their tropism, long-term expression, low immunogenicity, and transduction efficiencies. However, many of the researchers investigating the use of viral vectors for the treatment of NCLs (Cabrera-Salazar et al., 2007; Griffey et al., 2004; Griffey et al., 2005; Griffey et al., 2006; Passini et al., 2006) are using vectors with a tropism for neuronal transduction (i.e. AAV-1, -2, and -5) (Burger et al., 2004). Given the significant glial pathology in INCL and other forms of NCLs, findings from these therapy studies could mistakenly suggest that viral vectors are inefficient therapeutic tools. Therefore, experiments need to be performed that directly compare the efficacy of glial- or neuronal-directed therapies for the treatment of INCL and other LSDs.

Given that the pathology encompasses the entire neuraxis in INCL, the task of directing therapies is quite challenging. In mouse models of LSDs like

INCL, researchers are using novel therapies and methodologies in attempt to treat the brain in its entirety (Bobo et al., 1994; Chen et al., 2009; Daly et al., 2001; Dodge et al., 2009). Although this approach is ideal for disorders like INCL, there may be alternative ways to slow disease progression until a comprehensive treatment strategy is developed. For example, the first area to display neuronal loss and glial activation is the thalamus, specifically the lateral geniculate nucleus (LGN). Since previous research has demonstrated that early interventions increase therapeutic efficacy (Cabrera-Salazar et al., 2007), the thalamus should be targeted early to evaluate the effect of focal treatments on disease progression in INCL. While safety and ethical issues surrounding the use of stem cell and gene therapies remain unanswered, direct infusions of recombinant enzyme into the CNS is a promising treatment for LSDs. Therefore, preclinical experiments targeting the thalamus should be performed in the PPT1-/- mouse to determine if a single infusion of recombinant enzyme, viral vectors, or stem cells can significantly delay or treat the clinical features of disease.

Glial activation as a therapeutic target

Based on our findings that cytokine levels are highly elevated in both the 3KO mice and PPT1-/- brain due to glial activation, we hypothesized that disrupting the cytokine cascade is a possible target for therapeutic intervention. Our data demonstrate that when cytokines are increased to a certain threshold, leukocyte entry in the CNS occurs and the disease course is exacerbated. We observed leukocyte entry into the CNS in the 3KO mice, but not the PPT1-/- mice, because of the relative cytokine elevation. Therefore, by keeping the

cytokine levels stable, we believe we can delay the neuroinflammatory process response for accelerating the disease course of INCL.

Recently, the laboratory of Dr. Martin Watterson developed a novel, small molecule called Minozac that targets the neuroimmune response generated by astrocytes and microglia (Hu et al., 2007; Ralay Ranaivo et al., 2006). Minozac is non-toxic, bioavailable and able to cross the blood brain barrier (BBB). It selectively acts on glia by knocking down pro-inflammatory cytokines that recruit circulating immune cells into the CNS. When administered to mice, it showed positive results in models of Alzheimer's(Ralay Ranaivo et al., 2006), EAE(Karpus et al., 2008), TBI(Lloyd et al., 2008; Somera-Molina et al., 2007), and epilepsy(Lloyd et al., 2008; Somera-Molina et al., 2007), all of which present with gliosis and neuroinflammation. In each of the four diseases, treatment of Minozac reduced the number of activated astrocytes and microglia, decreased cytokine levels and improved behavioral deficits. Of particular interest, in a kainic acid-induced model of epilepsy(Tian et al., 2005), researchers demonstrated that Minozac diminished the glial activation associated with seizure onset, which decreased the susceptibly of mice to future seizures. Thus, the effects of Minozac in models of CNS disease show great promise, suggesting that Minozac is a good candidate for treating INCL.

Combination therapy in INCL

Treatment for LSDs is as simple as it is complex. Contrary to other CNS diseases like Alzheimer's, Parkinson's, or Huntington's disease, the etiology of INCL is known. Disease pathology in INCL is due to an enzyme deficiency and

thus, enzyme replacement therapy rescues the deficits. Thus, in many ways, the treatment strategies for LSDs are quite simple and unsophisticated. The problem arises in the scope of therapy necessary to treat those afflicted with these diseases. Contrary to other CNS disorders, the disease pathology associated with INCL involves the entire neuraxis as well as many visceral tissues. Thus, an effective treatment strategy must include targeting a variety of cell types in a diverse set of tissues. It is unlikely that one therapy will be able to accomplish this feat in isolation. Thus, we propose to use several therapies in combination for the treatment of INCL.

The use of viral vectors to target PPT1 expression to the CNS is partially efficacious in newborn PPT1-/- mice(Griffey et al., 2004; Griffey et al., 2005). Although many histopathological parameters and behavioral deficits are improved, the therapeutic benefit is only partial. Thus, future work needs to use gene therapy in combination with other possible treatments for INCL. For example, Minozac, which targets the toxic effects of reactive gliosis, when used singularly this therapy will only be partially efficacious since the primary cause of INCL, a deficiency in PPT1, remains untreated. Therefore, treating PPT1-/- mice with Minozac, in combination with other approaches might result in an additive or better yet, synergistic effect in patients with INCL.

Furthermore, gene therapy and Minozac could be paired with a third drug for the treatment of INCL. Cystagon, or phosphocysteamine, is responsible for disrupting thioester linkages in s-acylated proteins, a similar mode of action to the deficient enzyme, PPT1 (Lu and Hofmann, 2006; Zhang et al., 2001). In vitro

studies demonstrated that Cystagon is capable of decreasing ceroid accumulation in lymphoblasts from INCL patients. We have initiated preliminary studies using once daily injections of Cystagon into PPT1-/- mice. The cystagon treatment is non-toxic, well tolerated, and results in some clinical benefit benefit early in disease progression. Therefore, we hypothesize that Minozac in concert with Cystagon and gene therapy will result in an efficacious, synergistic treatment for INCL.

REFERENCES

Armstrong, C.L., Krueger-Naug, A.M., Currie, R.W., and Hawkes, R. (2000). Constitutive expression of the 25-kDa heat shock protein Hsp25 reveals novel parasagittal bands of purkinje cells in the adult mouse cerebellar cortex. J Comp Neurol *416*, 383-397.

Armstrong, C.L., Krueger-Naug, A.M., Currie, R.W., and Hawkes, R. (2001). Constitutive expression of heat shock protein HSP25 in the central nervous system of the developing and adult mouse. J Comp Neurol *434*, 262-274.

Aschner, M. (1998a). Astrocytes as mediators of immune and inflammatory responses in the CNS. Neurotoxicology *19*, 269-281.

Aschner, M. (1998b). Immune and inflammatory responses in the CNS: modulation by astrocytes. Toxicol Lett *102-103*, 283-287.

Ballabio, A., and Gieselmann, V. (2009). Lysosomal disorders: from storage to cellular damage. Biochim Biophys Acta *1793*, 684-696.

Bates, K.A., Fonte, J., Robertson, T.A., Martins, R.N., and Harvey, A.R. (2002). Chronic gliosis triggers Alzheimer's disease-like processing of amyloid precursor protein. Neuroscience *113*, 785-796.

Belayev, L., Busto, R., Zhao, W., and Ginsberg, M.D. (1996). Quantitative evaluation of blood-brain barrier permeability following middle cerebral artery occlusion in rats. Brain Res *739*, 88-96.

Bennett, M.J., and Hofmann, S.L. (1999). The neuronal ceroid-lipofuscinoses (Batten disease): a new class of lysosomal storage diseases. J Inherit Metab Dis *22*, 535-544.

Bible, E., Gupta, P., Hofmann, S.L., and Cooper, J.D. (2004). Regional and cellular neuropathology in the palmitoyl protein thioesterase-1 null mutant mouse model of infantile neuronal ceroid lipofuscinosis. Neurobiol Dis *16*, 346-359.

Bobo, R.H., Laske, D.W., Akbasak, A., Morrison, P.F., Dedrick, R.L., and Oldfield, E.H. (1994). Convection-enhanced delivery of macromolecules in the brain. Proc Natl Acad Sci U S A *91*, 2076-2080.

Burger, C., Gorbatyuk, O.S., Velardo, M.J., Peden, C.S., Williams, P., Zolotukhin, S., Reier, P.J., Mandel, R.J., and Muzyczka, N. (2004). Recombinant AAV viral vectors pseudotyped with viral capsids from serotypes 1, 2, and 5 display differential efficiency and cell tropism after delivery to different regions of the central nervous system. Mol Ther *10*, 302-317.

Cabrera-Salazar, M.A., Roskelley, E.M., Bu, J., Hodges, B.L., Yew, N., Dodge, J.C., Shihabuddin, L.S., Sohar, I., Sleat, D.E., Scheule, R.K.*, et al.* (2007). Timing of therapeutic intervention determines functional and survival outcomes in a mouse model of late infantile batten disease. Mol Ther *15*, 1782-1788.

Calero, G., Gupta, P., Nonato, M.C., Tandel, S., Biehl, E.R., Hofmann, S.L., and Clardy, J. (2003). The crystal structure of palmitoyl protein thioesterase-2 (PPT2) reveals the basis for divergent substrate specificities of the two lysosomal thioesterases, PPT1 and PPT2. J Biol Chem *278*, 37957-37964.

Camp, L.A., Verkruyse, L.A., Afendis, S.J., Slaughter, C.A., and Hofmann, S.L. (1994). Molecular cloning and expression of palmitoyl-protein thioesterase. J Biol Chem *269*, 23212-23219.

Chang, M., Cooper, J.D., Sleat, D.E., Cheng, S.H., Dodge, J.C., Passini, M.A., Lobel, P., and Davidson, B.L. (2008). Intraventricular enzyme replacement improves disease phenotypes in a mouse model of late infantile neuronal ceroid lipofuscinosis. Mol Ther *16*, 649-656.

Chavarria, A., and Alcocer-Varela, J. (2004). Is damage in central nervous system due to inflammation? Autoimmun Rev *3*, 251-260.

Chen, Y.H., Chang, M., and Davidson, B.L. (2009). Molecular signatures of disease brain endothelia provide new sites for CNS-directed enzyme therapy. Nat Med *15*, 1215-1218.

Cocchi, F., DeVico, A.L., Garzino-Demo, A., Arya, S.K., Gallo, R.C., and Lusso, P. (1995). Identification of RANTES, MIP-1 alpha, and MIP-1 beta as the major HIV-suppressive factors produced by CD8+ T cells. Science *270*, 1811-1815.

Cooper, J.D. (2003). Progress towards understanding the neurobiology of Batten disease or neuronal ceroid lipofuscinosis. Curr Opin Neurol *16*, 121-128.

Cooper, J.D., Russell, C., and Mitchison, H.M. (2006). Progress towards understanding disease mechanisms in small vertebrate models of neuronal ceroid lipofuscinosis. Biochim Biophys Acta *1762*, 873-889.

Daginakatte, G.C., Gadzinski, A., Emnett, R.J., Stark, J.L., Gonzales, E.R., Yan, P., Lee, J.M., Cross, A.H., and Gutmann, D.H. (2008). Expression profiling identifies a molecular signature of reactive astrocytes stimulated by cyclic AMP or proinflammatory cytokines. Exp Neurol *210*, 261-267.

Daly, T.M., Ohlemiller, K.K., Roberts, M.S., Vogler, C.A., and Sands, M.S. (2001). Prevention of systemic clinical disease in MPS VII mice following AAV-mediated neonatal gene transfer. Gene Ther *8*, 1291-1298.

Daly, T.M., and Sands, M.S. (1998). Gene therapy for lysosomal storage diseases. Expert Opin Investig Drugs *7*, 1673-1682.

Das, A.K., Becerra, C.H., Yi, W., Lu, J.Y., Siakotos, A.N., Wisniewski, K.E., and Hofmann, S.L. (1998). Molecular genetics of palmitoyl-protein thioesterase deficiency in the U.S. J Clin Invest *102*, 361-370.

Doan, T., Melvold, R., Viselli, S., and Waltenbaugh, C. (2007). Immunology (Lippincott, Williams & Wilkins).

Dodge, J.C., Clarke, J., Treleaven, C.M., Taksir, T.V., Griffiths, D.A., Yang, W., Fidler, J.A., Passini, M.A., Karey, K.P., Schuchman, E.H.*, et al.* (2009). Intracerebroventricular infusion of acid sphingomyelinase corrects CNS manifestations in a mouse model of Niemann-Pick A disease. Exp Neurol *215*, 349-357.

Donato, R. (2003). Intracellular and extracellular roles of S100 proteins. Microsc Res Tech *60*, 540-551.

Dong, Y., and Benveniste, E.N. (2001). Immune function of astrocytes. Glia *36*, 180-190.

Eddleston, M., and Mucke, L. (1993). Molecular profile of reactive astrocytes--implications for their role in neurologic disease. Neuroscience *54*, 15-36.

Eng, L.F., Ghirnikar, R.S., and Lee, Y.L. (2000). Glial fibrillary acidic protein: GFAP-thirty-one years (1969-2000). Neurochem Res *25*, 1439-1451.

Galvin, N., Vogler, C., Levy, B., Kovacs, A., Griffey, M., and Sands, M. (2007). A murine model of infantile neuronal ceroid lipofuscinosis - Ultrastructural evaluation of storage in the central nervous system and viscera. Pediatr Dev Pathol, 1.

Galvin, N., Vogler, C., Levy, B., Kovacs, A., Griffey, M., and Sands, M.S. (2008). A murine model of infantile neuronal ceroid lipofuscinosis-ultrastructural evaluation of storage in the central nervous system and viscera. Pediatr Dev Pathol *11*, 185-192.

Goebel, H.H., and Wisniewski, K.E. (2004). Current state of clinical and morphological features in human NCL. Brain Pathol *14*, 61-69.

Goldstein, G.W. (1987). The blood-brain barrier: interacters between endothelial cells and astrocytes. Mead Johnson Symp Perinat Dev Med, 15-17.

Goncalves, C.A., Leite, M.C., and Nardin, P. (2008). Biological and methodological features of the measurement of S100B, a putative marker of brain injury. Clin Biochem *41*, 755-763.

Griffey, M., Bible, E., Vogler, C., Levy, B., Gupta, P., Cooper, J., and Sands, M.S. (2004). Adeno-associated virus 2-mediated gene therapy decreases autofluorescent storage material and increases brain mass in a murine model of infantile neuronal ceroid lipofuscinosis. Neurobiol Dis *16*, 360-369.

Griffey, M., Macauley, S.L., Ogilvie, J.M., and Sands, M.S. (2005). AAV2-mediated ocular gene therapy for infantile neuronal ceroid lipofuscinosis. Mol Ther *12*, 413-421.

Griffey, M.A., Wozniak, D., Wong, M., Bible, E., Johnson, K., Rothman, S.M., Wentz, A.E., Cooper, J.D., and Sands, M.S. (2006). CNS-directed AAV2-mediated gene therapy ameliorates functional deficits in a murine model of infantile neuronal ceroid lipofuscinosis. Mol Ther *13*, 538-547.

Griffin, W.S., Yeralan, O., Sheng, J.G., Boop, F.A., Mrak, R.E., Rovnaghi, C.R., Burnett, B.A., Feoktistova, A., and Van Eldik, L.J. (1995). Overexpression of the

neurotrophic cytokine S100 beta in human temporal lobe epilepsy. J Neurochem *65*, 228-233.

Guarnieri, F.G., Arterburn, L.M., Penno, M.B., Cha, Y., and August, J.T. (1993). The motif Tyr-X-X-hydrophobic residue mediates lysosomal membrane targeting of lysosome-associated membrane protein 1. J Biol Chem *268*, 1941-1946.

Gupta, P., Soyombo, A.A., Atashband, A., Wisniewski, K.E., Shelton, J.M., Richardson, J.A., Hammer, R.E., and Hofmann, S.L. (2001). Disruption of PPT1 or PPT2 causes neuronal ceroid lipofuscinosis in knockout mice. Proc Natl Acad Sci U S A *98*, 13566-13571.

Hafiz, F.B., and Brown, D.R. (2000). A model for the mechanism of astrogliosis in prion disease. Mol Cell Neurosci *16*, 221-232.

Haltia, M. (2003). The neuronal ceroid-lipofuscinoses. J Neuropathol Exp Neurol *62*, 1-13.

Haltia, M., Rapola, J., and Santavuori, P. (1973a). Infantile type of so-called neuronal ceroid-lipofuscinosis. Histological and electron microscopic studies. Acta Neuropathol (Berl) *26*, 157-170.

Haltia, M., Rapola, J., Santavuori, P., and Keranen, A. (1973b). Infantile type of so-called neuronal ceroid-lipofuscinosis. 2. Morphological and biochemical studies. J Neurol Sci *18*, 269-285.

Haltia, M., Tyynela, J., Baumann, M., Henseler, M., and Sandhoff, K. (1995). Immunological studies on sphingolipid activator proteins in the neuronal ceroid-lipofuscinoses. Gerontology *41 Suppl 2*, 239-248.

Heales, S.J., Lam, A.A., Duncan, A.J., and Land, J.M. (2004). Neurodegeneration or neuroprotection: the pivotal role of astrocytes. Neurochem Res *29*, 513-519.

Hers, H.G. (1965). Inborn Lysosomal Diseases. Gastroenterology *48*, 625-633.

Hoffmann, B., and Mayatepek, E. (2005). Neurological manifestations in lysosomal storage disorders - from pathology to first therapeutic possibilities. Neuropediatrics *36*, 285-289.

Hofmann, S.L., Atashband, A., Cho, S.K., Das, A.K., Gupta, P., and Lu, J.Y. (2002). Neuronal ceroid lipofuscinoses caused by defects in soluble lysosomal enzymes (CLN1 and CLN2). Curr Mol Med *2*, 423-437.

Hofmann, S.L., Das, A.K., Yi, W., Lu, J.Y., and Wisniewski, K.E. (1999). Genotype-phenotype correlations in neuronal ceroid lipofuscinosis due to palmitoyl-protein thioesterase deficiency. Mol Genet Metab *66*, 234-239.

Hofmann, S.L., and Peltonen, L. (2001). The neuronal ceroid lipofuscinosis. In The Metabolic and Molecular Basis of Inherited Disease, C.R. Scriver, A.L. Beaudet, W.S. Sly, and D. Valle, eds. (New York, McGraw-Hill), pp. 3877-3894.

Hu, W., Ranaivo, H.R., Roy, S.M., Behanna, H.A., Wing, L.K., Munoz, L., Guo, L., Van Eldik, L.J., and Watterson, D.M. (2007). Development of a novel therapeutic suppressor of brain proinflammatory cytokine up-regulation that attenuates synaptic dysfunction and behavioral deficits. Bioorg Med Chem Lett *17*, 414-418.

Hulse, R.E., Kunkler, P.E., Fedynyshyn, J.P., and Kraig, R.P. (2004). Optimization of multiplexed bead-based cytokine immunoassays for rat serum and brain tissue. J Neurosci Methods *136*, 87-98.

Kalman, M. (2004). Glial reaction and reactive glia, Vol 31 (Amsterdam, Elsevier).

Karpus, W.J., Reynolds, N., Behanna, H.A., Van Eldik, L.J., and Watterson, D.M. (2008). Inhibition of experimental autoimmune encephalomyelitis by a novel small molecular weight proinflammatory cytokine suppressing drug. J Neuroimmunol *203*, 73-78.

Kielar, C., Maddox, L., Bible, E., Pontikis, C.C., Macauley, S.L., Griffey, M.A., Wong, M., Sands, M.S., and Cooper, J.D. (2007). Successive neuron loss in the thalamus and cortex in a mouse model of infantile neuronal ceroid lipofuscinosis. Neurobiol Dis *25*, 150-162.

Kielian, T., and Esen, N. (2004). Effects of neuroinflammation on glia-glia gap junctional intercellular communication: a perspective. Neurochem Int *45*, 429-436.

Kinouchi, R., Takeda, M., Yang, L., Wilhelmsson, U., Lundkvist, A., Pekny, M., and Chen, D.F. (2003). Robust neural integration from retinal transplants in mice deficient in GFAP and vimentin. Nat Neurosci *6*, 863-868.

Kobayashi, K., Hayashi, M., Nakano, H., Fukutani, Y., Sasaki, K., Shimazaki, M., and Koshino, Y. (2002). Apoptosis of astrocytes with enhanced lysosomal activity and oligodendrocytes in white matter lesions in Alzheimer's disease. Neuropathol Appl Neurobiol *28*, 238-251.

Lane, E.B., and Pekny, M. (2004). Stress models for the study of intermediate filament function. Methods Cell Biol *78*, 229-264.

Levine, S., and Hoenig, E.M. (1972). Astrocytic gliosis of vascular adventitia and arachnoid membrane in infantile Gaucher's disease. J Neuropathol Exp Neurol *31*, 147-154.

Li, L., Lundkvist, A., Andersson, D., Wilhelmsson, U., Nagai, N., Pardo, A.C., Nodin, C., Stahlberg, A., Aprico, K., Larsson, K.*, et al.* (2008). Protective role of reactive astrocytes in brain ischemia. J Cereb Blood Flow Metab *28*, 468-481.

Lloyd, E., Somera-Molina, K., Van Eldik, L.J., Watterson, D.M., and Wainwright, M.S. (2008). Suppression of acute proinflammatory cytokine and chemokine upregulation by post-injury administration of a novel small molecule improves long-term neurologic outcome in a mouse model of traumatic brain injury. J Neuroinflammation *5*, 28.

Lu, J.Y., and Hofmann, S.L. (2006). Inefficient cleavage of palmitoyl-protein thioesterase (PPT) substrates by aminothiols: implications for treatment of infantile neuronal ceroid lipofuscinosis. J Inherit Metab Dis *29*, 119-126.

Lucas, S.M., Rothwell, N.J., and Gibson, R.M. (2006). The role of inflammation in CNS injury and disease. Br J Pharmacol *147 Suppl 1*, S232-240.

Lundkvist, A., Reichenbach, A., Betsholtz, C., Carmeliet, P., Wolburg, H., and Pekny, M. (2004). Under stress, the absence of intermediate filaments from Muller cells in the retina has structural and functional consequences. J Cell Sci *117*, 3481-3488.

Macauley, S.L., and Sands, M.S. (2009a). Promising CNS-directed enzyme replacement therapy for lysosomal storage diseases. Exp Neurol *218*, 5-8.

Macauley, S.L., and Sands, M.S. (2009b). Promising CNS-directed enzyme replacement therapy for lysosomal storage diseases. Exp Neurol.

Macauley, S.L., Sidman, R.L., Schuchman, E.H., Taksir, T., and Stewart, G.R. (2008b). Neuropathology of the acid sphingomyelinase knockout mouse model of Niemann-Pick A disease including structure-function studies associated with cerebellar Purkinje cell degeneration. Exp Neurol *214*, 181-192.

Macauley, S.L., Wozniak, D.F., Kielar, C., Tan, Y., Cooper, J.D., and Sands, M.S. (2009). Cerebellar pathology and motor deficits in the palmitoyl protein thioesterase 1-deficient mouse. Exp Neurol *217*, 124-135.

Maragakis, N.J., and Rothstein, J.D. (2006). Mechanisms of Disease: astrocytes in neurodegenerative disease. Nat Clin Pract Neurol *2*, 679-689.

Marathe, S., Miranda, S.R., Devlin, C., Johns, A., Kuriakose, G., Williams, K.J., Schuchman, E.H., and Tabas, I. (2000). Creation of a mouse model for non-neurological (type B) Niemann-Pick disease by stable, low level expression of lysosomal sphingomyelinase in the absence of secretory sphingomyelinase: relationship between brain intra-lysosomal enzyme activity and central nervous system function. Hum Mol Genet *9*, 1967-1976.

Margraf, L.R., Boriack, R.L., Routheut, A.A., Cuppen, I., Alhilali, L., Bennett, C.J., and Bennett, M.J. (1999). Tissue expression and subcellular localization of CLN3, the Batten disease protein. Mol Genet Metab *66*, 283-289.

Mazzanti, M., Sul, J.Y., and Haydon, P.G. (2001). Glutamate on demand: astrocytes as a ready source. Neuroscientist *7*, 396-405.

McCandless, E.E., and Klein, R.S. (2007). Molecular targets for disrupting leukocyte trafficking during multiple sclerosis. Expert Rev Mol Med *9*, 1-19.

Meikle, P.J., Hopwood, J.J., Clague, A.E., and Carey, W.F. (1999). Prevalence of lysosomal storage disorders. JAMA *281*, 249-254.

Messing, A., and Brenner, M. (2003). GFAP: functional implications gleaned from studies of genetically engineered mice. Glia *43*, 87-90.

Mitchison, H.M., Hofmann, S.L., Becerra, C.H., Munroe, P.B., Lake, B.D., Crow, Y.J., Stephenson, J.B., Williams, R.E., Hofman, I.L., Taschner, P.E.*, et al.* (1998). Mutations in the palmitoyl-protein thioesterase gene (PPT; CLN1) causing juvenile neuronal ceroid lipofuscinosis with granular osmiophilic deposits. Hum Mol Genet *7*, 291-297.

Mitchison, H.M., Lim, M.J., and Cooper, J.D. (2004). Selectivity and types of cell death in the neuronal ceroid lipofuscinoses. Brain Pathol *14*, 86-96.

Mrak, R.E., and Griffinbc, W.S. (2001). The role of activated astrocytes and of the neurotrophic cytokine S100B in the pathogenesis of Alzheimer's disease. Neurobiol Aging *22*, 915-922.

Murphy, G.M., Jr., Ellis, W.G., Lee, Y.L., Stultz, K.E., Shrivastava, R., Tinklenberg, J.R., and Eng, L.F. (1992). Astrocytic gliosis in the amygdala in Down's syndrome and Alzheimer's disease. Prog Brain Res *94*, 475-483.

Murray, C., Viehman, A., and Lippa, C.F. (2006). The corpus callosum in Pick's disease, Alzheimer's disease, and amyotrophic lateral sclerosis: gliosis implies possible clinical consequence. Am J Alzheimers Dis Other Demen *21*, 37-43.

Nakazawa, T., Takeda, M., Lewis, G.P., Cho, K.S., Jiao, J., Wilhelmsson, U., Fisher, S.K., Pekny, M., Chen, D.F., and Miller, J.W. (2007). Attenuated glial reactions and photoreceptor degeneration after retinal detachment in mice deficient in glial fibrillary acidic protein and vimentin. Invest Ophthalmol Vis Sci *48*, 2760-2768.

Nedergaard, M., Ransom, B., and Goldman, S.A. (2003). New roles for astrocytes: redefining the functional architecture of the brain. Trends Neurosci *26*, 523-530.

Nesic, O., Lee, J., Ye, Z., Unabia, G.C., Rafati, D., Hulsebosch, C.E., and Perez-Polo, J.R. (2006). Acute and chronic changes in aquaporin 4 expression after spinal cord injury. Neuroscience *143*, 779-792.

Neufeld, E.F. (1991). Lysosomal storage diseases. Annu Rev Biochem *60*, 257-280.

Neufeld, E.F., and Fratantoni, J.C. (1970). Inborn errors of mucopolysaccharide metabolism. Science *169*, 141-146.

Oberheim, N.A., Tian, G.F., Han, X., Peng, W., Takano, T., Ransom, B., and Nedergaard, M. (2008). Loss of astrocytic domain organization in the epileptic brain. J Neurosci *28*, 3264-3276.

Palmer, D.N., Fearnley, I.M., Walker, J.E., Hall, N.A., Lake, B.D., Wolfe, L.S., Haltia, M., Martinus, R.D., and Jolly, R.D. (1992). Mitochondrial ATP synthase subunit c storage in the ceroid-lipofuscinoses (Batten disease). Am J Med Genet *42*, 561-567.

Passini, M.A., Dodge, J.C., Bu, J., Yang, W., Zhao, Q., Sondhi, D., Hackett, N.R., Kaminsky, S.M., Mao, Q., Shihabuddin, L.S.*, et al.* (2006). Intracranial delivery of CLN2 reduces brain pathology in a mouse model of classical late infantile neuronal ceroid lipofuscinosis. J Neurosci *26*, 1334-1342.

Pekny, M. (2001). Astrocytic intermediate filaments: lessons from GFAP and vimentin knock-out mice. Prog Brain Res *132*, 23-30.

Pekny, M., Johansson, C.B., Eliasson, C., Stakeberg, J., Wallen, A., Perlmann, T., Lendahl, U., Betsholtz, C., Berthold, C.H., and Frisen, J. (1999). Abnormal reaction to central nervous system injury in mice lacking glial fibrillary acidic protein and vimentin. J Cell Biol *145*, 503-514.

Pekny, M., and Nilsson, M. (2005). Astrocyte activation and reactive gliosis. Glia *50*, 427-434.

Pekny, M., and Pekna, M. (2004). Astrocyte intermediate filaments in CNS pathologies and regeneration. J Pathol *204*, 428-437.

Perea, G., Navarrete, M., and Araque, A. (2009). Tripartite synapses: astrocytes process and control synaptic information. Trends Neurosci *32*, 421-431.

Pontikis, C.C., Cotman, S.L., MacDonald, M.E., and Cooper, J.D. (2005). Thalamocortical neuron loss and localized astrocytosis in the Cln3Deltaex7/8 knock-in mouse model of Batten disease. Neurobiol Dis *20*, 823-836.

Potokar, M., Kreft, M., Li, L., Daniel Andersson, J., Pangrsic, T., Chowdhury, H.H., Pekny, M., and Zorec, R. (2007). Cytoskeleton and vesicle mobility in astrocytes. Traffic *8*, 12-20.

Ralay Ranaivo, H., Craft, J.M., Hu, W., Guo, L., Wing, L.K., Van Eldik, L.J., and Watterson, D.M. (2006). Glia as a therapeutic target: selective suppression of human amyloid-beta-induced upregulation of brain proinflammatory cytokine production attenuates neurodegeneration. J Neurosci *26*, 662-670.

Ransom, B., Behar, T., and Nedergaard, M. (2003). New roles for astrocytes (stars at last). Trends Neurosci *26*, 520-522.

Rengarajan, J., Szabo, S.J., and Glimcher, L.H. (2000). Transcriptional regulation of Th1/Th2 polarization. Immunol Today *21*, 479-483.

Renkawek, K., Stege, G.J., and Bosman, G.J. (1999). Dementia, gliosis and expression of the small heat shock proteins hsp27 and alpha B-crystallin in Parkinson's disease. Neuroreport *10*, 2273-2276.

Rider, J.A., and Rider, D.L. (1988). Batten disease: past, present, and future. Am J Med Genet Suppl *5*, 21-26.

Ridet, J.L., Malhotra, S.K., Privat, A., and Gage, F.H. (1997). Reactive astrocytes: cellular and molecular cues to biological function. Trends Neurosci *20*, 570-577.

Rothermundt, M., Peters, M., Prehn, J.H., and Arolt, V. (2003). S100B in brain damage and neurodegeneration. Microsc Res Tech *60*, 614-632.

Sands, M.S., and Davidson, B.L. (2006). Gene therapy for lysosomal storage diseases. Mol Ther *13*, 839-849.

Sands, M.S., and Haskins, M.E. (2008). CNS-directed gene therapy for lysosomal storage diseases. Acta Paediatr Suppl *97*, 22-27.

Santavuori, P. (1988). Neuronal ceroid-lipofuscinoses in childhood. Brain Dev *10*, 80-83.

Santavuori, P., Haltia, M., and Rapola, J. (1974). Infantile type of so-called neuronal ceroid-lipofuscinosis. Dev Med Child Neurol *16*, 644-653.

Sarna, J., Miranda, S.R., Schuchman, E.H., and Hawkes, R. (2001). Patterned cerebellar Purkinje cell death in a transgenic mouse model of Niemann Pick type A/B disease. Eur J Neurosci *13*, 1873-1880.

Sarna, J.R., and Hawkes, R. (2003). Patterned Purkinje cell death in the cerebellum. Prog Neurobiol *70*, 473-507.

Schousboe, A., Sonnewald, U., Civenni, G., and Gegelashvili, G. (1997). Role of astrocytes in glutamate homeostasis. Implications for excitotoxicity. Adv Exp Med Biol *429*, 195-206.

Schriner, J.E., Yi, W., and Hofmann, S.L. (1996). cDNA and genomic cloning of human palmitoyl-protein thioesterase (PPT), the enzyme defective in infantile neuronal ceroid lipofuscinosis. Genomics *34*, 317-322.

Scriver, C.R. (2001). The Metabolic and Molecular Basis of Inherited Disease (New York, McGraw-Hill).

Shrestha, B., Gottlieb, D., and Diamond, M.S. (2003). Infection and injury of neurons by West Nile encephalitis virus. J Virol *77*, 13203-13213.

Sleat, D.E., Wiseman, J.A., El-Banna, M., Kim, K.H., Mao, Q., Price, S., Macauley, S.L., Sidman, R.L., Shen, M.M., Zhao, Q.*, et al.* (2004). A mouse model of classical late-infantile neuronal ceroid lipofuscinosis based on targeted disruption of the CLN2 gene results in a loss of tripeptidyl-peptidase I activity and progressive neurodegeneration. J Neurosci *24*, 9117-9126.

Slemmer, J.E., Haasdijk, E.D., Engel, D.C., Plesnila, N., and Weber, J.T. (2007). Aldolase C-positive cerebellar Purkinje cells are resistant to delayed death after cerebral trauma and AMPA-mediated excitotoxicity. Eur J Neurosci *26*, 649-656.

Sofroniew, M.V. (2005). Reactive astrocytes in neural repair and protection. Neuroscientist *11*, 400-407.

Sofroniew, M.V. (2009). Molecular dissection of reactive astrogliosis and glial scar formation. Trends Neurosci.

Sofroniew, M.V., Bush, T.G., Blumauer, N., Lawrence, K., Mucke, L., and Johnson, M.H. (1999). Genetically-targeted and conditionally-regulated ablation

of astroglial cells in the central, enteric and peripheral nervous systems in adult transgenic mice. Brain Res *835*, 91-95.

Somera-Molina, K.C., Robin, B., Somera, C.A., Anderson, C., Stine, C., Koh, S., Behanna, H.A., Van Eldik, L.J., Watterson, D.M., and Wainwright, M.S. (2007). Glial activation links early-life seizures and long-term neurologic dysfunction: evidence using a small molecule inhibitor of proinflammatory cytokine upregulation. Epilepsia *48*, 1785-1800.

Sondhi, D., Peterson, D.A., Edelstein, A.M., del Fierro, K., Hackett, N.R., and Crystal, R.G. (2008). Survival advantage of neonatal CNS gene transfer for late infantile neuronal ceroid lipofuscinosis. Exp Neurol *213*, 18-27.

Sondhi, D., Peterson, D.A., Giannaris, E.L., Sanders, C.T., Mendez, B.S., De, B., Rostkowski, A.B., Blanchard, B., Bjugstad, K., Sladek, J.R., Jr*., et al.* (2005). AAV2-mediated CLN2 gene transfer to rodent and non-human primate brain results in long-term TPP-I expression compatible with therapy for LINCL. Gene Ther *12*, 1618-1632.

Sullivan, S.M., Lee, A., Bjorkman, S.T., Miller, S.M., Sullivan, R.K., Poronnik, P., Colditz, P.B., and Pow, D.V. (2007). Cytoskeletal anchoring of GLAST determines susceptibility to brain damage: an identified role for GFAP. J Biol Chem *282*, 29414-29423.

Switzer, R.C., 3rd (2000). Application of silver degeneration stains for neurotoxicity testing. Toxicol Pathol *28*, 70-83.

Taupin, P. (2006). HuCNS-SC (StemCells). Curr Opin Mol Ther *8*, 156-163.

Tayama, M., O'Brien, J.S., and Kishimoto, Y. (1992). Distribution of saposins (sphingolipid activator proteins) in tissues of lysosomal storage disease patients. J Mol Neurosci *3*, 171-175.

Tian, G.F., Azmi, H., Takano, T., Xu, Q., Peng, W., Lin, J., Oberheim, N., Lou, N., Wang, X., Zielke, H.R*., et al.* (2005). An astrocytic basis of epilepsy. Nat Med.

Tyynela, J., Palmer, D.N., Baumann, M., and Haltia, M. (1993). Storage of saposins A and D in infantile neuronal ceroid-lipofuscinosis. FEBS Lett *330*, 8-12.

Vajda, F.J. (2002). Neuroprotection and neurodegenerative disease. J Clin Neurosci *9*, 4-8.

Vanhanen, S.L., Sainio, K., Lappi, M., and Santavuori, P. (1997). EEG and evoked potentials in infantile neuronal ceroid-lipofuscinosis. Dev Med Child Neurol *39*, 456-463.

Verardo, M.R., Lewis, G.P., Takeda, M., Linberg, K.A., Byun, J., Luna, G., Wilhelmsson, U., Pekny, M., Chen, D.F., and Fisher, S.K. (2008). Abnormal reactivity of muller cells after retinal detachment in mice deficient in GFAP and vimentin. Invest Ophthalmol Vis Sci *49*, 3659-3665.

Vesa, J., Hellsten, E., Verkruyse, L.A., Camp, L.A., Rapola, J., Santavuori, P., Hofmann, S.L., and Peltonen, L. (1995). Mutations in the palmitoyl protein thioesterase gene causing infantile neuronal ceroid lipofuscinosis. Nature *376*, 584-587.

Volterra, A., and Meldolesi, J. (2005). Astrocytes, from brain glue to communication elements: the revolution continues. Nat Rev Neurosci *6*, 626-640.

Voskuhl, R.R., Peterson, R.S., Song, B., Ao, Y., Morales, L.B., Tiwari-Woodruff, S., and Sofroniew, M.V. (2009). Reactive astrocytes form scar-like perivascular barriers to leukocytes during adaptive immune inflammation of the CNS. J Neurosci *29*, 11511-11522.

Wainwright, M.S., Craft, J.M., Griffin, W.S., Marks, A., Pineda, J., Padgett, K.R., and Van Eldik, L.J. (2004). Increased susceptibility of S100B transgenic mice to perinatal hypoxia-ischemia. Ann Neurol *56*, 61-67.

Walkley, S.U. (1998). Cellular pathology of lysosomal storage disorders. Brain Pathol *8*, 175-193.

Walz, W. (2000). Role of astrocytes in the clearance of excess extracellular potassium. Neurochem Int *36*, 291-300.

Welsh, J.P., Yuen, G., Placantonakis, D.G., Vu, T.Q., Haiss, F., O'Hearn, E., Molliver, M.E., and Aicher, S.A. (2002). Why do Purkinje cells die so easily after global brain ischemia? Aldolase C, EAAT4, and the cerebellar contribution to posthypoxic myoclonus. Adv Neurol *89*, 331-359.

Wilhelmsson, U., Bushong, E.A., Price, D.L., Smarr, B.L., Phung, V., Terada, M., Ellisman, M.H., and Pekny, M. (2006). Redefining the concept of reactive astrocytes as cells that remain within their unique domains upon reaction to injury. Proc Natl Acad Sci U S A *103*, 17513-17518.

Winchester, B. (2004). Primary defects in lysosomal enzymes (Oxford, Oxford University Press).

Wisniewski, K.E., Rapin, I., and Heaney-Kieras, J. (1988). Clinico-pathological variability in the childhood neuronal ceroid-lipofuscinoses and new observations on glycoprotein abnormalities. Am J Med Genet Suppl *5*, 27-46.

Worgall, S., Sondhi, D., Hackett, N.R., Kosofsky, B., Kekatpure, M.V., Neyzi, N., Dyke, J.P., Ballon, D., Heier, L., Greenwald, B.M.*, et al.* (2008). Treatment of late infantile neuronal ceroid lipofuscinosis by CNS administration of a serotype 2 adeno-associated virus expressing CLN2 cDNA. Hum Gene Ther *19*, 463-474.

Wu, Y.P., McMahon, E.J., Matsuda, J., Suzuki, K., and Matsushima, G.K. (2001). Expression of immune-related molecules is downregulated in twitcher mice following bone marrow transplantation. J Neuropathol Exp Neurol *60*, 1062-1074.

Young, P.P., Fantz, C.R., and Sands, M.S. (2004). VEGF disrupts the neonatal blood-brain barrier and increases life span after non-ablative BMT in a murine model of congenital neurodegeneration caused by a lysosomal enzyme deficiency. Exp Neurol *188*, 104-114.

Zhang, Z., Butler, J.D., Levin, S.W., Wisniewski, K.E., Brooks, S.S., and Mukherjee, A.B. (2001). Lysosomal ceroid depletion by drugs: therapeutic implications for a hereditary neurodegenerative disease of childhood. Nat Med *7*, 478-484.

Curriculum Vitae

SHANNON L. MACAULEY-RAMBACH

address: 6945 Lindenwood Place
St Louis, MO 63109

email: macauley.rambach@gmail.com
cell: 508.667.7655

EDUCATION

Washington University, St Louis, MO.

- PhD candidate in Neuroscience, 2003 - Present
- Dissertation Title: The role of astrocyte activation in a mouse model of infantile neuronal ceroid lipofuscinosis (INCL)

Middlebury College, Middlebury, VT.

- BA February 1999
- Joint Major in Biology and Psychology
- Senior Project: The role of vasoactive intestinal polypeptide and arginine-vasopressin in the regulation of circadian rhythms in the suprachiasmatic nuclei of *mus domesticus*

EXPERIENCE

Washington University School of Medicine, Saint Louis, MO.
PhD student in Neuroscience, Laboratory of Mark S. Sands (March 2004 - Present)

- Identification of the underlying cellular mechanisms that lead to pathological changes and functional deficits in a mouse model of Infantile Neuronal Ceroid Lipofuscinosis (INCL).
- Development of mouse models to test the role of quiescent astrocytes, activated astrocytes, and neurons in the disease pathogenesis of INCL.
- Use of gene therapies and small molecules for the treatment of INCL.

Genzyme Corporation, Framingham, MA.
Neuroscience Research Associate (December 2000 - July 2003)
Neuroscience Research Assistant (December 1999 - 2000)

- Characterization of the CNS histopathology in different models of lysosomal storage disorders; identifying endpoints used to determine therapeutic efficacy.
- Development of test batteries that characterize the behavioral deficits found in animal models of lysosomal storage diseases; identifying endpoints used to determine therapeutic efficacy.
- Evaluation of novel cell, protein, and gene therapies, as well as various modes of intracranial delivery, for the treatment of CNS disorders.
- Histological evaluation of a neural transplantation model for the treatment of Parkinson's disease.

Genzyme Corporation, Framingham, MA.
Immunology Research Assistant (April 1999 - December 1999)

- Researched and developed methods aimed at tolerance induction to therapeutic agents for the treatment of Fabry Disease.

Middlebury College, Middlebury, VT.
Neurobiology Research Assistant (June 1998 - February 1999)

- Investigated the relationship between circadian behavior and the neuroanatomy of the suprachiasmatic nucleus in mouse models.

RESEARCH SUPPORT

- Batten Disease Research and Support Association (BDSRA) Postdoctoral Fellowship, November 2009 – November 2011
- NINDS National Research Service Award (NRSA) Predoctoral Fellowship, March 2007 - Present

AWARDS AND HONORS

- J. Alfred Rider Memorial Research Award Recipient, July 2009
  - Awarded to the #1 ranked, peer reviewed research proposal by the BDSRA
- 12th International Congress on Neuronal Ceroid Lipofuscinoses (NCL) - Travel Award Recipient, May 2009
- National Graduate Student Research Festival at the National Institute of Health – Selected Participant, September 2009
- Markey Special Emphasis Pathway in Human Pathobiology Fellow, 2004 - 2006
- Genzyme Corporation Vice President's Award, June 2003

INVITED SPEAKER

- Society for Neuroscience, Chicago, IL, October 2009
- Batten Disease Research and Support Association's Annual Family Meeting, St. Louis, MO, July 2009
- 12th International Congress on NCL, Hamburg, Germany, June 2009

TEACHING EXPERIENCE

- Neurobiology of Disease Biology 5663 Teaching Assistant, January 2006 – May 2006
- Research mentor to Washington University Undergraduate, June 2009 - Present

PUBLICATIONS

1. **Macauley SL**, Reddy AS, Pekny M, Sands MS. The role of astrocyte activation in a mouse model of Infantile Neuronal Ceroid Lipofusciniosis. *In preparation.*
2. Kielar C, Wishart TM, Palmer A, Dihanich S, **Macauley SL**, Sands MS, Pearce DA, Cooper JD, Gillingwater TH. Molecular correlates of axonal and synaptic pathology in mouse models of Batten disease. *Hum. Mol. Genet*. 2009 18(21):4066-80.
3. **Macauley SL**, Wozniak D, Kielar C, Tang Y, Cooper JD, and Sands M. Cerebellar pathology and motor deficits in the palmitoyl protein thioesterase 1 deficient mouse. *Exp. Neurol*. 2009; 217(1):124-35.
4. **Macauley SL**, and Sands MS. Promising CNS-directed enzyme replacement therapy for lysosomal storage diseases. *Exp. Neurol.* 2009; 218(1):5-8
5. **Macauley SL***, Sidman RL, Taksir TV, Schuchman EH, Stewart GR. Investigation of the structure-functional relationship in mouse model of Niemann-Pick A Disease. *Exp. Neurol*. 2008; 214(2):181-92. *** Corresponding Author**
6. Kielar C., Maddox L, Bible E, Pontikis CC, **Macauley SL**, Griffey MA, Wong M, Sands MS, and Cooper JC. Neuron loss occurs in the thalamus before the cortex in

a mouse model of infantile neuronal ceroid lipofuscinosis. *Neurobiol Dis.* 2007;25(1):150-62.

7. Lin D, Donsante A, **Macauley SL**, Levy B, Vogler C, Sands MS. CNS-directed AAV2/5-mediated gene therapy synergizes with myeloreductive BMT in the murine model of globoid-cell leukodystrophy. *Mol Ther*. 2007;15(1):44-52.
8. Griffey M, **Macauley SL**, Ogilvie JM, Sands MS. AAV2-mediated ocular gene therapy for infantile neuronal ceroid lipofuscinosis. *Mol. Ther.* 2005;12(3):413-21.
9. Passini MA, **Macauley SL**, Huff MR, Taksir TV, Bu J, Wu IH, Piepenhagen PA, Dodge JC, Shihabuddin LS, O'Riordan CR, Schuchman EH, Stewart GR. AAV vector-mediated correction of brain pathology in a mouse model of Niemann-Pick A disease. *Mol Ther*. 2005;11(5):754-62.
10. Shihabuddin LS, Numan S, Huff MR, Dodge JC, Clarke J, **Macauley SL**, Yang W, Taksir TV, Parsons G, Passini MA, Gage FH, Stewart GR. Intracerebral transplantation of adult mouse neural progenitor cells into the Niemann-Pick-A mouse leads to a marked decrease in lysosomal storage pathology. *J Neurosci.* 2004;24(47):10642-51.
11. Sleat DE, Wiseman JA, El-Banna M, Kim KH, Mao Q, Price S, **Macauley SL**, Sidman RL, Shen MM, Zhao Q, Passini MA, Davidson BL, Stewart GR, Lobel P. A mouse model of classical late-infantile neuronal ceroid lipofuscinosis based on targeted disruption of the CLN2 gene results in a loss of tripeptidyl-peptidase I activity and progressive neurodegeneration. *J Neurosci.* 2004;24(41):9117-26.
12. **Macauley SL**, Horsch AD, Otterdoom M, Zheng MH, Stewart GR. The effects of transforming growth factor-beta2 on dopaminergic graft survival. *Cell Transplant.* 2004;13(3):245-52.

ABSTRACTS

1. **Macauley SL**, Reddy AS, Pekny M, and Sands MS. The role of astrocyte activation in an inherited model of neurodegenerative disease. Glia in Health & Disease Meeting, Cold Spring Harbor, NY 2008.
2. **Macauley SL**, Vogler C, Wozniak D, and Sands MS. The relationship between cerebellar pathology and motor deficits in the PPT1-/- mouse model of INCL. International Council on Batten Disease, Rochester, NY 2007.
3. **Macauley SL**, Griffey M, Bible E, Vogler C, Wong M, Rothman S, Wozniak D, Cooper J, Sands MS. Chronic inflammation and its contribution to neurodegeneration in Batten disease: Implications for therapy. Society for Neuroscience Meeting, Washington, DC, 2005.
4. **Macauley SL**, Ness JK, Lee C, Snider BJ, Green SH, Sands MS, Goldberg MP. Lentiviral vector expression of GFP in cultured oligodendrocytes. Society for Neuroscience Meeting, San Diego, CA, 2004.
5. Zhao Q, **Macauley SL**, Raben N, Mattaliano R, Stewart GR. Neuropathology in a muscle-wasting disase: observations from the 6neo/neo mouse model of Pompe Disease. Society for Neuroscience Meeting, San Diego, CA, 2004.
6. Stewart GR, **Macauley SL**, Mao Q, Davidson BL, Passini MA, Chang M, Sidman RL, Wiseman JA, El-banna M, Kim K, Price S, Shen MM, Sleat DE, Lobel P. A mouse model of late infantile neuronal ceroid lipofuscinosis (LINCL) based on targeted disruption of the CLN2 gene. Society for Neuroscience Meeting, San Diego, CA, 2004.
7. Bu J, Dodge JC, Zhoa Q, Barbon CM, Song AN, Collins HA, Taksir TV, Griffiths DA, **Macauley SL**, O'Riordan CR, Stewart GR, Passini MA. Restoration of cerebellar motor function and global reduction of sphingomyelin storage in the Niemann-Pick A

brain after intracranial injection of recombinant AAV stereotype 1. Society for Neuroscience Meeting, San Diego, CA, 2004.

8. Passini MA, **Macauley SL**, Huff MR, Taksir TV, Yew NS, O'Riordan CR, Schuchman EH, Stewart GR. Widespread gene delivery and reversal of pathology in the brains of Niemann-Pick A mice by retrograde axonal transport of a therapeutic AAV vector. Society for Neuroscience Meeting, New Orleands, LO, 2003.
9. Shihadbuddin LS, Huff MR, **Macauley SL**, Clarke J, Parsons G, Taksir TV, Gage FH, Stewart GR. Intracerebral transplantation of adult mouse neural progenitor cells into Niemann-Pick A mouse leads to marked decrease in storage deposits. Society for Neuroscience Meeting, New Orleands, LO, 2003.
10. Passini MA, Numan S, Huff MR, Taksir TV, **Macauley SL**, O'Riordan CR, Stewart GR. Distribution of acid sphingomyelinase in the brains of Niemann-Pick A mice following AAV2 gene therapy. American Society of Gene Therapy Meeting, Washington, DC, 2003.
11. Switzer III RC, **Macauley SL**, Schuchman EH, Griffey M, Sands M, Stewart GR. Comparative pathology of neurometabolic disease animal models using silver degeneration staining: Infantile Batten (PPT1), Krabbe (twitcher), and Niemann-Pick A (ASMKO). Society for Neuroscience Meeting, Orlando, FL, 2002.
12. Stewart GR, Schuchman, **Macauley SL**. Behavioral pathology of the Niemann-Pick A (ASMKO) mouse: structure-function studies on Purkinje cell degeneration. Society for Neuroscience Meeting, Orlando, FL, 2002.
13. **Macauley SL**, Shihabuddin LS, Schuchman, EH, Mervis RF, Taksir T, Stewart GR. Neuropathology of Niemann-Pick A (ASMKO) mouse. Society for Neuroscience Meeting, Orlando, FL, 2002.
14. **Macauley SL,** Otterdoom M, Horsch AD, Zheng M, Stewart GR. The effects of TGF-ß on dopaminergic graft survival. American Society for Neural Transplantation and Repair Meeting, Coldwater, FL, 2001.
15. Numan S, Huff MR, **Macauley SL**, Ziegler R, Cheng S, Stewart GR. Optimizing viral vector-based gene therapy to the brain: a comparative study of intracranial delivery systems and approaches. Society for Neuroscience Meeting, New Orleans, LO, 2000.

ACTIVITIES

- Neuroscience Week at the Saint Louis Science Center – Presenter, September 2008
- WASHU Student Advisory Committee (SAC), Member, 2004-2006
- WASHU Neuroscience Retreat Committee, Organizer, 2003- 2006
- WASHU Student-Run Neuroscience Works in Progress Seminar (NeuroWIP), Founder and Organizer, 2005-2007
- WASHU BioMED Rap 2006